

Emissions of Biogenic Volatile Organic Compounds and Ozone Balance under Future Climate Conditions

Cheng Wu



Forschungszentrum Jülich GmbH
Institute of Energy and Climate Research
Troposphere (IEK-8)

Emissions of Biogenic Volatile Organic Compounds and Ozone Balance under Future Climate Conditions

Cheng Wu

Schriften des Forschungszentrums Jülich
Reihe Energie & Umwelt / Energy & Environment

Band / Volume 308

ISSN 1866-1793

ISBN 978-3-95806-121-7

Bibliographic information published by the Deutsche Nationalbibliothek.
The Deutsche Nationalbibliothek lists this publication in the Deutsche
Nationalbibliografie; detailed bibliographic data are available in the
Internet at <http://dnb.d-nb.de>.

Publisher and
Distributor: Forschungszentrum Jülich GmbH
Zentralbibliothek
52425 Jülich
Tel: +49 2461 61-5368
Fax: +49 2461 61-6103
Email: zb-publikation@fz-juelich.de
www.fz-juelich.de/zb

Cover Design: Grafische Medien, Forschungszentrum Jülich GmbH

Printer: Grafische Medien, Forschungszentrum Jülich GmbH

Copyright: Forschungszentrum Jülich 2016

Schriften des Forschungszentrums Jülich
Reihe Energie & Umwelt / Energy & Environment, Band / Volume 308

D 82 (Diss. RWTH Aachen University, 2015)

ISSN 1866-1793
ISBN 978-3-95806-121-7

The complete volume is freely available on the Internet on the Jülicher Open Access Server (JuSER)
at www.fz-juelich.de/zb/openaccess.

Neither this book nor any part of it may be reproduced or transmitted in any form or by any
means, electronic or mechanical, including photocopying, microfilming, and recording, or by any
information storage and retrieval system, without permission in writing from the publisher.

Abstract

Ozone (O_3) is a phytotoxic trace gas in the troposphere where it is photochemically produced from volatile organic compounds (VOCs) and nitrogen oxides ($NO_x = NO + NO_2$). The dominant sink of O_3 in the air over areas with dense plant cover is dry deposition on plant surfaces. However, plants can also contribute to photochemical O_3 formation because they emit biogenic VOCs (BVOCs).

In this study, the role of vegetation for tropospheric ozone balance was investigated by considering the following processes: O_3 depletion by dry deposition on plant surfaces, O_3 depletion by gas phase reactions with plant emitted BVOCs, and photochemical O_3 production from BVOCs. Furthermore, drought and heat stress were applied to the plants, and possible impacts of these stresses on plant performance and on the tropospheric ozone balance were investigated.

Dry deposition of O_3 was dominated by O_3 uptake through the plants stomata with negligible losses on cuticle and stem. For strong BVOC emitter, O_3 destruction by gas phase reactions with BVOCs was significant at low NO_x conditions. Switching from low NO_x to high NO_x conditions led to O_3 production. A ratio of O_3 formation rates over BVOC loss rates was measured for α -pinene as single BVOC and for BVOC mixtures emitted from real plants. For O_3 formation under BVOC limited conditions, this ratio was in the range of 2–3 ppb/ppb. The ratio of O_3 uptake/BVOC emission reflects the capability of a plant as a potential source of O_3 , while NO_x concentration and BVOC/ NO_x ratio determine whether the emitted BVOCs act as an additional sink or a source of O_3 .

O_3 uptake rates and BVOC emission rates are affected by environmental variables such as temperature, light intensity and stresses to plants. The impacts of them are different and thus the capability of a plant to be a source of O_3 is also affected by these variables. The focus of this work was the evaluation of the impact of drought and heat stress because future climate change will bring more and intense heat waves and elongated drought periods.

With the application of moderate drought, the capability of a plant to be a source of O_3 increased; under conditions of severe drought the impact of plants in the O_3 balance decreased to almost zero. Heat stress also changes the capability of the plant to be a source of O_3 . However, this change depends on the basic emission mechanisms of BVOCs and the severity of stress.

Zusammenfassung

Ein großer Teil des phytotoxischen Spurengases Ozon (O_3) in der Troposphäre ist photochemischen Ursprungs. Es wird aus flüchtigen organischen Verbindungen (VOCs, volatile organic compounds) und Stickstoffoxiden ($NO_x = NO + NO_2$) gebildet. Hauptsenke für O_3 in Gebieten mit dichtem Pflanzenbewuchs ist die trockene Deposition auf Pflanzenoberflächen. Umgekehrt spielen auch von Pflanzen emittierten VOCs (BVOCs, biogenic volatile organic compounds) eine wichtige Rolle bei der Bildung von troposphärischem O_3 .

Im Rahmen dieser Arbeit wurde der Einfluss von Pflanzen auf die Ozonbilanz in der Troposphäre untersucht. Dazu wurden folgende Prozesse berücksichtigt: O_3 -Abbau durch trockene Deposition auf Pflanzenoberflächen, O_3 -Abbau durch Gasphasenreaktionen mit den von Pflanzen emittierten BVOCs und photochemische O_3 -Bildung aus BVOCs. Darüber hinaus wurden die Auswirkungen der Trocken- und Hitzestress auf die Ozonbilanz untersucht.

Die trockene Deposition von O_3 auf Pflanzenoberflächen wird durch die stomatare Aufnahme dominiert. Im Vergleich dazu spielt die kutikuläre Aufnahme eine geringe Rolle. Für starke BVOC-Emitter ist der O_3 -Abbau durch chemische Reaktionen mit BVOCs signifikant so lange die NO_x -Konzentrationen niedrig sind. Bei hohen NO_x -Konzentrationen wird O_3 photochemisch produziert. Verhältnisse zwischen O_3 -Bildungsraten und BVOC-Verlustraten wurden für BVOC-Mischungen aus Pflanzen sowie für α -Pinen als einzelnes BVOC gemessen. Unter BVOC-limitierten Bedingungen wurden pro verbrauchtem BVOC 2–3 Moleküle O_3 gebildet. Das Verhältnis O_3 -Aufnahme/BVOC-Emission reflektiert das Potential einer Pflanze eine Quelle für O_3 zu sein. Die NO_x -Konzentrationen bzw. die BVOC/ NO_x -Verhältnisse bestimmen ob die BVOCs als zusätzliche Senke oder Quelle von O_3 wirken.

O_3 -Aufnahmeraten und BVOC-Emissionsraten werden von Umweltvariablen wie Temperatur, Lichtintensität und Stresseinflüssen für Pflanzen beeinflusst. Die Auswirkungen dieser Variablen sind unterschiedlich und das Potential einer Pflanze als Quelle oder Senke für O_3 zu fungieren wird auch von diesen Variablen beeinflusst. Durch fortschreitenden Klimawandel werden häufigere Trocken- und Hitzeperioden erwartet. Ein Schwerpunkt dieser Arbeit war daher, die Auswirkungen von Trocken- und Hitzestress auf die Rolle von Pflanzen bei der Ozonbilanz zu bewerten.

Moderater Trockenstress erhöht sich die Fähigkeit einer Pflanze als eine Quelle für O_3 ; starke Trockenheit verringert die Auswirkungen von Pflanzen auf die Ozonbilanz auf fast Null. Auch Hitzestress verändert das Potential einer Pflanze als eine Quelle für O_3 . Die exakten Auswirkungen hängen von den Emissionsmechanismen und der Stärke der Stressbelastung ab.

Contents

- 1 Introduction..... 1
 - 1.1 Tropospheric ozone..... 1
 - 1.2 The role of vegetation for tropospheric ozone balance..... 2
 - 1.3 Impacts of future climate change on tropospheric ozone balance 2
 - 1.4 Focus of this work..... 3
- 2 Material and Methods..... 5
 - 2.1 Instrumentation of Jülich Plant Atmosphere Chamber..... 5
 - 2.2 Concepts 8
 - 2.2.1 Basic rate equations of substances in CSTRs..... 8
 - 2.2.2 Dry deposition of ozone on plant surfaces..... 9
 - 2.2.3 Ozone losses by gas phase reactions 12
 - 2.2.4 BVOC emissions under multi-stress 12
 - 2.2.5 Photochemical ozone formation..... 16
 - 2.3 Experimental procedures 20
 - 2.3.1 Dry deposition of ozone on plant surfaces..... 20
 - 2.3.2 BVOC emissions under drought and heat stress..... 21
 - 2.3.3 Ozone losses by gas phase reaction 23
 - 2.3.4 Ozone formation of single compound and BVOC mixtures 23
 - 2.3.5 Ozone balance 24
- 3 Results 27
 - 3.1 Ozone losses on leaf surfaces..... 27
 - 3.1.1 Temporal change of ozone losses under drought stress..... 27
 - 3.1.2 Stomatal and non-stomatal ozone losses 28
 - 3.1.3 Impacts of severe drought stress on ozone losses..... 29
 - 3.1.4 Summary..... 30
 - 3.2 BVOC emissions under drought and heat stress..... 31

3.2.1	Impacts of drought stress.....	31
3.2.2	Impacts of heat stress	42
3.2.3	Summary.....	44
3.3	Ozone losses by gas phase reaction.....	45
3.4	Photochemical ozone formation.....	47
3.4.1	Determination of ozone formation rates.....	47
3.4.2	Ozone formation from single compound: α -pinene	48
3.4.3	Ozone formation from VOCs emitted by Holm oak	52
3.4.4	Summary.....	53
3.5	The role of plants for tropospheric ozone balance	55
3.5.1	Impacts of temperature, PAR and drought stress.....	55
3.5.2	Case study of ozone balance under high NO _x conditions.....	57
3.5.3	Summary.....	59
4	Discussion.....	61
4.1	Dry deposition of ozone on plant surfaces	61
4.1.1	Comparison to literatures	61
4.1.2	Higher slopes under severe drought stress.....	62
4.2	BVOC emissions under drought and heat stress.....	64
4.2.1	<i>De-novo</i> emissions under drought stress.....	64
4.2.2	Comparison of <i>de-novo</i> and pool emissions	66
4.2.3	Impacts of heat stress	68
4.3	Gas phase reaction.....	69
4.4	Photochemical ozone formation.....	71
4.4.1	Uncertainty of ozone formation rate	71
4.4.2	NO _x -VOC sensitivity - effective control of tropospheric ozone.....	72
4.4.3	Ozone formation potential.....	73
4.5	The role of vegetation for tropospheric ozone balance.....	75
4.5.1	The ratio of ozone uptake/BVOC emission - the potential to be an ozone source.....	75
4.5.2	Vegetation under future climate conditions - a sink or a source of ozone?	76
5	Summary and conclusion	79
6	Reference	81
7	Appendix.....	87
8	Abbreviations	91
9	Acknowledgement.....	93

1 Introduction

1.1 Tropospheric ozone

Ozone (O_3) is an important constituent of the planetary boundary layer with mixing ratios ranging from 10 parts per billion (ppb) in the air over remote areas up to more than 100 ppb downwind of polluted regions. It is one of the tropospheric air pollutants, which has impacts on scales ranging from local to global (Finlayson-Pitts and Pitts, 1997).

O_3 photolysis in the near UV by sunlight is the main source of hydroxyl radicals (OH), the main oxidant in the Earth's troposphere. In addition, O_3 is an oxidant of alkenes and such O_3 -alkene reactions also produce OH radicals. Hence increasing concentration of O_3 might lead to increased OH concentrations and increased oxidation capacity of the troposphere (Lefohn, 1992). Meanwhile, O_3 acts as a greenhouse gas and contributes to anthropogenic radiative forcing (IPCC, 2013). It is phytotoxic and impacts human respiratory health (WHO, 2006) and vegetation at the surface (Ashmore, 2005; Felzer et al., 2005), for example by reducing photosynthesis capacity (Fiscus et al., 2005; Karnosky et al., 2005).

There are two sources of tropospheric ozone. It arises either from stratosphere-troposphere exchange or formed during the photochemical oxidation of carbon monoxide (CO), methane (CH_4), and other volatile organic compounds (VOCs) in the presence of nitrogen oxides ($NO_x = NO + NO_2$) (Stevenson et al., 2006; Monks et al., 2009). The major sinks of tropospheric ozone include chemical destruction and dry deposition to surface. According to the studies of global ozone budget (Wang et al., 1998; Horowitz et al., 2003; Stevenson et al., 2006), the sources and sinks of tropospheric O_3 are dominated by photochemical production and destruction processes. Stevenson et al. (2006) reported that dry deposition on plant surfaces is estimated to lead to losses in the range of 800 to 1100 Tg yr⁻¹, approximately 15% of the total O_3 loss, and the transport from the stratosphere contributes ~10% of the global source of O_3 in the troposphere.

1.2 The role of vegetation for tropospheric ozone balance

Vegetation plays an important role in biosphere-atmosphere interactions (Calfapietra et al., 2013) and affects both the sink and the source processes of tropospheric ozone balance by gas exchanges with the atmosphere.

On the one hand, dry deposition of O_3 on plant surfaces is a major sink of O_3 in the air over agricultural and forest areas. On the other hand, plants emit a considerable amount of different compounds known as biogenic volatile organic compounds (BVOCs), which are involved in photochemical O_3 formation and impact the oxidation capacity of the troposphere (Chameides et al., 1988; Jacob and Wofsy, 1988; Derwent et al., 1996; Kulmala et al., 2004). Compared to most anthropogenic VOCs, BVOCs are very reactive because of the presence of C-C double bond(s). In regions where NO_x mixing ratios are low, O_3 is depleted by reactions with BVOCs emitted by the plants. In regions with high NO_x mixing ratios, O_3 is produced by photochemical reactions involving BVOCs and NO_x . Thus, vegetation can act as a source of O_3 .

On a global scale, the source strengths of BVOC is estimated to $\sim 1000 \text{ Tg yr}^{-1}$ (Guenther et al., 1995; 2012) which exceeds the source strengths of anthropogenic volatile organic compounds by about an order of magnitude (Müller, 1992). Most studies on impacts of BVOCs on tropospheric chemistry focused on isoprene (C_5H_8), since isoprene represents approximately one half of the total BVOC emissions (Guenther et al., 1995; 2012). Less is known about mono- ($C_{10}H_{16}$) and sesquiterpenes ($C_{15}H_{24}$), which have also sizeable sources, and contribute $\sim 15\%$ and $\sim 3\%$ of the total emissions, respectively (Guenther et al., 1995; 2012).

1.3 Impacts of future climate change on tropospheric ozone balance

The future changes in global and regional climate include increases in temperature, changes in the hydrological cycle, and increasing probabilities of extreme events such as heat waves and drought (IPCC, 2013). In the 21st century, heat waves will become more intense, longer and more frequent (Meehl and Tebaldi, 2004). Global warming will also induce further severe and widespread droughts over many land areas (Dai, 2013). Both stresses, heat and drought, will have impacts on BVOC emissions, on dry deposition of O_3 on plant surfaces, and also on atmospheric chemistry (Strong et al., 2013; Allen et al., 2010). Thus, for the future tropospheric O_3 balance, it is essential to quantitatively understand the impacts of heat and drought stress on BVOC emissions by plants and also the behavior of uptake of O_3 .

Empirical algorithms are often used for modelling the global source strengths of BVOC emissions (Guenther et al., 1993; 1995; 2006; 2012). In general, they follow the procedure: BVOC emission rates of representative species with standard conditions are used as basic model input. Dependencies of BVOC emissions on variables such as temperature, light intensity and soil moisture are considered by applying phenomenological algorithms. In the Model of Emissions of

Gases and Aerosols from Nature (MEGAN) (Guenther et al., 2006;2012), impacts of soil moisture are so far only considered for isoprene emissions. Fewer studies on impacts of soil moisture on monoterpene (MT) emissions have been done. Different reference quantities were used, but most can hardly be used for up-scaling.

1.4 Focus of this work

In order to control whether plants act as a sink or a source for O₃, the efficiencies of the individual processes, dry deposition of O₃ on plant surfaces, BVOC emissions by plants, O₃ destruction in gas phase reactions and photochemical O₃ production from the BVOC emissions were studied. Laboratory measurements with typical species from Temperate, Boreal and Mediterranean forests were conducted under well-defined conditions.

Mechanisms of O₃ deposition on leaf surfaces and BVOC emissions from plants, especially MT emissions, were studied in a plant chamber. These two processes were checked under stress-free and stressed (drought and heat) conditions. For *de-novo* MT emissions, volumetric water content of the soil was used as a reference quantity to parameterize the dependency of *de-novo* MT emissions on soil moisture and to characterize the severity of drought. Afterwards, the plant emitted BVOC was introduced into a reaction chamber. At low NO_x conditions, depletion of O₃ by reactions with BVOCs was investigated while at high NO_x conditions, photochemical O₃ formation was studied. Finally, ozone balance was built up using a two-chamber system by combining all processes. The possible impacts of drought and heat stress on the behaviors of vegetation and on the ozone balance were studied.

2 Material and Methods

2.1 Instrumentation of Jülich Plant Atmosphere Chamber

The experiments were performed at Jülich Plant Atmosphere Chamber (JPAC) in Jülich, Germany. The setup of the chambers is already described in detail elsewhere (Mentel et al., 2009;2013;Schimang et al., 2006). There are three chambers with volumes of 164 L, 1150 L and 1450 L. These chambers could be used singly or in combination, depending on the requirements of the experiments. Fig. 2-1 shows a two-chamber system combining a plant chamber and a reaction chamber. In this study, such design was used for the experiments regarding the ozone balance.

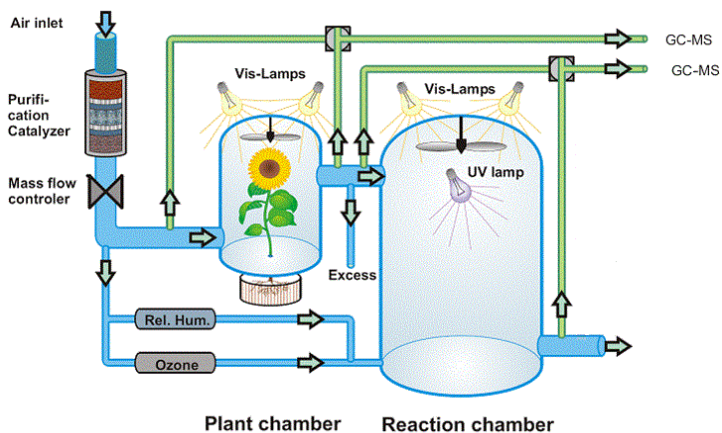


Fig. 2-1 Two-chamber system: the plant chamber (left) is coupled to the reaction chamber (right), where the plant emitted BVOCs could either cause gas phase loss of O_3 or react together with NO_x and cause photochemical O_3 formation (adapted from Mentel et al. (2009)).

The chambers were made of borosilicate glass and operated as continuously stirred tank reactors (CSTRs). To keep the temperature (T) constant, the CSTRs were mounted in separate walk-in climate chambers. Each CSTR was equipped with a Teflon fan providing homogeneous mixing and diminishing the boundary layer resistance at leaf surfaces. The chambers were

equipped with several connections to introduce temperature sensors, a light-intensity sensor and to connect the tubes for gas phase analysis and air supply.

Either one of the two smaller chambers was used as the plant chamber. These two chambers were equipped with 11 (1150 L chamber) and 7 (164 L chamber) discharge lamps, respectively, resulting in photosynthetic active radiation (PAR) at full illumination and at typical mid-canopy heights of $440 \mu\text{mol m}^{-2} \text{s}^{-1}$ and $700 \mu\text{mol m}^{-2} \text{s}^{-1}$. Infrared (IR) radiation (between 750 and 1050 nm) from the lamps was reflected by filters placed between the lamps and the chambers in order to minimize radiative heating of the plants. In order to minimize wall losses also all tubes were either made of Teflon (PTFE or PFA) or of glass.

The chamber with the volume of 1450 L was used as the reaction chamber. This chamber was equipped with 12 discharge lamps, resulting $360 \mu\text{mol m}^{-2} \text{s}^{-1}$ as the maximum visible light flux. In order to obtain sufficient NO_2 photolysis frequencies and O_3 photolysis frequencies, the chamber was equipped with another type of discharge lamps (from here on termed as UVA lamps) and an internal Ultraviolet (UV) lamp (from here on termed as TUV lamps), subsequently.

Ambient air was purified by an adsorptive drying device (Zander Aufbereitungstechnik GmbH & Co. KG, Essen, Germany, KEA 70) and by a palladium catalyst operating at 450°C . O_3 , NO , NO_2 , and volatile organic compounds ($> \text{C}_3$) were removed after the air had passed the purification system. Concentrations of CO_2 and water vapor were also reduced by the adsorption dryer. The CO_2 concentration in the plant chamber was kept at levels of about 350 parts per million (ppm) by adding CO_2 at the inlet. The air flow through the chambers was kept constant by mass flow controllers. Typical air flows used were in the range of $20\text{--}70 \text{ L min}^{-1}$ when using the small chamber and $20\text{--}100 \text{ L min}^{-1}$ when using the large chamber. Residence times of air in these two chambers were $2\text{--}8 \text{ min}$ in the small chamber and $10\text{--}60 \text{ min}$ in the larger chamber.

The reaction chamber has two inlets. One was used for adding VOC, another one for adding O_3 and regulating relative humidity (RH). For adding VOC, either a portion of the air leaving the plant chamber or flow from a diffusion source was fed into the reaction chamber. For this, substances were evaporated from diffusion sources, diluted by synthetic air and continuously flushed into the reaction chamber. The second air flow used for adding O_3 and controlling RH was humidified by a self-made, temperature controlled glass bubbler. The RH was held constant during individual experiment.

Table 2-1 shows analytical equipment at JPAC. The details are described in previous publications (Schuh et al., 1997; Wildt et al., 1997; Schimang et al., 2006). O_3 concentrations were measured by UV absorption. NO concentrations were measured by chemiluminescence and for the measurements of NO_2 the analyzed air was led through a photolytic converter. Differences in mixing ratios of H_2O and CO_2 between chamber inlet and outlet were measured by infrared absorption. Absolute H_2O concentrations were determined with dew point mirrors. Absolute CO_2 concentrations were measured by feeding CO_2 free synthetic air to the reference channel of the IR absorption device. Mixing ratios of BVOCs were measured using gas chromatography-mass spectrometry (GC-MS) or proton-transfer-reaction mass spectrometry (PTR-MS). Calibration of the GC-MS and the PTR-MS systems was performed using a diffusion source containing pure chemicals in individual vials in combination with a dynamic dilution system. Concentrations of the compounds released from the calibration source were determined from the mass loss rates

of the individual compounds and the dilution fluxes. The VOC mixing ratios were in the parts per trillion (ppt) to lower ppb range. For the details of the GC systems and calibration procedure, see e.g. Heiden et al. (2003).

Table 2-1 Instrumentation at the Jülich Plant Atmosphere Chamber (JPAC).

Quantity	Instrument	Principle	Company
BVOC	GC HP 5890 Serie II + MSD HP 5972A	Gas chromatography for separation, mass spectrometry for quantification and identification of BVOC	Agilent Technologies
	GC HP 6890 + MSD HP 5973		
	GC HP 7890 + MSD HP 5975C		
	PTR-MS	Chemical reaction mass spectrometry for quantification of BVOC	Ionicon
NO _x	Tecan CLD 770 AL PPT + Tecan PLC 760 & CLD TR 780	Chemiluminescence + photolytic converter	ECO Physics
CO ₂ and H ₂ O	Binos 100 4P	IR absorption	Fisher-Rosemount
CO ₂	LI-820 CO ₂ gas analyzer	IR absorption	LI-COR Bioscience
O ₃	Model 49	UV absorption	Thermo Environmental Instruments
Dew point	Dew point mirror MTS-MK-1	-	Walz
O ₃ generator	-	O ₂ photolysis at 189 nm	Self-made
Temperature sensor	Type K, Ni-CrNi	-	Newport
PAR sensor	LI-189	-	LI-COR
Discharge lamps	HQI 400W/D	-	Osram
Filter	IR3	-	Prinz Optics
UVA	TL60 W/10-R, 60W	$\lambda = 365 \text{ nm}$	Philips
TUV	TUV 40W	$\lambda = 254 \text{ nm}$	Philips
Balance	MC1	-	Sartorius

2.2 Concepts

In this section, the first part is the basic rate equations for substances in continuously stirred tank reactors (CSTRs). The concepts of individual processes: dry deposition of O₃ on plant surfaces, gas phase reactions of O₃ and BVOCs, BVOC emissions by plant and photochemical O₃ formation from BVOCs are described afterwards.

2.2.1 Basic rate equations of substances in CSTRs

In CSTRs, the basic processes to be considered for a compound X are: introduction in the chamber together with the inflowing air, removal together with the outflowing air, losses at the chamber walls, gas phase reactions, photolysis, and in case of plants being in the chamber, uptake and emission from the plants. Assuming mass balance, the change of X with time is given by

$$V \times \frac{d[X]}{dt} = F \times ([X]_{\text{in}} - [X]) + X_{\text{source}} - X_{\text{sink}} \quad (2-1)$$

where V is the volume of the chamber, F is the air flow through the chamber, $[X]_{\text{in}}$ and $[X]$ are the mixing ratios of compound X at the chamber inlet and outlet, respectively. X_{source} is the sum of source terms of X , and X_{sink} is the sum of all loss terms of X . Since the chambers were operated as CSTRs with the mixing times below 2 minutes, the concentrations measured at chamber outlet represent the average of the concentrations in the chamber.

For steady-state conditions, the change of the concentration, $d[X]/dt$, is zero and the difference between concentrations measured in the chamber and at the chamber inlet equal the sum of all loss and sink terms

$$F \times ([X] - [X]_{\text{in}}) = X_{\text{source}} - X_{\text{sink}} \quad (2-2)$$

Individual source and sink terms were determined in separate experiments. Wall losses were determined without plants and oxidants in the chamber and in darkness using equation (2-3)

$$F \times ([X] - [X]_{\text{in}}) = \Phi^{\text{W}} \times A^{\text{W}} \quad (2-3)$$

where Φ^{W} is the flux density of X to the wall and A^{W} is the wall area. From former experiments (Schuh et al., 1997; Heiden et al., 2003; Schimang et al., 2006) it is known that except for a few compounds (methyl jasmonate, some sesquiterpenes (SQT)) wall losses are negligible. Repeating such measurements with O₃ confirmed these findings and therefore wall losses are neglected in the following.

Gas phase reactions of O_3 with BVOCs were also measured without a plant in the chamber. When using emissions from real plants, a second chamber was used for this purpose. The exhaust from the plant chamber was fed to a reaction chamber. In the example of VOC ozonolysis ($X = \text{VOC}$), equation (2-4) shows how measured losses are compared to theoretical losses.

$$F \times ([X] - [X]_{\text{in}}) = V \times k_{X+O_3} \times [X] \times [O_3] \quad (2-4)$$

In equation (2-4), $[X]$ is the concentration of the VOC under consideration, and $[O_3]$ is the O_3 concentration in the chamber and k_{X+O_3} is the rate constant.

Flux densities $\Phi(X)$ with a plant were determined in the chamber using equation (2-5)

$$F \times ([X] - [X]_{\text{in}}) = \Phi(X) \times A^L \quad (2-5)$$

where A^L is the leaf area of the plant in the chamber. Flux densities depend on concentration gradients. Assuming flux densities to be proportional to the concentration gradients, conductivities or deposition velocities g_x are defined as

$$g_x = \frac{\Phi(X)}{\Delta[X]} \quad (2-6)$$

where $\Delta[X]$ is the concentration gradient between the air in the substomatal cavity of the plant and the air in the chamber. Using $\Delta[X]$ in units of molecules cm^{-3} leads to a deposition velocity in units of cm s^{-1} . Using mixing ratios to express $\Delta[X]$ leads to conductivities (molecules $\text{cm}^{-2} \text{s}^{-1}$) that are connected to deposition velocities by the molar volume (in units of cm^3).

Equations (2-3) to (2-6) are the basic equations. Depending on the experiment, X was different and correction factors had to be considered. More detailed equations and the theoretical background are described separately in the following.

2.2.2 Dry deposition of ozone on plant surfaces

The exchange of water vapor (transpiration) and CO_2 (photosynthesis) is regulated by the aperture of stomata and the concentration gradients between air and plants. If stomata are open and the concentrations in the atmosphere and in the substomatal cavity are different, gas molecules will move from the region with a high concentration to the region with a low concentration. This causes also uptake of trace gases such as O_3 , NO , and NO_2 .

As a convention, for the exchange of gases between plants and the atmosphere, flux densities are positive in case the plants emit a compound (e.g. water vapor, BVOC), and are negative when plants take up a gas (CO_2 , O_3). In this study, flux densities of CO_2 and O_3 were multiplied by

-1 for better visual comparison in diagram. In the example of O_3 , basic mechanisms of trace gas uptake were determined by following steps:

As the first step, the total uptake rates of O_3 (flux densities), $\Phi(O_3)_{\text{uptake}}$, were approximated using equation (2-5a) and conductivities to O_3 were then determined using equation (2-6a)

$$\Phi(O_3)_{\text{uptake}} = \frac{F}{A^L} \times ([O_3]_{\text{in}} - [O_3]) \quad (2-5a)$$

$$g_{O_3} = \frac{\Phi(O_3)_{\text{uptake}}}{\Delta[O_3]} \quad (2-6a)$$

where $\Delta[O_3]$ is equivalent to the O_3 concentration in the chamber $[O_3]$ by assuming the O_3 concentration in the intercellular air spaces to be zero (Neubert et al., 1993),

In the second step, stomatal conductivity of O_3 , $g_{O_3}^S$, was determined independent of O_3 data. Since release of water through the stomata is a diffusion process as well as diffusion processes of traces gases. Stomatal conductance to O_3 therefore can be determined from the stomatal conductivity to water vapour in consideration of the respective diffusion coefficients (Neubert et al., 1993) as

$$g_{O_3}^S = g_{H_2O}^S \times \frac{D_{O_3}}{D_{H_2O}} \quad (2-7)$$

where $D_{H_2O} = 0.25 \text{ cm}^2 \text{ s}^{-1}$ was taken from Marrero and Mason (1972) and $D_{O_3} = 0.167 \text{ cm}^2 \text{ s}^{-1}$ was taken from Laisk et al. (1989). Transpiration and stomatal conductivity to water vapour can be calculated in the same way as for O_3 using equations (2-5b) and (2-6b)

$$\Phi(H_2O) = \frac{F}{A^L} \times ([H_2O] - [H_2O]_{\text{in}}) \quad (2-5b)$$

$$g_{H_2O}^S = \frac{\Phi(H_2O)}{[H_2O]_p - [H_2O]} \quad (2-6b)$$

where $[H_2O]$ and $[H_2O]_{\text{in}}$ are the mixing ratios of water vapour measured at chamber outlet and inlet, respectively. $[H_2O]_p$ is the concentration of water vapour in the substomatal cavity. $[H_2O]_p$ was calculated from the measured leaf temperatures assuming the relative humidity inside the plants to be 100 % (Neubert et al., 1993).

In order to analyse the conductivity g_{O_3} , a resistance network (Fig. 2-2) was used (Laisk et al., 1989; Neubert et al., 1993). This resistance network includes resistances against the fluxes through the stomata (R_s), fluxes from the substomatal cavity into the mesophyll (R_m), and fluxes

through the cuticle (R_C). The respective conductivities are stomatal conductivity ($g_{O_3}^S$), mesophyll conductivity ($g_{O_3}^M$) and cuticular conductivity ($g_{O_3}^C$), which are the inverses of the resistances.

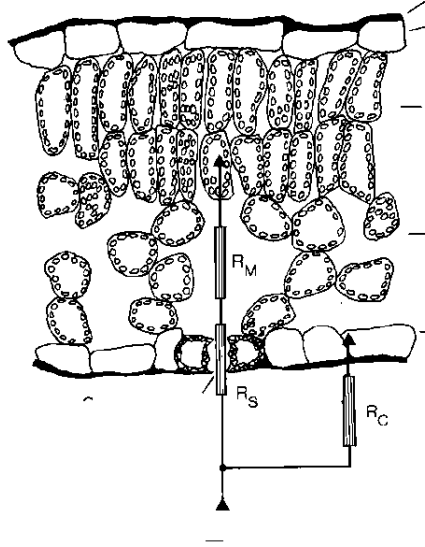


Fig. 2-2 Resistance network (Neubert et al., 1993).

According to the resistance network g_{O_3} is expressed as

$$g_{O_3} = g_{O_3}^C + \frac{g_{O_3}^S \times g_{O_3}^M}{g_{O_3}^S + g_{O_3}^M} \quad (2-8)$$

Plotting g_{O_3} versus $g_{O_3}^S$ led to linear relationships with the intercept $g_{O_3}^C$ and the slope

$$\frac{dg_{O_3}}{dg_{O_3}^S} = \frac{(g_{O_3}^M)^2}{(g_{O_3}^S + g_{O_3}^M)^2} \quad (2-9)$$

Theoretically the slope is in the range of 0–1 and it shows the relation between $g_{O_3}^M$ and $g_{O_3}^S$. Maximum value for the slope is 1 and this maximum is reached if $g_{O_3}^M \gg g_{O_3}^S$, i.e. if further depletion of O_3 can proceed much faster than the delivery of O_3 through the stomata.

One assumption made for the calculation of O₃ uptake rate (equation 2-5a) was the negligible O₃ losses by gas phase reactions. In some cases with strong BVOC emitter, O₃ losses by gas phase reaction was controlled and calculated (see 2.2.3).

2.2.3 Ozone losses by gas phase reactions

Generally, gas phase reactions of O₃ with BVOCs were measured in a reaction chamber (1450 L chamber) fed with the air from the plant chamber, because the residence time of the air in the reaction chamber was much longer than that in the plant chamber.

The measured O₃ losses are compared to the calculated O₃ losses by equation (2-4a)

$$\frac{F}{V} \times ([O_3]_{in} - [O_3]) = \sum_i [VOC_i] \times [O_3] \times k_{VOC_i + O_3} \quad (2-4a)$$

where [VOC_{*i*}] is the concentration of VOC_{*i*} in the chamber, and $k_{VOC_i + O_3}$ is the rate constant of the reaction VOC_{*i*} + O₃.

Such O₃ losses by gas phase reactions were also considered when measuring O₃ losses in the plant chamber, when BVOC and O₃ concentrations were both high and the O₃ losses were significant, compared to the O₃ uptake on plant surfaces. The calculation was also based on equation (2-4a).

2.2.4 BVOC emissions under multi-stress

Plants take up O₃ and at the same time emit BVOCs. Since isoprene emissions have been most studied, this study concentrated on the impacts of drought and heat on MT emissions.

2.2.4.1 Basic algorithm to describe the isoprene and monoterpene emissions

BVOC emissions could be classified into two basic groups: pool emissions and *de-novo* emissions. The key to distinguish them is the size of the storage pool. Fig. 2-3 is adapted from Grote and Niinemets (2008) and it illustrates the relationship between the synthesis of isoprenoids and their emission rates in dependence on the size of the storage pool within the leaves. For those plants having extensive storage pools, such as conifer resin ducts, the emissions are generated from evaporation of these compounds out of storage pools; for those having only small storage capacity, the compounds were emitted directly from *de-novo* synthesis (Grote and Niinemets, 2008).

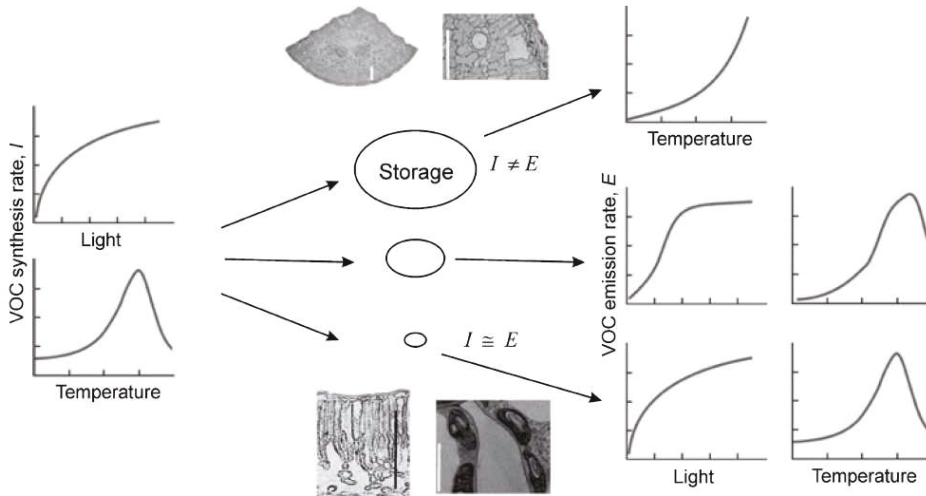


Fig. 2-3 Illustration of the relationships between the isoprenoid synthesis (*I*) and emission (*E*) rates in dependence on the size of the isoprenoid storage pool within the leaves. Isoprenoid synthesis rates depend on the production rate of photosynthetic intermediates, and thus respond to light and temperature according to basic enzyme-kinetic expressions. Contrary, isoprenoid evaporation and diffusion from storage pools depend on diffusion resistances and compound physico-chemical characteristics. In species with large storage pools such as conifers where the mono- and sesquiterpenes are stored in resin ducts, the synthesis and emission rates can be effectively decoupled. Storage pools for isoprene are small and the synthesis and emission rates are essentially equal. Because MT can be non-specifically stored in leaf lipid and liquid phases, a mixed situation may arise in broad-leaved monoterpene-emitting species that lack specific storage compartments for MT within the leaves (adapted from Grote and Niinemets (2008)).

For past decades, many models have used multiplicative approach to estimate the BVOC emissions under different conditions. Temperature and PAR are two basic environmental variables, which influence the emissions.

One of the first algorithms was developed by Tingey (1980;1991), who showed that MT emissions from Slash pine exponentially depend on temperature but are independent of PAR. The underlying reason is that MT emissions from conifers are pool emissions, which depend on temperature and not directly on PAR. In a modified syntax, Tingey's algorithm reads

$$\Phi = \Phi^S \times \exp(\beta \times (T - T_s)) \quad (2-10)$$

where Φ is the emission rate of the MT at the actual temperature T , Φ^S is the standard emission rate or emission activity factor, i.e. the emission rate measured at standard temperature T_s . β is the parameter describing the temperature dependence. β is in the range of 0.09 K^{-1} .

Schuh et al. (1997) found that for MT emissions from different species, both *de-novo* and pool mechanism can act in parallel. He suggested two additive terms to describe temperature and PAR dependence of MT emissions. One of them is similar to equation (2-10) and describes the temperature dependence of MT emissions from pools. The other one is similar to the algorithm by Guenther et al. (1993), which describes isoprene emissions, which are *de-novo* emissions. Both T and PAR are required, since the emission rate is directly related to synthesis and determined by biochemical and physiological processes. In a modified syntax, the algorithm of *de-novo* MT emissions in the study of Guenther et al. (2012) reads

$$\Phi = \Phi^S \times \frac{c_L \times \alpha \times \text{PAR}}{\sqrt{1 + \alpha^2 \times \text{PAR}^2}} \times \exp(\beta \times (T - T_s)) \quad (2-11)$$

where Φ is the emission rate at temperature T and at light intensity PAR. Φ^S is the emission activity factor i.e. the emission rate measured at standard light intensity (often set to 1000 $\mu\text{mol m}^{-2} \text{s}^{-1}$) and at standard temperature, T_s (often set to 30°C). α is the parameter describing the PAR dependence of the emission, and c_L is a normalization factor used to obtain $\Phi = \Phi^S$ when PAR is equal to the standard light intensity.

In the same study of Schuh et al. (1997), it was also noted that the high variability of MT standard emission rates. Measuring emissions from different individuals of a given species under identical conditions of T and PAR still result in highly variable emission rates. This clearly shows that MT emissions also depend on other variables than T and PAR alone, and one of these other variables is soil moisture.

2.2.4.2 Impacts of soil moisture on isoprene and monoterpene emissions

In the Model of Emissions of Gases and Aerosols from Nature (MEGAN) (Guenther et al., 2006;2012), impacts of soil moisture are considered, but only for isoprene emissions. Guenther et al. (2006) implemented the empirical algorithm by Pegoraro et al. (2004) who used the volumetric water content of the soil (θ) as reference quantity for characterizing the impacts of soil moisture. Three different regimes of θ are used in MEGAN to define the factor that describes the impact of soil moisture on isoprene emissions.

Above a threshold θ_1 , isoprene emissions are not affected by soil moisture and the factor is unity. Below θ_1 , isoprene emissions linearly decrease with decreasing θ until the wilting point θ_w is reached. The wilting point θ_w is the soil moisture below which plants cannot extract water from the soil. At and below θ_w isoprene emissions are set to zero. In MEGAN, θ_w is taken from a database by Chen and Dudhia (2001). The difference between θ_1 and θ_w , $\Delta\theta_1$, is the empirical parameter used to describe the dependence of isoprene emissions on soil moisture. Its value ($\Delta\theta_1 = 0.06 \text{ m}^3 \text{ m}^{-3}$) is taken from Pegoraro et al. (2004).

Compared to isoprene there are less studies on impacts of soil moisture on MT emissions. Some studies show increasing emissions with decreasing soil moisture (Bertin and Staudt, 1996; Blanch et al., 2007; Ormeño et al., 2007), others show decreasing emissions with increasing severity of drought (Lavoit et al., 2009; Šimpraga et al., 2011). Besides this, different reference quantities

have been used to characterize the soil moisture level. Among these are the plant water potential (Ormeño et al., 2007;Lavoire et al., 2009) and the diurnal variation of the radial stem diameter (Šimpraga et al., 2011) . As these plant parameters are highly variable between individuals and influenced by a larger number of factors, they can hardly be used for up-scaling.

2.2.4.3 Determination of θ and the θ -dependence of monoterpene emissions

The volumetric water content, θ , was determined from the mass loss of water during the respective experiments (equation 2-12)

$$\theta = \frac{V_{\text{water}}}{V_{\text{soil}}} = \frac{M_{\text{act}} - M_{\text{dry}}}{V_{\text{soil}}} \quad (2-12)$$

where M_{act} is the actual mass of the soil and M_{dry} is the dry mass of the soil. V_{soil} is the volume of the soil in the pots neglecting the volume of the roots. M_{act} was measured online and M_{dry} was estimated from soil samples taken from the top of the pots and oven dried at 110°C for five days. The measured mass loss was converted to volume loss by using the density of water, 1 kg L⁻¹.

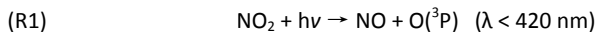
The procedure of determining M_{dry} by taking soil samples added the main uncertainty to the data given for θ . The error caused by this procedure for θ is estimated to be $\pm 15\%$ of the absolute data. In one case, the measured M_{act} were lower than M_{dry} . This led to slightly negative values for θ , which is physically impossible. However, since the deviation from zero was quite low, the negative values were kept.

The dependence of MT emission on θ was parameterized in the following way: maximum MT emissions were reached when θ had fallen near to the threshold below which MT emissions started to decrease (θ_1). The average of the emission rates measured around the maximum emissions was set as standard emission rate, Φ^S . Emission rates measured at the same light intensity and chamber temperature were normalized by dividing them by Φ^S . The normalised data were used to determine the relationship between MT emissions and θ . Although the decrease of emissions with decreasing θ appeared to be exponential, a linear approximation was applied to be comparable to other approaches of parameterization. Linear fits to the normalized data allowed for determining θ_1 as well as the volumetric water content θ_0 below which the extrapolated emissions became zero. Only data with $\theta < \theta_1$ and measured at the same PAR and the same chamber temperature were taken for the fits. Furthermore all data with $\Phi/\Phi^S < 0.05$ were discarded to diminish the impact of the exponential behaviour. Similar to the notation used in MEGAN, $\Delta\theta_1$, the difference $\theta_1 - \theta_0$, was calculated in this study. This procedure of determining the θ dependence of MT emissions was performed for all data sets.

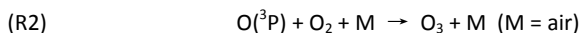
2.2.5 Photochemical ozone formation

2.2.5.1 Chemical fundamentals of photochemical ozone formation

Photochemical O_3 production in the troposphere requires the presence of NO_x . The only significant process forming O_3 in the troposphere is the photolysis of NO_2 , giving NO and ground state oxygen, $O(^3P)$,



$O(^3P)$ reacts with O_2 yielding O_3 ,



since O_3 reacts with NO rapidly,



if assuming no other net production or loss of O_3 , equilibrium between NO , NO_2 and O_3 (R1–R3) is established within minutes (Fig. 2-4, A) as photostationary steady state (PSS) (Leighton, 1961).

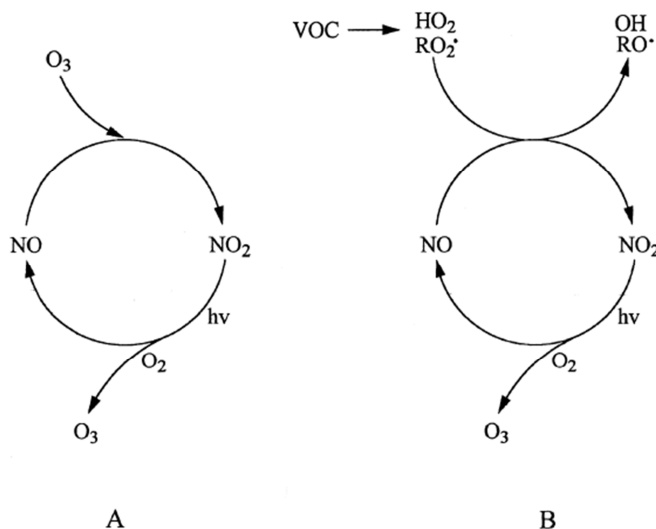
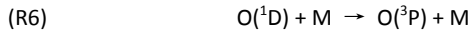
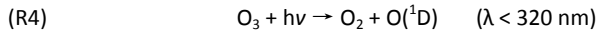


Fig. 2-4 Schematics of the reactions involved in NO -to- NO_2 conversion and O_3 formation in NO - NO_2 - O_3 systems without (A) and with the addition of VOCs (B) (Atkinson, 2000).

Extra O_3 production is initiated by oxidation of VOC by hydroxyl radicals, OH . At the wavelength $< 320 \text{ nm}$, photolysis of O_3 forms the excited oxygen, $O(^1D)$ atom. About 10% of $O(^1D)$ atom

reacts with water vapor (H_2O) to generate OH radicals (R5), and the rest is deactivated by air (R6), giving $\text{O}({}^3\text{P})$.



When VOCs and CO are present, they react with OH and form RO_2 and HO_2 radicals. These intermediate radicals react further with NO and convert NO to NO_2 (Fig. 2-4, B).



Thus, photolysis of NO_2 , which is produced from the reaction of NO and proxy radicals causes photochemical O_3 formation. In R7, the alkoxy radical (RO) reacts rapidly with O_2



and in general, the carbonyl $\text{R}'\text{CHO}$ can continue to be oxidized, leading to peroxy radicals and contributing to O_3 production.

2.2.5.2 VOC- NO_x -Ozone system

There are many studies about the VOC- NO_x -Ozone system (Finlayson-Pitts and Pitts Jr, 1986; Bowman and Seinfeld, 1994; Sillman, 1991, 1999). O_3 isopleth plots are frequently used to illustrate such relation (Fig. 2-5).

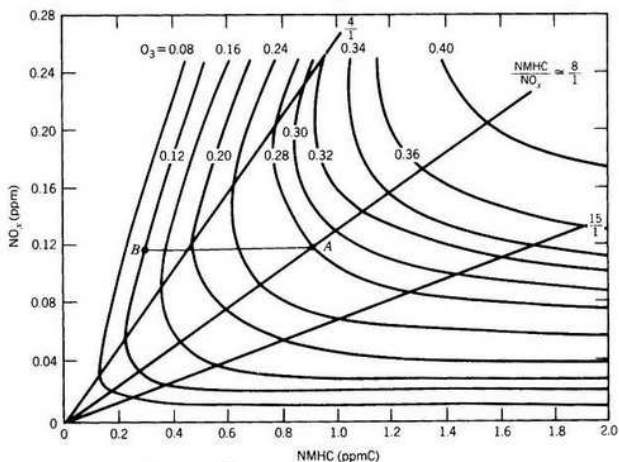


Fig. 2-5 Ozone isopleth plot used in EKMA approach (Finlayson-Pitts and Pitts Jr, 1986).

This O_3 isopleth plot used EKMA (Empirical Kinetic Modeling Approach) technique (Dodge, 1977b; Dodge, 1977a), which is based on a chemical box model called the O_3 isopleth plotting package. For each point in the Fig. 2-5, x- and y-value are the starting concentrations of two precursors NO_x and VOC (NMHC, non-methane hydrocarbon, in Fig. 2-5). For each point, modeled daily maximal hourly average O_3 concentration is taken. Isopleth lines link the points with the same maximal O_3 concentration but different initial conditions. Looking at Fig. 2-5, it becomes clear that the NO_x -VOC- O_3 system is highly nonlinear. O_3 production depends on both the absolute VOC and NO_x concentrations and the VOC/ NO_x ratio.

The key point of the chemistry of the NO_x -VOC- O_3 system is the competition between NO_2 and VOC for OH radicals. The full plot could be separated to two regions with the O_3 ridge line (NMHC/ NO_x =8/1, in Fig. 2-5). When VOC/ NO_x is lower than the ridge line value (e.g. point B in Fig. 2-5), OH radicals react mainly with NO_2 . Such reaction removes radicals, thus the O_3 production rate is limited by the conversion of NO to NO_2 . An addition of NO_x therefore decreases radical concentrations and thus O_3 formation, while increase of VOC concentration causes increase of peak O_3 (point A in Fig. 2-5). The system is VOC-limited. When VOC/ NO_x is high and the region is on the lower right of the ridge line, OH radicals react mainly with VOC. The VOC + OH reaction chain generates more radicals than it consumes. The O_3 production is limited by the amount of the precursor NO_2 , i.e., the system is NO_x -limited (Finlayson-Pitts and Pitts Jr, 1986; Seinfeld and Pandis, 2006).

Of course, there are many other factors affecting the separation into VOC-limited and NO_x -limited regimes. Sillman (1999) characterized these factors: VOC reactivity, biogenic hydrocarbons, photochemical aging, and rates of meteorological dispersion.

In this study, a vertical cut and a horizontal cut of O_3 isopleth plot were conducted to test the chemical mechanisms. The ratio of O_3 production rate $P(O_3)$, over BVOC loss rate $L(BVOC)$, $P(O_3)/L(BVOC)$ was calculated to show the potential of O_3 formation from VOCs.

2.2.5.3 Equations of ozone formation in the reaction chamber

For the determination of $P(O_3)$, the major source and loss terms of O_3 were considered: the source term is NO_2 photolysis, while the loss terms included O_3 photolysis, O_3 reactions with NO , $BVOC$, OH and HO_2 , and wall losses (Wildt et al., 2014).

According to Wildt et al. (2014) the loss terms due to reactions of O_3 with $BVOC$, with OH and with HO_2 were small compared to O_3 photolysis and O_3 outflow from the chamber. Therefore in the calculation of $P(O_3)$ only major loss terms photolysis of O_3 , reaction of O_3 with NO , and O_3 outflow were considered together with the source term NO_2 photolysis and O_3 inflow. Thus, the equation is given by

$$F \times ([O_3] - [O_3]_{in}) = -V \times J(O^1D) \times [O_3] \times f([H_2O]) + V \times J(NO_2) \times [NO_2] - V \times k_{NO+O_3} \times [NO] \times [O_3] \quad (2-14)$$

where $J(O^1D)$ and $J(NO_2)$ are photolysis rates of O_3 and NO_2 . $f(H_2O) \approx 0.09$, it is the branching ratio of $O^1D + H_2O$ reactions over O^1D quenching to O^3P by O_2 and N_2 which leads to reformation of O_3 . $k_{NO+O_3} = 1.8 \times 10^{-14} \text{ cm}^3 \cdot \text{s}^{-1}$ (IUPAC, 2009), is the rate constant for the reaction of NO with O_3 .

In the absence of $VOCs$, the dominant source term is NO_2 photolysis and the dominant loss term is reaction of O_3 with NO . In photostationary steady state (PSS), both rates are equal and cancel out. In the presence of VOC and OH , O_3 production by NO_2 photolysis exceeds O_3 losses in reactions with NO . The difference between NO_2 photolysis and the reaction of O_3 with NO is attributed to reaction R7 and termed as O_3 production rate

$$P(O_3) = \frac{F}{V} \times ([O_3] - [O_3]_{in}) + J(O^1D) \times [O_3] \times f([H_2O]) \quad (2-15)$$

where $J(O^1D)$ was determined on the days without NO_x addition, i.e., $P(O_3) = 0$ in equation (2-15), by measuring the dip of $[O_3]$ with TUV lamp. By assuming the loss of O_3 was entirely caused by the photolysis, $J(O^1D)$ was determined according to equation (2-16)

$$J(O^1D) = \frac{F}{V} \times \frac{[O_3]_{in} - [O_3]}{[O_3]} \times \frac{1}{f([H_2O])}. \quad (2-16)$$

2.3 Experimental procedures

Laboratory measurements of four individual processes were conducted under well-defined conditions: dry deposition of O₃ on leaf surface (2.3.1) and BVOC emissions by plants (2.3.2) were investigated in the plant chambers; destruction of O₃ by plant emitted VOCs (2.3.3) and photochemical O₃ formation from BVOCs (2.3.4) were studied separately in the reaction chamber. Finally, all of these processes were combined with the two-chamber system and the ozone balance (2.3.5) was built up. In 2.3.5, characterizing the O₃ balance was conducted twice. In a first step, a well-watered plant was used. After this, the experiment was repeated with the same individual but under drought stress which was supposed to change all individual processes determining the O₃ balance.

For these experiments, typical tree species from Temperate, Boreal and Mediterranean forests were used. Three to four years old seedlings of European beech (*Fagus sylvatica* L.), Scots pine (*Pinus sylvestris* L.) and Norway spruce (*Picea abies* L.) were taken from the forest, potted in buckets and stored outside for about a year before they were used for the experiments. Seedlings of Holm oak (*Quercus ilex*) were obtained from the forest nursery of Castelporziano Estate, Rome, central Italy. Together with seedlings of Aleppo pine (*Pinus halepensis* L.), which were brought from the Judean Mountains, Israel, they have been potted in 15 L buckets and stored in a growth room before using them in the CSTRs. All plants were potted in the same soil that was a mix of peat (Einheitserde ED73) with quartz sand (volumetric ratio 3:1, density 0.34 ± 0.07 kg L⁻¹).

Leaf area of broad-leaf species were determined by counting the total leaf number and painting edges of ten leaves on a transparency film and calculating the average value by scanning the film and counting of number of dark pixels with ImageJ. For the conifers, the length of all branches and the number of needles from 3 different branches was counted. The leaf area of single needle was estimated by multiplying length and diameter.

2.3.1 Dry deposition of ozone on plant surfaces

Two chambers with the volume of 164 L and 1150 L were used as plant chambers. O₃ analyser and dew point mirror were used and switched between the in- and outlet of the respective chamber automatically. By comparing the differences in the concentration of gases in the in- and outlet, total O₃ loss and transpiration rate were measured.

Before the experiments, wall losses were tested with the empty chambers. After that, different plant species were introduced into the chamber. O₃ deposition on leaf surfaces was investigated for an Aleppo pine (Exp. 1.1), and a Holm oak (Exp. 1.2) (Table 2-2).

For Aleppo pine, a diurnal rhythm of light was applied: 12 hours illumination, 10 hours darkness, 1 hour twilight in the morning and 1 hour twilight in the afternoon simulated by switching on or off individual lamps one by one within 1 hour, respectively. The duration of the whole

experiment was 30 days with three drought periods. O₃ was applied for ~10 days in between including the time periods when plant was under stress-free and water-stressed conditions.

Holm oak experienced a severe drought period followed by a recovery period. O₃ losses were measured firstly on test days when the plant was well-watered. Light program was set to 600 $\mu\text{mol m}^{-2} \text{s}^{-1}$ from 4:00 to 14:00, 300 $\mu\text{mol m}^{-2} \text{s}^{-1}$ from 14:00 to 17:00, and 100 $\mu\text{mol m}^{-2} \text{s}^{-1}$ from 17:00 to 22:00 local time. O₃ losses were then tested again on one day when the plant was under severe drought stress, and with very low transpiration. Light program was set to 600 $\mu\text{mol m}^{-2} \text{s}^{-1}$ for the whole day.

Table 2-2 Overview over experiments of O₃ deposition on leaf surfaces

Exp.	Species	Chamber [L]	T [°C]	PAR [$\mu\text{mol m}^{-2} \text{s}^{-1}$]	Remark
1.1	Aleppo pine	1150	23	440	O ₃ uptake under mild drought
1.2	Holm oak	164	25	600/300/100	O ₃ uptake under severe drought

2.3.2 BVOC emissions under drought and heat stress

Using the same plant chambers (164 L and 1150 L chambers) the experiments of BVOC emissions under drought and heat stress were conducted with four species. As species with storage pools for MT, Scots pine (Exp. 2.1) and Norway spruce (Exp. 2.2, Exp. 2.5) were tested; as species without storage pools for MT, European beech (Exp. 2.3) and Holm oaks (Exp. 2.4) were used. In total, 8 plants were used for the measurements: one individual each for European beech, Scots pine, two individuals for Norway spruce and four individuals of Holm oak. In Exp. 2.1 to Exp. 2.4, the plants were exposed to drought stress and in Exp. 2.5, the impacts of heat stress were investigated.

In Exp. 2.1 to 2.4, the weight of the investigated plants was measured. The pot containing the plants' roots was positioned in a shallow dish allowing for collecting excess water from the pot. Plant, pot and dish were mounted on a balance that was used to measure the weight together with the soil and the water in the soil. The flexibility of the bag that sealed the gap between stem and stem duct allowed weighing the plant/soil system on-line. The balance had a nominal resolution of 1 g but variations of the chamber's slight overpressure (5–10 mbar) imposed noise in the range of 20–30 g limiting the precision of weight measurements.

For the first three species (Exp. 2.1, 2.2&2.3), the plants were put in the same chamber (1150 L) and contained with similar temperature and illumination conditions (Table 2-3). A diurnal light rhythm was applied to the plants. They were exposed to diurnal rhythm of 12 hours illumination, 10 hours darkness, 1 hour twilight in the morning and 1 hour twilight in the afternoon. They were fully irrigated and the measurements started after an adaptation period of 2–3 days. In order to observe the plants' behavior during recovery, all plants went through 4 drought periods.

In Exp. 2.4a and 2.4b, we tested two Holm oaks in similar ways as mentioned above, but in different chambers which had different light intensities and temperatures causing different duration and severity of drought. In Exp. 2.4c temperature dependency was checked under drought stress. The period of illumination was elongated to 15 h allowing measuring at the 3 different temperatures but at the same PAR for each day. When volumetric water content of the soil (θ) had fallen below $0.02 \text{ m}^3 \cdot \text{m}^{-3}$, the chamber temperature was not changed for two days to in order to follow the drought induced decrease of MT emissions without changes of temperature and PAR. In Exp. 2.4d, PAR dependency was checked during drought period. Every second day, PAR was changed systematically during periods of illumination. More detailed data on PAR and temperatures applied to the plants are given in Table 2-3.

The impacts of heat stress were tested in Exp. 2.5 with another Norway spruce. This experiment lasted for 43 days. The plant was irrigated several times to keep the proper soil moisture and avoid any impacts of drought. Firstly, the emissions rates with three temperatures of 18°C, 23°C and 27°C were tested. Afterwards, 3-h 45°C and 3-h 55°C heat stresses were applied to the plant on two tests days (details see Table 2-3). The changes of both *de-novo* and pool emissions were measured during and after the heat stress.

Table 2-3 Overview over experiments of BVOC emissions under drought and heat stress

Exp.	Species	Duration [day] /Rewatering	T [°C]	PAR [$\mu\text{mol m}^{-2} \text{s}^{-1}$]	Remark
2.1	Norway spruce	44/4	23	440	<i>De-novo</i> &pool/drought
2.2	Scots pine	30/4	25	400	<i>De-novo</i> &pool/drought
2.3	European beech	27/4	23	440	<i>De-novo</i> /drought
2.4	Holm oak a	41/1	25	600	<i>De-novo</i> /drought
	Holm oak b	40/1	22	440	<i>De-novo</i> /drought
	Holm oak c	29/1	15/20/25 ^a	500	T-dependency/drought
	Holm oak d	20/1	20	200/400/ 700 ^b	PAR-dependency /drought
2.5	Norway spruce	43/7	18/23/27 /35(heat) ^c	700	<i>De-novo</i> &pool/heat

^a Except for two days, the chamber temperature was set to 15°C during the night and kept at 15°C for the next 6–7 hours of the following illumination period (from ~3:00 to ~10:00 local time). Then the temperature was set to 20°C for four hours (from ~10:00 to ~14:00) and thereafter to 25°C (from ~14:00 to ~18:00). The exact timing of temperature settings was adapted to the start of GC runs.

^b Every second day PAR was set to $700 \mu\text{mol m}^{-2} \text{s}^{-1}$ for 6 hours (from ~4:00 to ~10:00 local time), thereafter to $400 \mu\text{mol m}^{-2} \text{s}^{-1}$ for 5 hours (from ~10:00 to ~15:00), and then to $200 \mu\text{mol m}^{-2} \text{s}^{-1}$ for 5 hours (from ~15:00 to ~20:00). From ~20:00 to 4:00 PAR was zero. During the other days, PAR was held constant at $400 \mu\text{mol m}^{-2} \text{s}^{-1}$ from 4:00 to 20:00.

^c Chamber temperature was set to 23°C (day 1–11), 18°C (day 12–16) and 27°C (day 17–37). On day 38 and day 40, 3-h 45°C and 3-h 55°C heat stresses were applied to the plant. The chamber temperature was reduced to 35°C after each heat stress.

2.3.3 Ozone losses by gas phase reaction

Gas phase reactions of O₃ with VOCs from plants were tested in the reaction chamber (1450 L) connected with one plant chamber (164 L). O₃ was directly added in one of the inlets of the reaction chamber, causing ~84 ppb O₃ during night when there were no emissions. A portion of outlet flow of the plant chamber, which contained MT mixture emitted by Holm oak was introduced in another inlet of the reaction chamber. Table 2-4 shows the details of this experiment.

Table 2-4 Overview over experiment of ozone losses by gas phase reactions.

Exp.	VOCs	Chamber [L]	T [°C]	PAR [$\mu\text{mol m}^{-2} \text{s}^{-1}$]	Remark
3.1	MT mixture of Holm oak	164*	25	700	Gas phase reaction
		1450	20	360	

*Plant chamber

The concentrations of O₃ and VOCs in the in- and outlet of the reaction chamber were measured with O₃ device and GC-MS. The gas phase reactions of O₃ with VOCs were calculated based on equation (2-4a). The measured and calculated ozone losses and VOCs losses by gas phase reaction were compared.

2.3.4 Ozone formation of single compound and BVOC mixtures

Photochemical O₃ formation was observed in 1450 L chamber. Similar as the experiment of gas phase reactions, O₃ was added in one of the inlets and VOCs, either from the diffusion source or the plant chamber, were added in another inlet together with NO_x.

The photochemical O₃ formation of single compound, α -pinene was firstly tested. This compound was from the diffusion source. Based on the O₃ isopleth plot (Fig. 2-5), one vertical cut (Exp. 4.1) and one horizontal cut (Exp. 4.2) of the plot were tested. For the vertical cut, 11 events of O₃ formation were investigated with constant VOC concentration but varying NO_x concentrations and for the horizontal cut, 10 events were investigated with constant NO_x concentration but varying VOC concentrations.

In Exp. 4.1, the initial α -pinene concentrations were 18.9 ± 0.2 ppb and the initial NO_x concentrations varied between 7.5 and 137.8 ppb. NO_x were added only on event days. In each event, after 3–4 hours of adding NO_x, when the NO_x, VOC, and O₃ concentrations as well as RH were constant, TUV lamp was switched on. O₃ formation was driven by increasing OH produced

from O_3 photolysis. The experiment was continued until NO_x and O_3 reached steady state again. O_3 formation rate was calculated. In Exp. 4.2, α -pinene mixing ratios varied between 0 and 58.9 ppb by adjusting the inlet flow from the diffusion source. On the event days, the same amount of NO_x 64.7 ± 1.0 ppb was added in the morning. The process was similar as Exp. 4.1. Between every two events, there was at least one day as blank day. On the blank days, no NO_x was added. $J(O^1D)$ and the background of O_3 were checked.

One test of $J(O^1D)$ was performed after all four series of O_3 formation experiments. 1,8-cineole was used, instead of α -pinene or BVOC mixtures from plants, since it only reacts with OH but not with O_3 ($k_{O_3+1,8\text{-cineole}}$ is very low, $1 \times 10^{-19} \text{ cm}^3 \text{ s}^{-1}$). The aim was to scavenge OH and avoid the impacts of the reaction of O_3 with BVOCs or with OH on the calculation of $J(O^1D)$.

After testing α -pinene, the reaction chamber was coupled with the plant chamber and the VOC source was switched to the natural sources, Holm oak. 164 L chamber was used as the plant chamber. The amount of VOCs introduced into the reaction chamber was varied by varying PAR and inlet flows. In total, three different concentrations of VOC were tested in Exp. 4.3, in the range of 1.7 to 13.6 ppb. O_3 formation from BVOC mixture was measured under VOC-limited conditions. Table 2-5 shows an overview of these experiments.

Table 2-5 Overview over experiments of photochemical ozone formation

Exp.	No. of events	NO_x [ppb]	VOC		T [°C]	PAR [$\mu\text{mol m}^{-2} \text{ s}^{-1}$]	Remark
			Compound	[ppb]			
4.1	11	7.5–137.8	α -pinene	18.9 ± 0.2	15	60	NO_x limited
4.2	10	64.7 ± 1.0	α -pinene	0–58.9	15	60	VOC limited
4.3	5	72.5–213.8	MT mixture from Holm oak	1.7–13.6	20	270	VOC limited

2.3.5 Ozone balance

As the last part of this study, one experiment including all major processes was carried out by combining the plant chamber (164 L) and the reaction chamber (1450 L). One Holm oak was used. The experiment lasted for 6 weeks including one severe drought period, which started on day 28. T was set to 20°C for first 11 days and 25°C for day 26–28, and 30°C for the rest days. The impacts of T on the ratio of O_3 uptake/BVOC emission were observed (Exp. 5.1).

In the plant chamber, ~ 45 ppb O_3 was added in the first 9 days, thereafter O_3 was increased to ~ 85 ppb for the rest experiment. We measured the BVOC emissions flux and O_3 uptake rate with full illumination (6 lamps) for the whole period except 15 days in between, when we changed the light program during the days to vary the stomatal opening and to test the ratio of O_3 uptake/BVOC emission with different PAR (Exp. 5.2).

In Exp. 5.3, the O_3 uptake rates and BVOC emission rates were collected during the whole drought stress with the same T (30°C) and PAR ($600 \mu\text{mol m}^{-2} \text{ s}^{-1}$).

During this period, a part of the outlet air of the plant chamber including BVOC emissions and O₃ was introduced in the reaction chamber. In this chamber, longer residence time (~50 min) enables the measurement of gas phase reactions. The O₃ loss by the reactions with VOCs was measured when no NO₂ was added. On four test days (Exp. 5.4) ~76 ppb NO₂ was added in the reaction chamber. Photochemical O₃ formation was measured in this chamber together with the O₃ uptake and BVOC emissions in the plant chamber, at either different T or soil moisture conditions. The change of total O₃ balance of this system was studied based on these 4 cases.

Table 2-6 Overview over experiments of ozone balance.

Exp.	T [°C]	PAR [μmol m ⁻² s ⁻¹]	Drought	Remark
5.1	20/25/30	600	No	O ₃ uptake/BVOC emission ratio /temperature
5.2	30	200/400/600	No	O ₃ uptake/BVOC emission ratio /PAR
5.3	30	600	Mild to severe	O ₃ uptake/BVOC emission ratio /drought
5.4				
case 1	30	600	No	Ozone balance/standard
case 2	20	600	No	Ozone balance/lower temperature
case 3	30	600	Mild	Ozone balance/mild drought
case 4	30	600	Severe	Ozone balance/severe drought

Compared to case 1 in Exp. 5.4, case 2 had lower T = 20°C; in case 3 and case 4, different severities of drought stress were applied. Case 3 was performed under mild drought stress when the transpiration started to decrease. In case 4, the plant was under severe drought stress with quite low transpiration.

In case 4, the emissions from the plant were too low to be measured if O₃ was added to the plant chamber. Therefore O₃ was added directly in the reaction chamber with the same level as the O₃ concentration added to the reaction chamber by the outflow from the plant chamber in the other cases. The O₃ uptake rate on this day was estimated with the interpolation of the O₃ uptake rates measured before and after the test day when O₃ was added in the plant chamber.

The change of total O₃ balance of this system was studied based on these 4 case studies. Net O₃ flux, $\Phi(\text{O}_3)_{\text{net}}$, was calculated by combining O₃ uptake flux, $\Phi(\text{O}_3)_{\text{uptake}}$ and O₃ production flux

$$\Phi(\text{O}_3)_{\text{net}} = -\Phi(\text{O}_3)_{\text{uptake}} + \Phi(\text{VOC}) \times \frac{P(\text{O}_3)}{L(\text{VOC})}. \quad (2-17)$$

3 Results

3.1 Ozone losses on leaf surfaces

Dry deposition of O_3 by uptake through leaf surfaces was measured in the plant chamber. Total O_3 loss in the plant chamber was measured by comparing the O_3 concentrations in the in- and outlet. Stomatal uptake of O_3 was calculated based on stomatal conductivity of water vapor and compared to the total O_3 losses in the plant chamber. Non-stomatal O_3 loss in the plant chamber included losses on the surface of leaves (cuticular uptake) and gas phase losses, which was calculated by Equation (2-4). An Aleppo pine and a Holm oak were used and the O_3 losses caused by the plants were measured under well-watered and water-stressed conditions.

3.1.1 Temporal change of ozone losses under drought stress

The Aleppo pine went through two drought periods. O_3 was applied for the 6 days when the plant was irrigated and recovered from the first drought period and went through the second drought period. Fig. 3-1 shows the temporal change of transpiration rate and O_3 uptake rate of this plant.

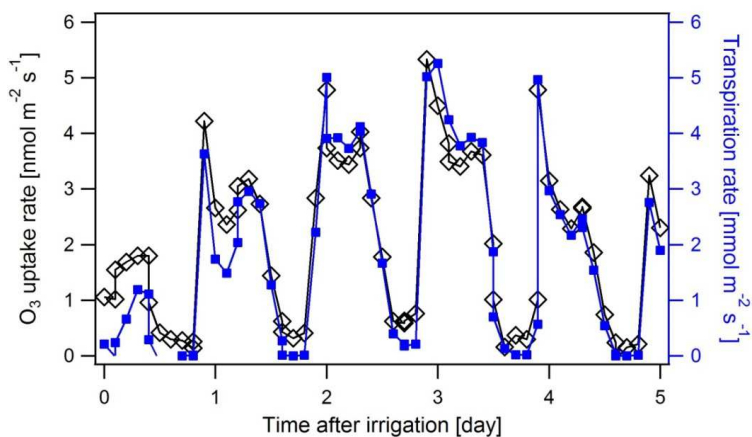


Fig. 3-1 Ozone uptake rate (black open diamonds) and transpiration rate (blue squares) of an Aleppo pine during the recovery (after the first drought) and second drought periods .

The diurnal variations of O₃ uptake rate and transpiration rate measured in the plant chamber showed a quite similar temporal shape: they were high during illumination and quite low without illumination. During daytime, morning peaks of both O₃ uptake and transpiration were found. They decreased afterwards and showed slight peaks in the afternoon again. During night, transpiration rates were almost zero, which shows the stomata were nearly closed, while O₃ uptake rates were also quite low, but somewhat above zero during periods without severe drought. This implies that there were some O₃ losses which were not related to stomatal opening.

The trends of O₃ uptake rate and transpiration rate during the recovery and the drought periods were similar. After irrigation, the plant reacted with higher transpiration and higher O₃ uptake. Both of them increased for about 3 days and decreased thereafter. These two processes were affected by soil water status and related to each other even when the plant was under drought stress.

3.1.2 Stomatal and non-stomatal ozone losses

In order to separate stomatal and non-stomatal uptake of O₃, the measured total conductivity of O₃ (g_{O_3}) was plotted as a function of the calculated stomatal conductivity of O₃ ($g_{O_3}^S$) (Fig. 3-2, black open diamonds). The data was from day 4 in Fig. 3-1, when the plant was in the second drought period.

A clear relationship ($R^2 = 0.97$) was found between the measured total conductivity and the calculated stomatal conductivity of O₃. The intercept of 0.001 indicates that when stomata were closed during the night, the O₃ losses were negligible, while the slope of 1.5 indicates around 1/3 of total O₃ loss were non-stomatal but related to stomatal aperture.

Since the Aleppo pine emitted high amount of MT and SQT, O₃ losses by gas phase reaction had to be considered. The main compounds were α -pinene, trans- β -ocimene and β -caryophyllene, which contributed more than 85% of total emissions.

For cases, when the concentrations of O₃ and VOCs were both measurable, the gas phase reaction can be calculated based on equation (2-4). In this case, since β -caryophyllene reacts fast with O₃ ($k_{O_3} = 1.16 \times 10^{-14} \text{ cm}^3 \text{ molecule}^{-1} \text{ s}^{-1}$), its concentrations at chamber outlet were below the detection limit. The gas phase losses of O₃ were calculated based on the results obtained from the experiment of gas phase reaction (Exp. 3.1, see section 3.3) where the O₃ losses in gas phase reactions were measured to be ~50% of the BVOC losses. The O₃ losses by gas phase reactions in relation to BVOC emissions was then estimated to $0.5 \times \Phi(\text{BVOC})$. With the correction, the slope of blue open diamonds reduced from 1.54 to 1.12, i.e., gas phase reactions explained large parts of excess non-stomatal O₃ losses.

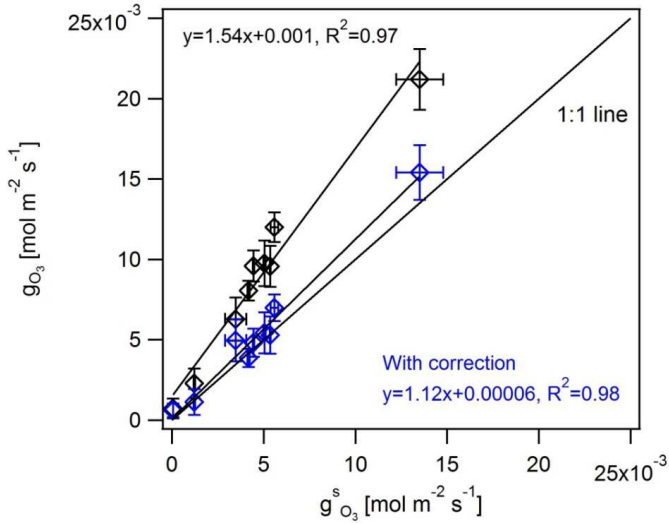


Fig. 3-2 The measured total conductivity of O_3 (g_{O_3}) versus the calculated stomatal conductivity to O_3 ($g_{O_3}^s$) of an Aleppo pine. Black and blue open diamonds represent the data without and with the consideration of gas phase reaction.

In the same way, the total conductivity of O_3 corrected for the gas phase losses and the stomatal conductivity of O_3 were checked for the rest of the days. The intercepts of the linear fittings were negligible and the averaged slopes were 1.06 ± 0.06 , close to 1. The drought stress in this experiment was not that severe, the lowest daily transpiration rate was $\sim 1/4$ compared to that at well-watered condition. Such change of soil water status didn't affect the relationship between the measured total stomatal conductivity (g_{O_3}) and the calculated stomatal conductivity ($g_{O_3}^s$). During both recovery and drought periods, the stomatal uptake contributed most of the O_3 losses on leaf surface and the non-stomatal O_3 loss was mainly explained by the gas phase reaction of VOCs with O_3 .

3.1.3 Impacts of severe drought stress on ozone losses

The experiment with the Holm oak focused on the impacts of severe drought stress on O_3 losses. The plant experienced a severe drought period followed by a recovery period. O_3 losses were measured on one day when the plant was well-watered and another day when it was under severe drought stress. In Fig. 3-3, the measured total conductivity of O_3 and the calculated stomatal conductivity of O_3 were compared under these two conditions.

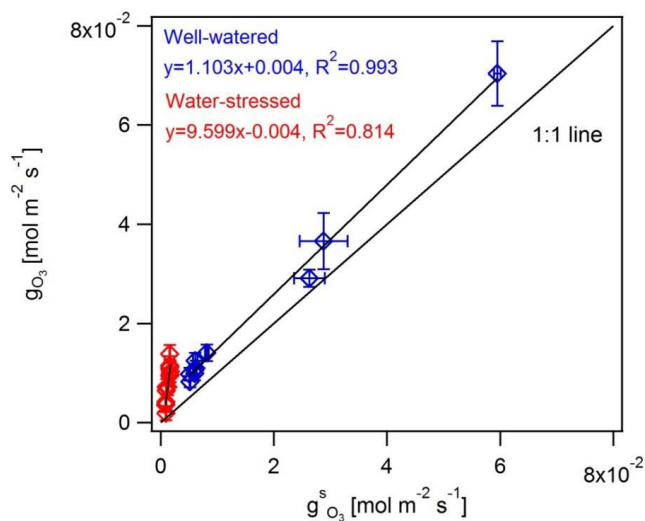


Fig. 3-3 The measured total conductivity of O_3 (g_{O_3}) versus the calculated stomatal conductivity of O_3 ($g_{O_3}^s$) of a Holm oak under well-watered (blue open diamonds) and water-stressed conditions (red open diamonds).

The measured total conductivity of O_3 was corrected by gas phase reaction based on equation (2-4). When the plant was well watered, the points (blue open diamonds) were close to 1:1 line and the slope was 1.1. But when the plant was exposed to severe drought stress, transpiration rates reduced a lot, from 1.5×10^{-3} to 8×10^{-5} $\text{mol m}^{-2} \text{s}^{-1}$, accompanied by a reduction of O_3 uptake rates. The measured total conductivity of O_3 and the calculated stomatal conductivity of O_3 (Fig. 3-3, red open diamonds) were in the low range. All of the data points were above 1:1 line with a high slope near to 10.

3.1.4 Summary

In all cases, transpiration and O_3 uptake showed similar temporal behavior regardless of the soil water status. By plotting the measured total conductivities of O_3 versus the calculated stomatal conductivities to O_3 , good linear relationships were found, indicating that the total O_3 losses were mainly controlled by stomatal opening. For strong VOC emitters, like Aleppo pine and Holm oak, gas phase O_3 losses were significant. After subtracting gas phase losses, nearly all O_3 losses could be explained by stomatal uptake.

Under severe drought stress, both transpiration rates and O_3 uptake rates decreased to a very low level. But, the relationship between the measured total conductivity of O_3 and the calculated stomatal conductivity of O_3 was different. Higher slopes were found compared to that under well-watered conditions meaning that more O_3 was lost than that could be calculated from stomatal conductivity to O_3 .

3.2 BVOC emissions under drought and heat stress

3.2.1 Impacts of drought stress

3.2.1.1 Emission patterns

All plants tested for studying the impacts of drought stress emitted MT. The emissions of isoprene and SQT were quite low if detectable at all. Neither emissions of phenolic volatiles originating downstream of the shikimate pathway nor green leaf volatiles were observed, which indicated the plants didn't substantially suffer from other unintended stresses than drought.

As deciduous species, European beech and Holm oak exhibited only *de-novo* emissions. Sabinene was the dominant emission from the European beech contributing nearly 1/3 of the total emission. Other compounds were γ -terpinene, α -terpinene, β -phellandrene and α -terpinolene. The main MT emissions of the Holm oak were α -pinene, limonene, β -pinene, sabinene and myrcene.

High correlation coefficients ($R^2 > 0.95$) were found for cross-correlations of the dominant emissions. Fig. 3-4 shows limonene, α -pinene and β -pinene emissions from a Holm oak (Exp. 2.4b) as a function of the total emissions. Though the absolute values of both single and total emissions decreased during drought period, the high coefficients ($R^2 > 0.95$) indicated that the pattern of emissions didn't change. This behavior allowed using the emission of a single compound to represent the total emissions.

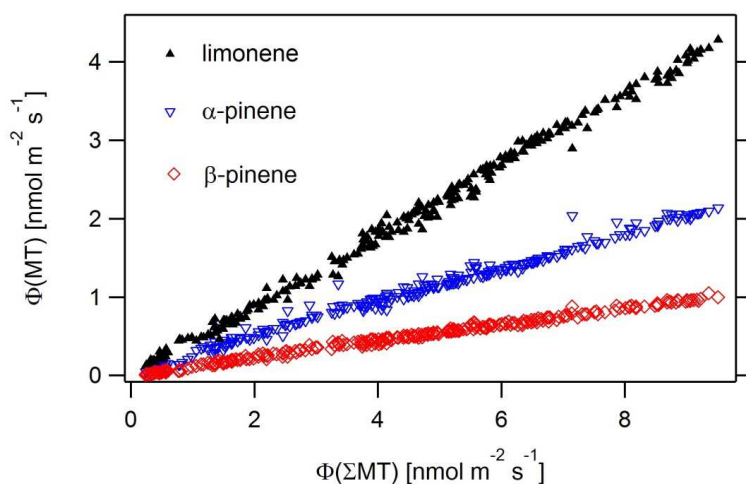


Fig. 3-4 Correlation plot of emission rates measured for a Holm oak, Exp. 2.4b. Only data measured at a PAR of $440 \mu\text{mol m}^{-2}\text{s}^{-1}$ and a chamber temperature of 22°C is plotted.

The main emissions from the two conifers, Norway spruce and Scots pine, were pool emissions, comprised α -pinene and Δ -3-carene. The former was used to represent pool emissions. Besides these pool emissions, both conifers also emitted 1,8-cineole which is a *de-novo* emission (Tarvainen et al.,

2005; Kleist et al., 2012). In order to confirm this, both individuals were exposed to $^{13}\text{CO}_2$ for three hours. After 3-h, strongly labeled 1,8-cineole emission was detected, which indicated 1,8-cineole was a *de-novo* emission with negligible contribution of pool storage. Thus 1,8-cineole was used to represent *de-novo* emissions of these two conifers and α -pinene was used as representative for pool emissions. Both types of emissions responded differently to drought.

3.2.1.2 Impacts of drought on *de-novo* emissions

Temporal changes of *de-novo* emissions under drought stress

Fig. 3-5 shows the temporal shape of sabinene emissions, net assimilation and volumetric water content of the soil, θ , as measured for a European beech seedling over a period of about three weeks (Exp. 2.3). This experiment started with full irrigation, θ was near to the field capacity ($\sim 0.4 \text{ m}^3 \text{ m}^{-3}$). On days 3 and 4, θ fell below $0.2 \text{ m}^3 \text{ m}^{-3}$, and net assimilation decreased by almost half, while sabinene emissions were even higher than that without drought stress. On day 5, θ was lower than $0.1 \text{ m}^3 \text{ m}^{-3}$ and the emissions sharply decreased with decreasing θ . It is obvious that both net photosynthesis and the emission of sabinene were related to the θ , but the changes of net assimilation appeared earlier than that of the emissions.

The plant was irrigated on day 5 when θ dropped to $\sim 0.1 \text{ m}^3 \text{ m}^{-3}$. After another 3 days, both net assimilation and sabinene emission recovered. As θ decreased again, net assimilation and sabinene emission dropped and followed the same trends as that in the first drought period. During severe drought from day 10 to day 16, both net assimilation and sabinene emissions decreased day by day, to almost zero. After re-watering, the emissions increased again but with a longer recovery time. For other species, similar temporal behavior of transpiration, net assimilation and the emissions was found (Appendix, Fig. A1&A2).

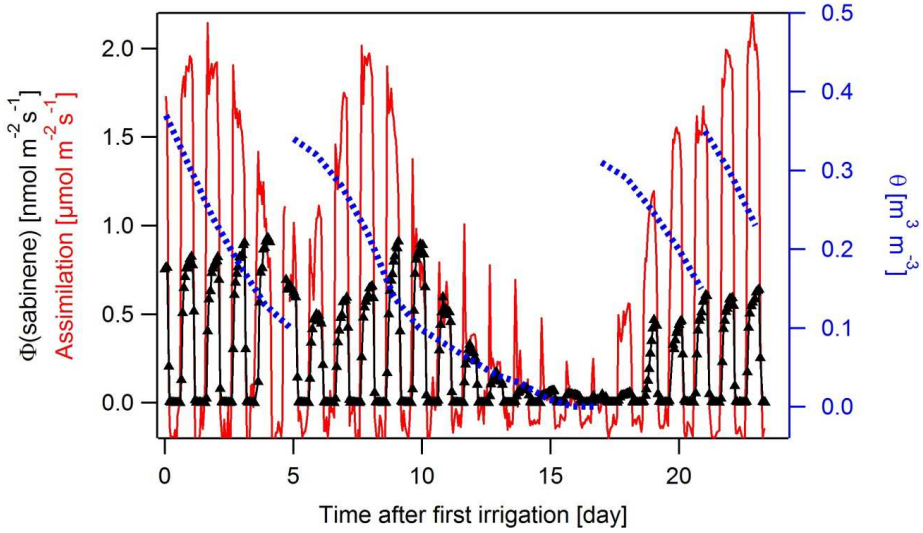


Fig. 3-5 Long term time series of sabinene emissions from a European beech seedling (black triangles, left y scale), assimilation (multiplied by -1, red line, left y scale) and volumetric water content of the soil θ (blue dashed line, right y scale).

Sabinene emissions and net assimilation were plotted again in dependence on θ in Fig. 3-6. The data includes one mild drought (day 0 to day 5, in Fig. 3-5) and one severe drought (day 6 and 17, in Fig. 3-5). During the mild drought period, net assimilation (red diamonds) dropped when θ falling below $0.2 \text{ m}^3 \text{ m}^{-3}$, while the emission (black diamonds) increased slightly when θ was between $0.2 \text{ m}^3 \text{ m}^{-3}$ and $0.1 \text{ m}^3 \text{ m}^{-3}$ and decreased when θ dropped further and became lower than $0.1 \text{ m}^3 \text{ m}^{-3}$. On day 5, the plant was irrigated and θ was high again. Neither net assimilation nor the emissions recovered immediately. Both took about 3-4 days to reach the level before drought stress. During the second drought period, net assimilation (red open circles) started to decrease at $\theta = \sim 0.2 \text{ m}^3 \text{ m}^{-3}$ and sabinene emission (black open circles) decreased with θ falling below $0.1 \text{ m}^3 \text{ m}^{-3}$. It is clear that their responses to drought were the same as that in the first drought period.

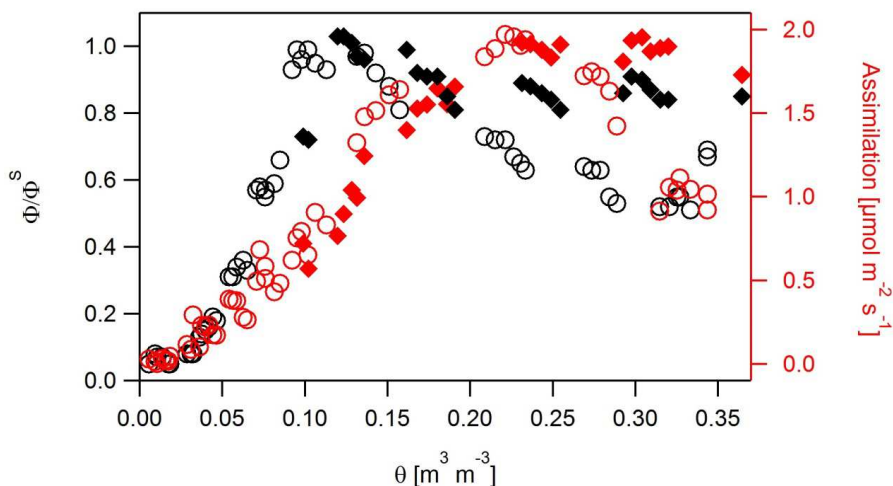


Fig. 3-6 Normalized sabinene emissions from a European beech (black symbols, left scale) and rates of net photosynthesis (red symbols, right scale, multiplied by -1) in dependence on θ . Closed diamonds represent data taken during a first drought period that was stopped when θ had fallen to $0.1 \text{ m}^3 \text{ m}^{-3}$, open circles represent data taken during the following period of recovery until severe drought. Only data taken at a chamber temperature of 23°C and a PAR of $440 \text{ } \mu\text{mol m}^{-2} \text{ s}^{-1}$ are considered.

Comparison of fast and slow progressions of drought

In the following two experiments Exp. 2.4a and Exp. 2.4b, the behaviors of two individual Holm oaks under drought stress were compared. Different chamber conditions caused different transpiration rates and evaporation rates of water from the soil. Fig. 3-7 shows the normalized α -pinene emissions of two Holm oaks in dependence on time. In Exp. 2.4a, higher temperature and PAR had caused higher transpiration rate and net assimilation. The normalized α -pinene emission started to decrease on day 10 and dropped from $\sim 0.1 \text{ m}^3 \text{ m}^{-3}$ to $\sim 0.03 \text{ m}^3 \text{ m}^{-3}$ within 8 days. In Exp. 2.4b, with lower temperature and PAR, the decreasing period lasted for about 18 days, much longer than in Exp. 2.4a.

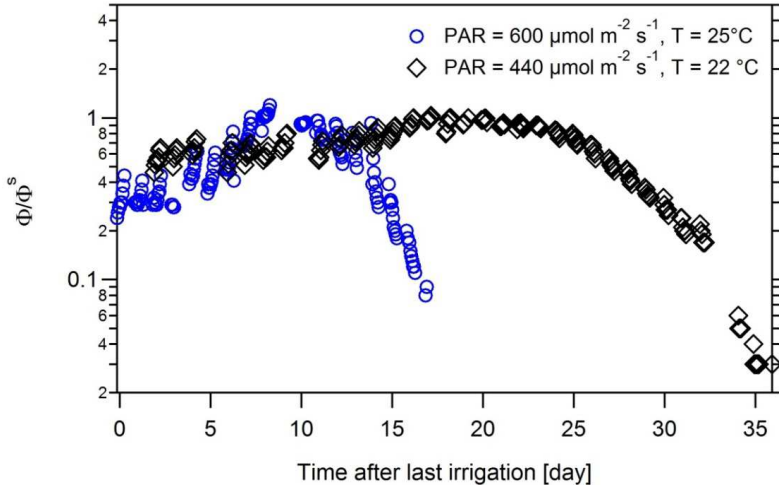


Fig. 3-7 Temporal shape of normalized α -pinene emissions from two individuals of Holm oak, experiments Exp. 2.4a and Exp. 2.4b. Blue circles show the data obtained at higher PAR and at higher chamber temperature. Black squares show the data obtained for the plant investigated at lower temperature and PAR. Only data taken during periods of full illumination are shown. For better comparison the emissions were separately normalized to the emission rates measured for the respective individual at $\theta = \sim 0.12 \text{ m}^3 \text{ m}^{-3}$.

Fig. 3-8 plots the same normalized α -pinene emissions but in dependence on θ . Although, the MT emissions decreased on different time scales in the two experiments (see Fig. 3-7).

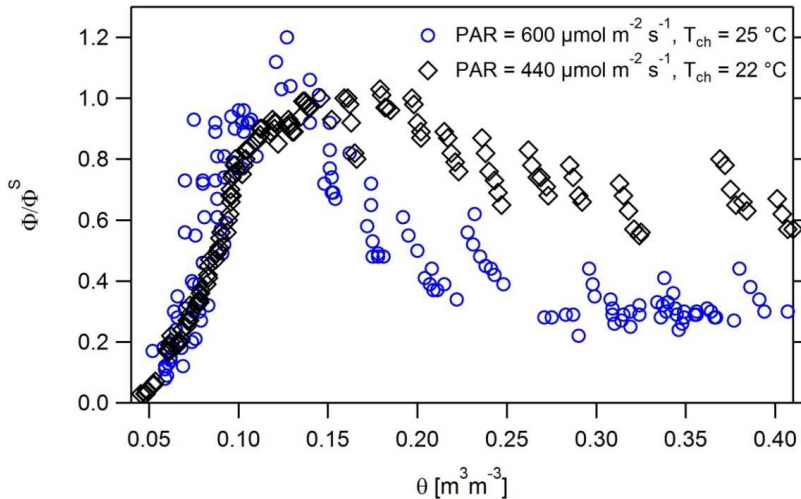


Fig. 3-8 Normalized α -pinene emissions from two individuals of Holm oak in dependence of θ . Blue circles show the data measured for the plant investigated at higher PAR and higher chamber temperature, black squares show data taken for the plant investigated at lower PAR and lower temperature.

It is clear that the same dependence of α -pinene emissions on θ was found in these two experiments. Similar as for beech, increase of MT emissions were observed when θ declined from $\sim 0.4 \text{ m}^3 \text{ m}^{-3}$ to $\sim 0.15 \text{ m}^3 \text{ m}^{-3}$. The decay of α -pinene emissions started with $\theta = \sim 0.12 \text{ m}^3 \text{ m}^{-3}$, and ended with $\theta = \sim 0.05 \text{ m}^3 \text{ m}^{-3}$. When θ was below $0.05 \text{ m}^3 \text{ m}^{-3}$, the emissions were near to zero. This experiment proved that the decay of the emissions with decreasing θ was not affected by temperature, PAR and the length of drought.

Parameterization of *de-novo* MT emissions

Similar behaviors of *de-novo* emissions from European beech (Exp. 2.3, Fig. 3-6) and two Holm oaks (Exp. 2.4a & 2.4b, Fig. 3-8) were found under drought stress, as well as in other experiments with Holm oaks (Exp. 2.4c and 2.4d), Norway spruce (Exp. 2.1, Appendix, Fig. A3) and Scots pine (Exp. 2.2, Appendix, Fig. A4). In order to parameterize of *de-novo* MT emissions, we defined three regimes of θ

$$\gamma_{SM} = 1 \quad \theta > \theta_1 \quad (3-1a)$$

$$\gamma_{SM} = \frac{\theta - \theta_0}{\Delta\theta_1} \quad \theta_0 < \theta < \theta_1 \quad (3-1b)$$

$$\gamma_{SM} = 0 \quad \theta < \theta_0 \quad (3-1c)$$

where γ_{SM} describes variations of emissions due to soil moisture θ . Above the threshold θ_1 , emissions are not directly affected by soil moisture, i.e. $\gamma_{SM} = 1$. Below θ_1 , emissions linearly decrease with decreasing θ until θ_0 , $\gamma_{SM} = (\theta - \theta_0) / \Delta\theta_1$, $\Delta\theta_1 = \theta_1 - \theta_0$. Below θ_0 , the extrapolated emissions became zero, $\gamma_{SM} = 0$. This formalism is identical to the emission activity factor of soil moisture in the Model of Emissions of Gases and Aerosols from Nature (MEGAN), to simulate the impacts of drought on isoprene emissions.

The emission rates were normalized to their maxima measured at θ near to θ_1 (termed as Φ^{th}) for each experiment and the relationships of the emissions rates and θ were fitted with linear approximation. Table 3-1 summarizes the data from the linear fits to the normalized *de-novo* emissions of the emission rates versus θ . For Exp. 2.4c, the dependency of α -pinene emission rates on θ were analyzed for chamber temperatures of 15, 20 and 25°C, respectively. Similarly in Exp. 2.4d, the θ dependencies of α -pinene emission rates were also calculated for PAR of 700, 400 and 200 $\mu\text{mol m}^{-2} \text{ s}^{-1}$, respectively. In Exp. 2.1 and 2.2, only fluxes of 1,8-cineole emissions were listed, since most of the emissions of two conifers were pool emission.

Table 3-1 Data from fits of emission rates versus θ . NS = Norway spruce, SP = Scots pine, EB = European beech, HO = Holm oak. Data behind the slash give chamber temperatures in °C and PAR in $\mu\text{mol m}^{-2} \text{s}^{-1}$, respectively. $\Phi^{\text{th}}(\text{MT})$ and $\Phi^{\text{th}}(\Sigma\text{MT})$ are the emission rates measured for the MT listed in the third column and for the sum of all MT emissions, respectively as measured near to θ_1 . θ_1 is the volumetric water content of the soil when emissions start to decrease ($\theta_1 = \Delta\theta_1 + \theta_0$). θ_0 = intercept of linear regression analysis when MT emissions are extrapolated to be zero. $\Delta\theta_1$ is the range of θ in which the emissions drop from their maximum to zero.

Exp.	Species	MT	$\Phi^{\text{th}}(\text{MT})$ [nmol m ⁻² s ⁻¹]	$\Phi^{\text{th}}(\Sigma\text{MT})$ [nmol m ⁻² s ⁻¹]	$\Delta\theta_1$ [m ³ m ⁻³]	θ_0 [m ³ m ⁻³]
2.1	NS	1,8-cineole	$(3.3 \pm 1.1) \cdot 10^{-4}$	/	0.19 ± 0.01	0.02 ± 0.007
2.2	SP	1,8-cineole	0.88 ± 0.15	/	0.068 ± 0.005	0.041 ± 0.004
2.3	EB	Sabinene	0.9 ± 0.03	2.6 ± 0.04	0.09 ± 0.004	0.03 ± 0.002
2.4a	HO1	α -pinene	4.9 ± 0.45	10.2 ± 0.47	0.044 ± 0.004	0.058 ± 0.002
2.4b	HO2	α -pinene	2.1 ± 0.05	9.2 ± 0.25	0.063 ± 0.003	0.071 ± 0.002
2.4c	HO3 / 15	α -pinene	3.5 ± 0.08	7.9 ± 0.74	0.055 ± 0.01	-0.006 ± 0.007
		α -pinene	4.8 ± 0.22	11.7 ± 0.6	0.058 ± 0.008	-0.01 ± 0.004
		α -pinene	6.5 ± 0.34	15.9 ± 0.8	0.079 ± 0.016	-0.021 ± 0.008
2.4d	HO4 / 700	α -pinene	1.6 ± 0.18	6.7 ± 0.8	0.065 ± 0.008	0.016 ± 0.006
		α -pinene	0.7 ± 0.1	2.6 ± 0.4	0.045 ± 0.015	0.018 ± 0.012
		α -pinene	0.3 ± 0.04	1.2 ± 0.17	0.044 ± 0.015	0.019 ± 0.012

The different species had different emission fluxes and patterns, but all of them showed θ_0 lower than $0.07 \text{ m}^3 \text{ m}^{-3}$, and $\Delta\theta_1$ in the range of 0.04 to $0.09 \text{ m}^3 \text{ m}^{-3}$. An average value of $\Delta\theta_1 = 0.08 \pm 0.05 \text{ m}^3 \text{ m}^{-3}$ was obtained from all these experiments.

Interdependence of the impacts of temperature, PAR and drought

In the Exp. 2.3, the temperature dependency of the emissions from Holm oak was tested with different severities of drought. On test days, we changed temperature and measured the changes of the emission rates. The temperature dependences of the emissions on individual test days were calculated.

Meanwhile, θ changed permanently. The decay was quite fast during the day time because of the loss by transpiration and slower during the night time, and affected also the emission rates. For the periods when the plant was well-watered and the emissions were not affected by θ , the changes of emissions on the test days were assumed mostly caused by the change of temperature. For the period, when the plant was under drought stress and the change of θ caused decrease of emissions during the day ($\theta < 0.1 \text{ m}^3 \text{ m}^{-3}$), the emissions were corrected in consideration of the parallel impacts of the decreasing θ . We assume that the temporal decay on these test days was similar as on the two chosen days (day 14 and day 15). On these two days ($0.04 < \theta < 0.07 \text{ m}^3 \text{ m}^{-3}$), temperature was kept constant and the changes of emissions, which were only caused by drought, were measured. An exponential function was fitted to the temporal decay yielding a decay rate of $0.04 \pm 0.002 \text{ h}^{-1}$ ($R^2 = 0.85$). For the data from test days, the correction factor was set to 1 for the time when the chamber

had reached steady state conditions after twilight in the morning (chamber temperature was constant and the emissions were relative constant). Correction factors were then calculated for each time with the decay rate.

In Fig. 3-9, the temperature coefficient β of α -pinene emission was plotted in dependence of θ . β was determined by linear regression analysis of $\ln(\Phi)$ versus leaf temperature. Closed black circles represent the data when θ was higher than $0.1 \text{ m}^3 \text{ m}^{-3}$ and the oak was stress-free. The average value from these data points was $0.12 \pm 0.007 \text{ K}^{-1}$. Red squares represent the data obtained when θ was lower than $0.1 \text{ m}^3 \text{ m}^{-3}$ and the plant was under drought stress. Although these points had high variability, the average value was $0.13 \pm 0.024 \text{ K}^{-1}$, didn't show significant difference compared to the data without drought stress.

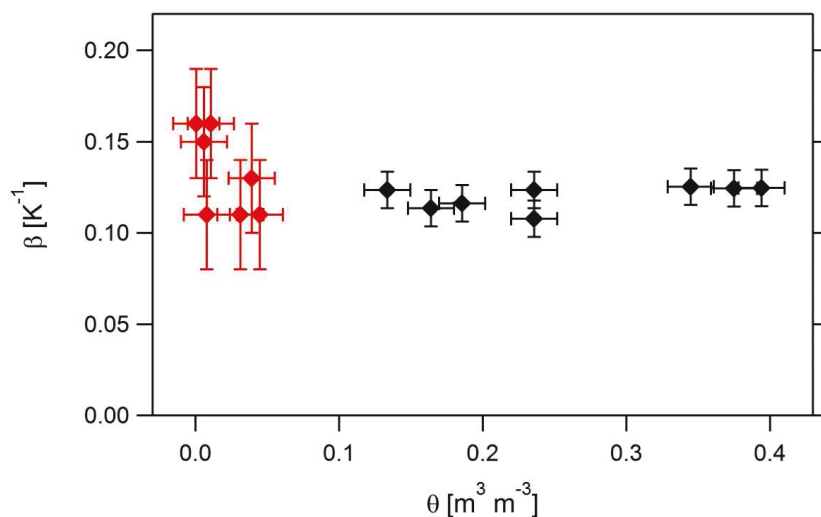


Fig. 3-9 Temperature coefficient β for α -pinene emissions from a Holm oak (Exp. 2.4c) at different soil moisture. Black diamonds represent the data obtained without impacts of drought on MT emissions. Red diamonds represent the data obtained for $\theta < 0.06 \text{ m}^3 \text{ m}^{-3}$ after correcting for the drought induced decrease of emissions. Errors in β were about $\pm 0.01 \text{ K}^{-1}$ for the data obtained without drought stress. For the data obtained during drought stress the errors from the normalization procedure had to be taken into account and errors in β are estimated to $\pm 0.03 \text{ K}^{-1}$. Error in θ is estimated to $\pm 0.016 \text{ m}^3 \text{ m}^{-3}$.

Similar as for the temperature dependence, the relationship of the normalized α -pinene emission and PAR with different severities of drought was plotted in Fig. 3-10. In this experiment (Exp. 2.4d), the absolute emission rates measured at $700 \mu\text{mol m}^{-2} \text{ s}^{-1}$ dropped by a factor of ~ 40 with θ falling from $0.055 \text{ m}^3 \text{ m}^{-3}$ to $0.018 \text{ m}^3 \text{ m}^{-3}$. Blue diamonds, black triangles, and red triangles represent the data from 3 test days with $\theta \sim 0.055 \text{ m}^3 \text{ m}^{-3}$, $\sim 0.043 \text{ m}^3 \text{ m}^{-3}$, and $\sim 0.018 \text{ m}^3 \text{ m}^{-3}$. For every test day, we got the emission rates with PAR = 0, 200, 400 and $700 \mu\text{mol m}^{-2} \text{ s}^{-1}$.

For correcting the changes of emissions caused by drought, the same method was used as in the previous section. The temporal decay was measured one day before the test day with constant temperature and PAR ($400 \mu\text{mol m}^{-2} \text{ s}^{-1}$). It was assumed that the temporal decay of emissions on the

test day was similar as the day before. An exponential function fitting the decay on the day before was used to correct the emissions on test days.

After correction, the data were normalized using the emission rates with $\text{PAR} = 700 \mu\text{mol m}^{-2} \text{s}^{-1}$ as the reference. Similar relationships of the normalized emissions and PAR were found with different soil water status. The interdependency of PAR and soil moisture was also negligible.

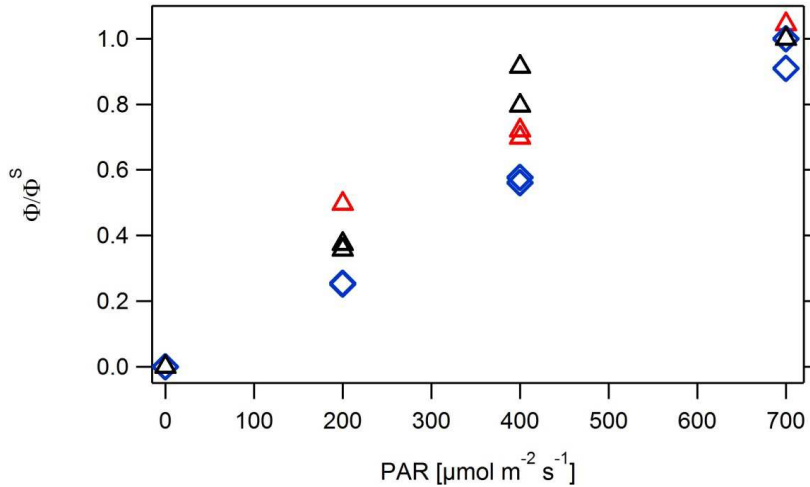


Fig. 3-10 Normalized emission rates corrected for the temporal decrease due to the progressing drought and normalized to the emission rates measured the respective day at $\text{PAR} = 700 \mu\text{mol m}^{-2} \text{s}^{-1}$ as function of PAR. Blue diamonds represent data taken at $\theta = \sim 0.055 \text{ m}^3 \text{ m}^{-3}$, black triangles show data taken at $\theta = \sim 0.043 \text{ m}^3 \text{ m}^{-3}$ and red triangles show the data at $\theta = \sim 0.018 \text{ m}^3 \text{ m}^{-3}$.

3.2.1.3 Impacts of drought on pool emissions

The experiments with Scots pine and Norway spruce included four drought periods each and at least one of them was severe with $\theta < 0.01 \text{ m}^3 \text{ m}^{-3}$. Two drought periods from each experiment were chosen to show the behaviors of pool emissions under drought stress and during recovery periods. In both experiments, α -pinene emissions, as a representative of pool emissions from two species were plotted. The behavior of *de-novo* emissions (e.g. 1,8-cineole) in dependence of θ of these two conifers see Appendix Fig. A3 and Fig. A4 or supplement to Wu et al. (2015). The temporal changes of transpiration and net assimilation under drought stress were also similar (Appendix Fig. A2).

The Norway spruce was irrigated twice during the 20 days shown in Fig. 3-11. The trend of θ was similar during the two drought periods: after irrigation, θ approached to the field capacity ($\sim 0.4 \text{ m}^3 \text{ m}^{-3}$), and took 6-8 days to fall to the low range ($\theta < 0.1 \text{ m}^3 \text{ m}^{-3}$). The decrease of α -pinene emission was not that significant and was only found when $\theta < 0.1 \text{ m}^3 \text{ m}^{-3}$. On day 9 (the last day of the first drought period), the average day time emission rate was $4.8 \times 10^{-2} \text{ nmol m}^{-2} \text{ s}^{-1}$, 34 % lower compared to the average emission rate from day 2 to 5, $7.3 \times 10^{-2} \text{ nmol m}^{-2} \text{ s}^{-1}$. On day 10, the plant was irrigated. About 3 hours after re-watering, a huge peak of the emission appeared. After the peak emission, both daytime and nighttime emission remained still high, and lasted for 5–6 days. In the last two days, when θ fell below $0.1 \text{ m}^3 \text{ m}^{-3}$ again, the emission decreased below $6 \times 10^{-2} \text{ nmol m}^{-2} \text{ s}^{-1}$.

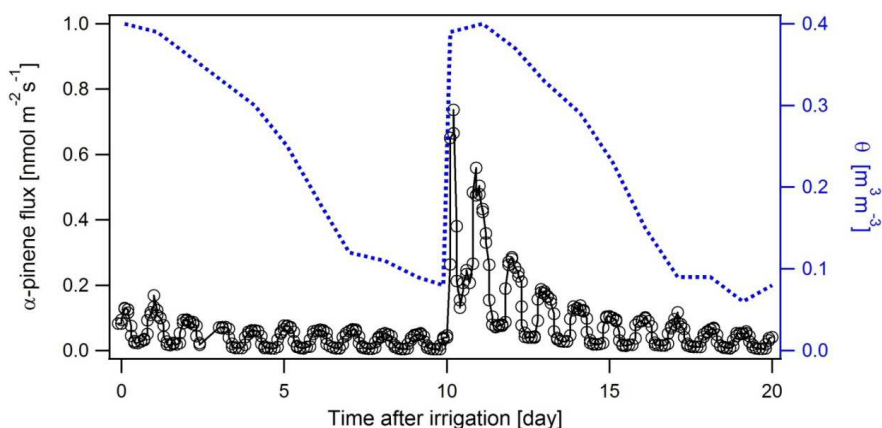


Fig. 3-11 temporal change of α -Pinene emission (black circles), volumetric water content of the soil (θ , blue dashed line) of a Norway spruce during the drought and the recovery periods. The plant was irrigated on day 0 and re-watered on day 10.

In Fig. 3-12, the ratios of daytime and nighttime α -pinene emissions were plotted. As an average, the daytime emission flux was 7 times (± 1.3) higher than the nighttime emission flux. There was no obvious change of this ratio under drought stress or during recovery time.

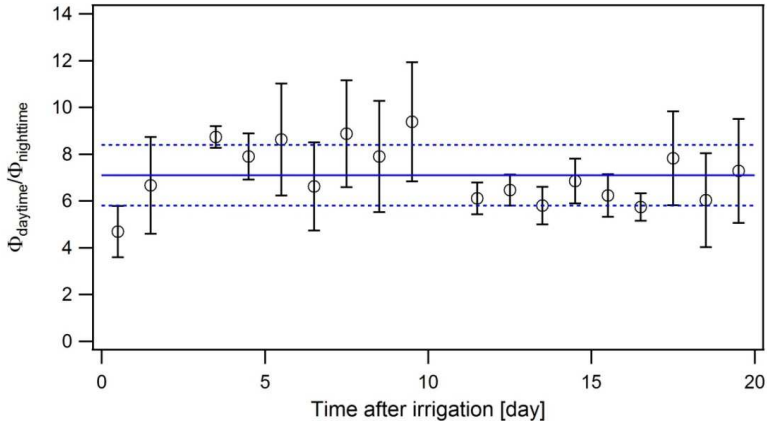


Fig. 3-12 Ratio of day time emission flux versus night time emission flux of a Norway spruce under drought and recovery periods. The blue line represents the average of the ratios with standard deviation (dashed lines).

The behavior of α -pinene emission of the Scots pine was similar. Fig. 3-13 shows the emission flux and θ from the second and third drought period. After the irrigation, θ approached to the field capacity ($\sim 0.35 \text{ m}^3 \text{ m}^{-3}$), and the emissions increased slightly during the first 4 days. Then it reduced slightly when θ fell below $0.1 \text{ m}^3 \text{ m}^{-3}$. On day 8, the plant was irrigated. After re-watering, the emission increased immediately and showed an increasing trend for the next four days. It was then followed by a decrease.

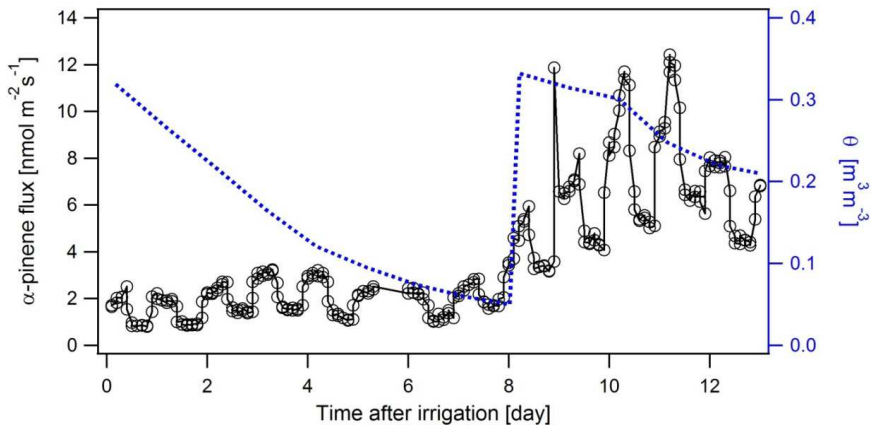


Fig. 3-13 Temporal changes of α -pinene emission (black circles), volumetric water content of the soil (θ , blue dashed line) of a Scots pine during the drought and the recovery periods.

The ratios of daytime emission and nighttime emission also didn't change a lot, were 1.9 ± 0.3 for the whole period (Fig. 3-14).

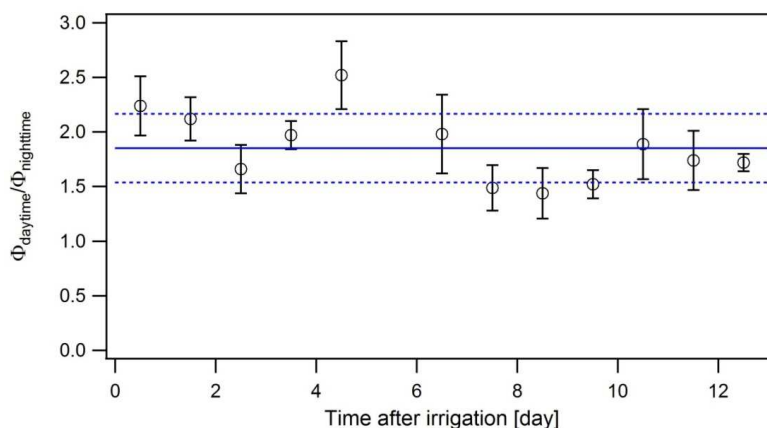


Fig. 3-14 The ratio of day time emission versus night time emission of a Scots pine under drought and recovery periods. The blue line represents the average of the ratios with standard deviation (dashed lines).

3.2.2 Impacts of heat stress

One experiment with a Norway spruce was conducted for the impacts of heat stress on both *de-novo* and pool emissions. The major emissions of the spruce were MT: α -pinene, camphene, sabinene, β -pinene, myrcene, careen, 1,8-cineole and SQT: β -farnesene, Δ -cadinene and junipene. Most of them were from pool storage (α -pinene, camphene, β -pinene, carene), and some, like myrcene, was a mixture of *de-novo* and pool emissions. SQT emissions were mainly *de-novo* emissions. Fig. 3-15 shows the changes of α -pinene, myrcene and β -farnesene with chamber temperature of 18°C, 23°C and 27°C and after 3-h 55°C heat stress.

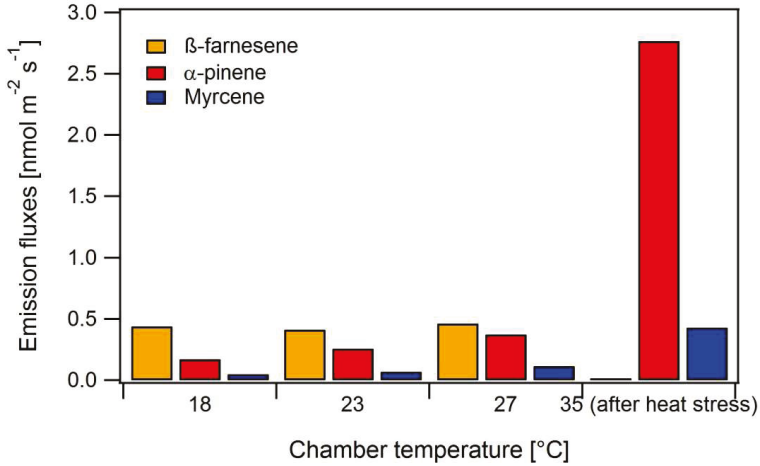


Fig. 3-15 Emission fluxes of α -pinene, myrcene and β -farnesene of Norway spruce before heat stress with different chamber temperatures and after 3-h heat stress with chamber temperature of 35°C.

Both *de-novo* and pool emissions of Norway spruce were affected by temperature. Before the heat stress, α -pinene and myrcene emissions show an increase of emission rates with the increasing temperature. The β -farnesene emissions were not that affected by temperature and reduced to the very low level even before the heat stress (not shown here). After 3-h heat stress of 55°C, the chamber temperature was reduced to 35°C. Both α -pinene and myrcene emissions increased and β -farnesene emission decreased to almost zero. In Fig. 3-16, the linear fittings were done for the data of $\ln(\Phi_{\text{myrcene}})$ and $\ln(\Phi_{\alpha\text{-pinene}})$ versus leaf temperature before the heat stress.

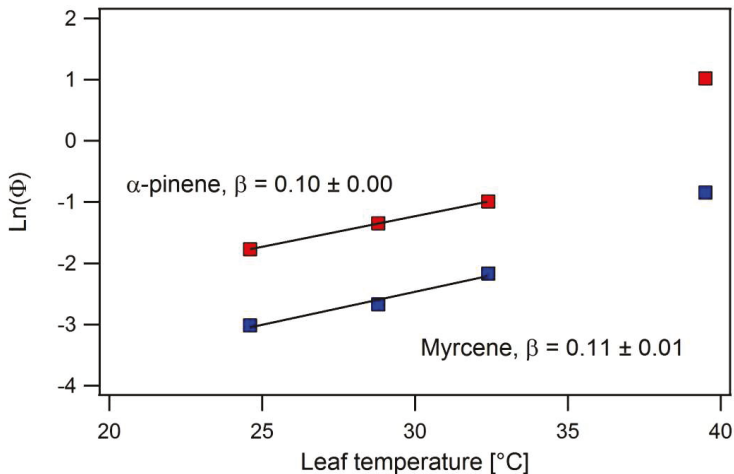


Fig. 3-16 $\ln(\Phi_{\alpha\text{-pinene}})$ and $\ln(\Phi_{\text{myrcene}})$ of Norway spruce in dependence on leaf temperatures before and after heat stress.

The fittings of $\ln(\Phi_{\alpha\text{-pinene}})$ and $\ln(\Phi_{\text{myrcene}})$ versus leaf temperatures show similar temperature coefficients $\beta = 0.1 \text{ K}^{-1}$ and 0.11 K^{-1} respectively. After heat stress, α -pinene emission showed high peak, ~ 7.4 times higher than that before heat stress and with $T = 27^\circ\text{C}$. It is clear that the high emission rate with 35°C after heat stress was not explainable by the temperature dependence alone. However, the increase of myrcene was not as high as that of the pure pool emission α -pinene, probably because of its mixed source.

3.2.3 Summary

De-novo and pool emissions have different diurnal variations. They also showed different behaviors when the soil moisture varies or when the plants were exposed to heat stress.

Impacts of drought. For *de-novo* MT, mild drought had no direct impacts on emissions. Severe drought caused decreases of *de-novo* MT emissions near to zero. Volumetric water content of soil (θ) was used as reference quantity to describe the effect of drought stress on BVOC emissions. The emissions reduced when θ was lower than the threshold. This tendency could be described by assuming linear behavior. Temperature and light dependencies of emissions were checked with different severities of drought. The results show that such dependencies were not substantially changed by drought. This enables to model impacts of drought on *de-novo* MT emissions together with changes of other environmental factors by multiplicative approach.

The decrease of pool emissions under severe drought stress were not that significant compared to that of *de-novo* emissions. Re-watering caused immediate huge amount of pool emissions. The high emissions lasted for several days with constant ratios of daytime- and nighttime emissions.

Impacts of heat. In the experiment with Norway spruce, 3-h heat stress changed the behavior of both *de-novo* and pool MT emissions. After heat stress, pure pool emissions increased much more than that could be explained by temperature dependency while *de-novo* emissions showed different behavior.

3.3 Ozone losses by gas phase reaction

When leading the air exiting the plant chamber to a reaction chamber, gas phase reaction occurred in both plant chamber and reaction chamber. The residence time of the gases in the reaction chamber (40–70 min for 1450 L chamber) was much longer than that in the reaction chamber (2–8 min for 164 L chamber). Therefore O₃ losses by gas phase reaction were measured in the reaction chamber. However, if the VOC and O₃ concentrations were both high in the plant chamber, the O₃ losses by gas phase reaction could not be ignored. For example in Fig. 3-2, gas phase reaction was also considered to better determine stomatal O₃ uptake.

Gas phase reactions of O₃ and VOCs from a Holm oak were tested in the reaction chamber. The total O₃ and VOCs losses were measured and compared to the calculated O₃ and VOCs losses based on [O₃], [VOC] and reaction rate constants (equation 2-4a), respectively. In table 3-2, the main compounds emitted by the plant were listed, together with their concentrations at the in- and outlet of the reaction chamber and the reaction rate constants with O₃. The dilution factor of the reaction chamber was considered when calculating the concentrations in the inlet. The measured and calculated O₃ losses were also listed in the table. Since the reaction rate constants of neo-allo-cimene + O₃ reactions and (Z)- β -ocimene + O₃ reactions are not known, the same value as for (E)- β -ocimene was used for these two compounds.

Table 3-2 The measured and the calculated VOC and O₃ losses by gas phase reactions. VOC_{*i*,in} and VOC_{*i*} are the concentrations of VOC_{*i*} at the in- and outlet of the chamber, $k_{O_3+VOC_i}$ is the reaction rate constant of VOC_{*i*} with O₃. O_{3,in} and O₃ are the O₃ concentrations at the in- and outlet of the chamber. The calculated sum of VOC losses is equal to the calculated O₃ losses.

	VOC _{<i>i</i>,in} [ppb]	VOC _{<i>i</i>} [ppb]	$k_{O_3+VOC_i}$ [10 ⁻¹⁸ cm ³ s ⁻¹]	Calc. VOC loss [ppb]	Meas. VOC loss [ppb]
α -pinene	20.7	10.2	86.6 ^a	3.9	10.5
β -pinene	11.25	7	15 ^a	0.5	4.3
(E)- β -ocimene	1.48	0.4	540 ^a	0.9	1.1
Myrcene	3.92	1	470 ^a	2.0	2.9
Limonene	1.35	0.5	200 ^a	0.5	0.9
Sabinene	5.76	2.9	86 ^a	1.1	2.9
(Z)- β -ocimene	4.41	0.9	540 ^a	2.2	3.5
Neo-allo-ocimene	21.65	4.2	540 ^a	10.1	17.5
Sum				21.2	43.4
	O _{3,in} [ppb]	O ₃ [ppb]		Calc. O ₃ loss [ppb]	Meas. O ₃ loss [ppb]
O ₃	83.9	63.4	-	21.2	20.5

^aAtkinson et al. (1997)

Compared to the calculated O₃ losses of 21.2 ppb, the measured O₃ losses were 20.5 ppb, which were well explained by the calculation. However, the calculated and the measured losses of VOCs showed a large discrepancy. The calculated VOC losses were 21.2 ppb (the same as the calculated O₃ losses) and the measured VOC losses were 43.4 ppb. Only 47% of the measured losses of VOCs could

be explained by the gas phase reactions with O₃. For the compounds with relative higher reaction rates, like (*E*)-β-ocimene and myrcene, the measured losses were 1.2 and 1.5 times higher than the calculated value. For those with lower reaction rates, like β-pinene, the measured value was even ~8 times higher than calculated. There were still additional losses of VOCs except the losses by the reactions with O₃.

The results proved that the calculation of gas phase reaction of O₃ with VOCs can explain the total O₃ losses quite well, while VOCs might react with other compounds, and showed higher losses.

3.4 Photochemical ozone formation

Three series of experiments were made with respect to photochemical O₃ formation from BVOC. α -pinene was tested firstly as sole VOC emitted from a diffusion source to avoid possible complications by varying emissions from a real plant. Two series of O₃ formation events were conducted: one with fixed initial α -pinene concentration but varied initial NO_x concentration and another with fixed initial NO_x concentration but varied initial α -pinene concentration. Another series was conducted for VOC mixtures from a Holm oak where the O₃ forming potential of VOC mixture was tested under high NO_x conditions.

3.4.1 Determination of ozone formation rates

During O₃ formation events, two processes dominated in the reaction chamber and determined gain or loss of O₃ as net effect. One was O₃ formation and another was O₃ photolysis. The net effect was measured by comparing the initial concentration and the final concentration of O₃ in the chamber under steady-state conditions. The amount of O₃ loss by photolysis was calculated by using $J(O^1D)$ measured on the blank days.

During the measurements, problems with determinations of O₃ concentrations by UV-absorption were found. Measuring the decay of O₃ concentrations in the chamber due to photolysis, different numbers were obtained when measuring without and with NO_x. Adding NO_x caused lower decreases of O₃ than without NO_x although the intensities of the UV lamp as well as water vapor concentrations were constant.

Furthermore, stopping the O₃ addition to the reaction chamber in the absence of NO_x caused nearly complete removal of O₃ whereas stopping the O₃ addition in the presence of NO_x always led to residual absorption signal in the O₃ detector. As this residual signal was observed for time periods exceeding the residence time on the reaction chamber tenfold this signal was assigned to fake O₃. The signal was equivalent to a fake O₃ mixing ratio of 2–5 ppb, it seemed to be related to the amount of NO_x added to the chamber and it vanished after flushing the reaction chamber for several days with air containing only low amounts of NO_x (< 300 ppt). Most probably other compounds produced in the reaction chamber were capable of absorbing light at 254 nm, the detection wavelength of the O₃ detector.

The 2-5 ppb background O₃ was measured after each experiment and subtracted when calculating $J(O^1D)$ and $P(O_3)$. But still, this cross sensitivity of the commercial device constrained exact quantitative analyses of O₃ forming potential of VOCs.

3.4.2 Ozone formation from single compound: α -pinene

3.4.2.1 Ozone formation: from high NO_x to low NO_x conditions

In order to show the detailed changes of different compounds during the O_3 formation events, three cases were chosen (Fig. 3-17) from Exp. 4.1. Fixed initial α -pinene concentration ($[\alpha\text{-pinene}]_0$) = 18.9 ± 0.2 ppb was added in the chamber with three different initial NO_x concentrations ($[\text{NO}_x]_0$) to demonstrate the impact of $[\text{NO}_x]$ on photochemical O_3 production from α -pinene. Other conditions in the chamber, such as RH, $J(\text{O}^1\text{D})$, and $J(\text{NO}_2)$, were kept constant.

Fig. 3-17 shows the $[\text{NO}]$, $[\text{NO}_2]$, $[\text{OH}]$ (left figure), $[\alpha\text{-pinene}]$ and $[\text{O}_3]$ (right figure) during these three events. The O_3 formation was driven by OH formed from photolysis of O_3 with UV light. The time periods shown in the figures were 0.5 h before the TUV lamps were switched on to 2.5 h after when the system was in steady state.

In the high NO_x system ($[\text{NO}_x]_0 = 138$ ppb), the ratio of $[\alpha\text{-pinene}]_0/[\text{NO}_x]_0$ was 0.14 ppb/ppb. After switching on the TUV light, the reaction $\text{OH} + \text{NO}_2 + \text{M} \rightarrow \text{HNO}_3 + \text{M}$ lowered the $[\text{OH}]$ which was $\sim 3 \times 10^7$ molecules cm^{-3} i.e. less than half of the $[\text{OH}]$ measured during the other two cases. The lower $[\text{OH}]$ caused a lower consumption of α -pinene. The left $[\alpha\text{-pinene}]$ was also higher than that in the other two cases, indicating there was less production of RO_2 radicals from the reaction $\alpha\text{-pinene} + \text{OH}$. In this system, adding more NO_x would not lead to higher O_3 formation. It was VOC-limited.

In case 2, reduced $[\text{NO}_x]_0$ (= 59 ppb) increased the $[\text{OH}]$ in the chamber to $\sim 8 \times 10^7$ molecules cm^{-3} and then increased the consumption of α -pinene. With the same $[\text{O}_3]_0$ as the first case, the final O_3 increased from ~ 83 ppb in case 1 to ~ 92 ppb in case 2. Higher $[\text{OH}]$ caused faster reaction of α -pinene with OH and more O_3 production.

In case 3, only 7.5 ppb initial NO_x were added to the reaction chamber. The ratio of $[\alpha\text{-pinene}]_0/[\text{NO}_x]_0 = 2.5$, was quite high. According to the k_{OH} of NO_2 and VOCs, the reaction $\text{VOCs} + \text{OH}$ dominated this system and the suppression of $[\text{OH}]$ by $\text{OH} + \text{NO}_2$ was less efficient. $[\text{OH}]$ was similar as that in case 2, high enough to cause substantial decrease of $[\alpha\text{-pinene}]$ in the chamber. The final $[\alpha\text{-pinene}]$ was similar as that in case 2. However, the O_3 production was even lower than the first case. The O_3 production was not limited by OH (or RO_2) but by NO_x .

These three cases show the switch of the system from VOC-limited to NO_x -limited by decreasing $[\text{NO}_x]_0$. The ratio of $[\alpha\text{-pinene}]_0/[\text{NO}_x]_0$ plays an important role in O_3 formation.

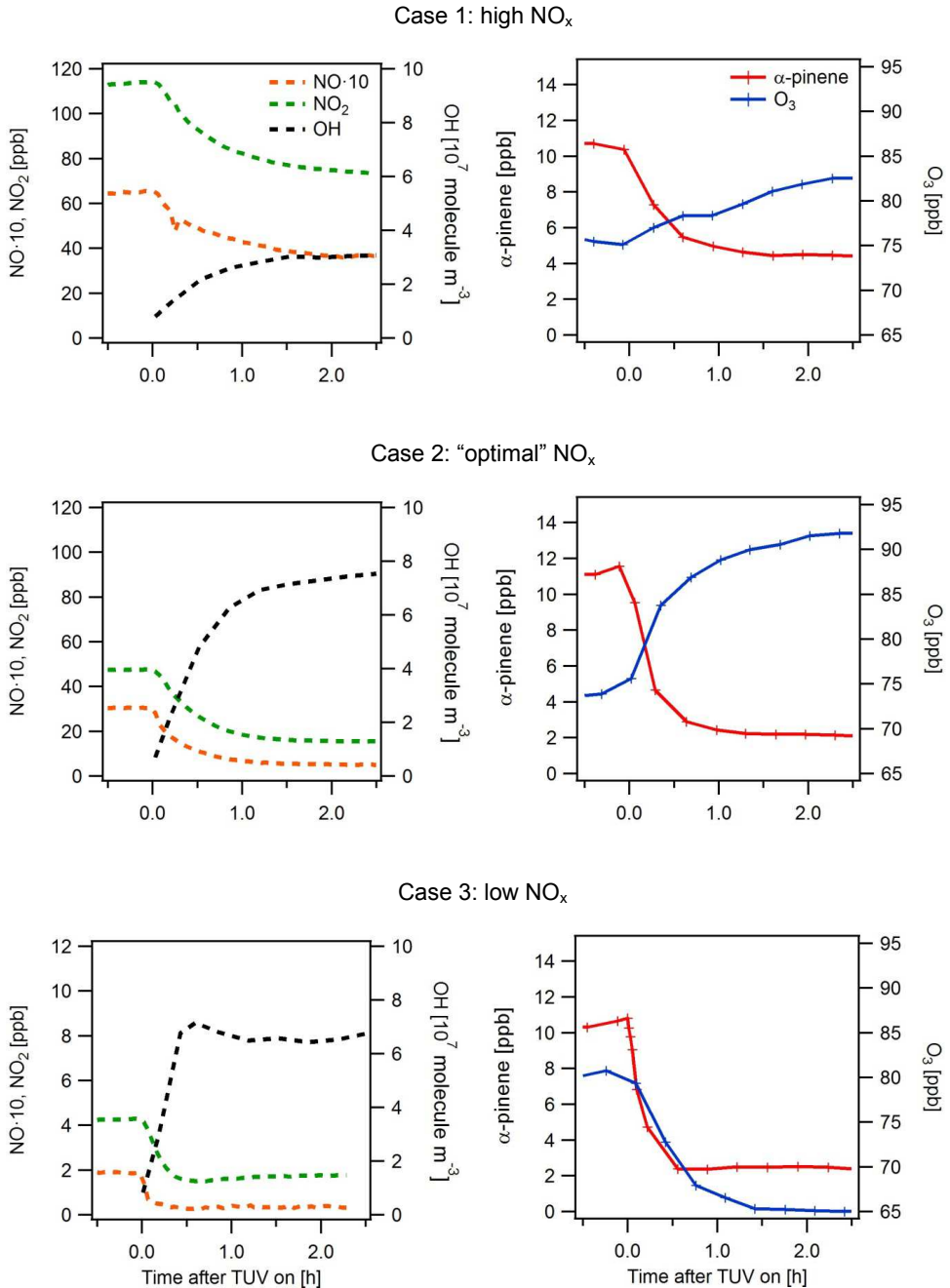


Fig. 3-17 Changes of $[\text{NO}_2]$ (green dashed line, left figure, left y scale), $[\text{NO}]$ (multiplied by 10, orange dashed line, left figure, left y scale), $[\text{OH}]$ (black dashed line, left figure, right y scale), $[\alpha\text{-pinene}]$ (red line, right figure, left y scale) and $[\text{O}_3]$ (blue line, right figure, right y scale) in three O_3 formation events.

3.4.2.2 Vertical cut of ozone isopleth plot

The following Fig. 3-18 shows the whole series of Exp. 4.1. A vertical cut of O₃ isopleth plot was conducted: O₃ production rates with different [NO_x]₀ but the same [α-pinene]₀ were tested. During this experiment, RH was kept constant (~53%). During the whole experiment, the baseline of O₃ was tested twice resulting in fake O₃ of 2.4 and 2.8 ppb, respectively. Thus, 2.6 ppb O₃ was subtracted when calculating J(O¹D) and P(O₃). The average J(O¹D) was $(2.00 \pm 0.11) \times 10^{-3} \text{ s}^{-1}$ for the whole series. J(O¹D) measured in the additional test with 1,8-cineole were $1.99 \times 10^{-3} \text{ s}^{-1}$ and $2.22 \times 10^{-3} \text{ s}^{-1}$ with and without the addition of 1,8-cineole, respectively. Without 1,8-cineole, the seemingly J-value was around 11% higher than with 1,8-cineole. This was due to scavenging OH produced by 1,8-cineole. For the calculation of P(O₃) in this series, a value of $2 \times 10^{-3} \text{ s}^{-1}$ was used.

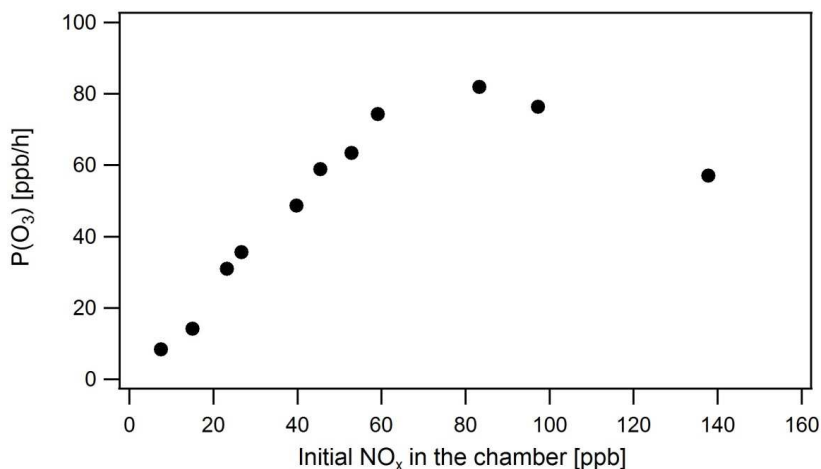


Fig. 3-18 Ozone production rate (P(O₃)) in dependence on initial NO_x. The initial α-pinene concentration was about 18.9 ppb in the chamber.

In Fig. 3-18 x-value represents the calculated [NO_x]₀ in the chamber, y-value represents O₃ production rate, P(O₃). It is obvious that a possible residual intercept of P(O₃) at [NO_x]₀ near to zero is negligible. This is expected as the fake O₃ was probably proportional to NO_x which is evidently low at low NO_x conditions. The error in the intercept may be low. However, substantial errors in the determination of the slope cannot be excluded. Therefore, data on the NO_x dependence of photochemical O₃ formation are not quantitatively interpreted.

Qualitatively, at low NO_x, the chemical system is limited by NO_x concentration. Increasing initial NO_x concentrations increases P(O₃) until the [NO_x]₀ exceeds 59 ppb. At [NO_x]₀ between 59 and 97 ppb the highest P(O₃) was obtained. With further increasing [NO_x]₀, O₃ production decreased again due to the suppressing impact of NO₂ on [OH]. The optimal ratio of [α-pinene]₀/[NO_x]₀ from this series was 0.19–0.32 ppb/ppb. The system is VOC-limited when the ratio is lower 0.19 ppb/ppb.

3.4.2.3 Horizontal cut of ozone isopleth plot

In Exp. 4.2, a horizontal cut of O_3 isopleth plot, i.e., photochemical O_3 production in dependence on $[\alpha\text{-pinene}]_0$ was measured. $[\text{NO}_x]_0$ was kept constant at 64.7 ± 1.0 ppb. The average $J(\text{O}^1\text{D})$ was $(2.35 \pm 0.13) \times 10^{-3} \text{ s}^{-1}$ for the whole series.

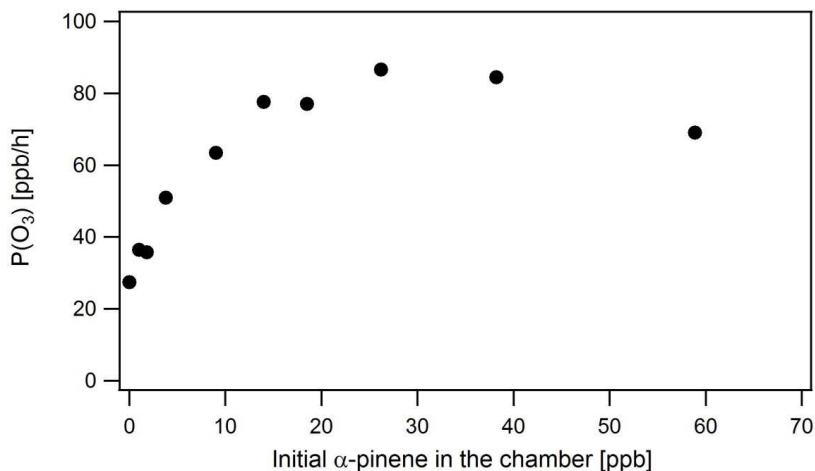


Fig. 3-19 Ozone production rate ($P(\text{O}_3)$) in dependence on initial α -pinene concentration. The initial NO_x concentration was 64.7 ppb in the chamber.

It is obvious from Fig. 3-19, that there is an intercept of $\sim 27 \text{ ppb h}^{-1}$ at $[\alpha\text{-pinene}]_0$ equals to zero. This intercept must be defective. As mentioned above, the error in the determination of the O_3 concentration using UV absorption might be induced by NO_x in the system. In this case, the error in the intercept was high, probably because of high NO_x concentrations when there was no α -pinene added.

However, a similar trend of $P(\text{O}_3)$ in dependence on $[\alpha\text{-pinene}]_0$ was found, compared to the trend of NO_x -dependency. The optimal $[\alpha\text{-pinene}]_0$ for the given $[\text{NO}_x]_0$ of 64.7 ppb was between 14 to 27.6 ppb. With $[\alpha\text{-pinene}]_0$ below this range, $P(\text{O}_3)$ increased almost linearly with increasing $[\alpha\text{-pinene}]_0$. When $[\alpha\text{-pinene}]_0$ was above 27.6 ppb, $P(\text{O}_3)$ didn't increase further. Increasing $[\alpha\text{-pinene}]_0$ to above 40 ppb caused decreasing $P(\text{O}_3)$. An optimal ratio of $[\alpha\text{-pinene}]_0/[\text{NO}_x]_0$ was calculated and was 0.22–0.43 ppb/ppb, similar as the ratio got in the last experiment. The system was VOC-limited with the ratio lower than 0.22.

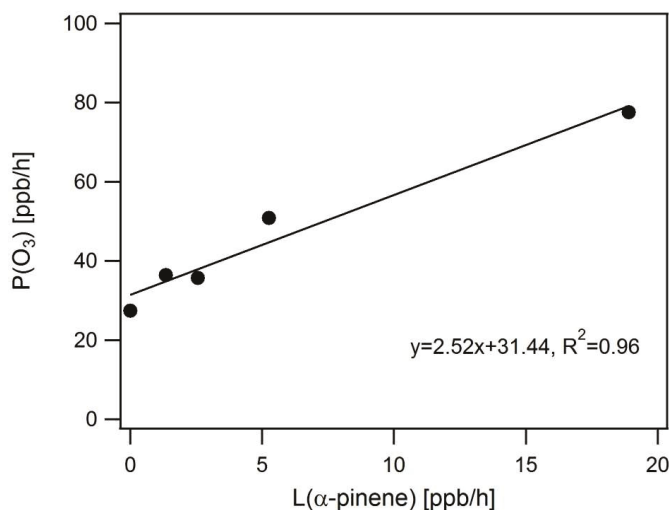


Fig. 3-20 Ozone formation rate ($P(O_3)$) versus loss rate of α -pinene ($L(\alpha\text{-pinene})$) under VOC-limited conditions ($[\alpha\text{-pinene}]_0/[\text{NO}_x]_0 \leq 0.22$).

In Fig. 3-20, the data points of O_3 formation rate versus loss rate of α -pinene under VOC-limited conditions ($[\alpha\text{-pinene}]_0/[\text{NO}_x]_0 \leq 0.22$) were plotted. Although the intercept was still high indicating an error in the determination of O_3 concentrations, the slope of 2.5 ppb/ppb ($R^2 = 0.96$) indicates 2.5 ppb O_3 was formed from 1 ppb α -pinene in the system.

3.4.3 Ozone formation from VOCs emitted by Holm oak

In order to test the O_3 forming potential of VOC mixtures emitted from real plants, one series of O_3 formation measurements was carried out with Holm oak as natural source. The main emission of the Holm oak was α -pinene, which accounted for $39 \pm 2\%$ of total emissions (average from 11:00–16:00) during the whole experiment. By varying light intensity and the inlet flow of the plant chamber, VOC concentrations were varied in the reaction chamber.

Three VOC concentrations in the range between 1.7–13.6 ppb were tested. According to the first two series, the ratio of $[\text{VOC}]_0/[\text{NO}_x]_0$ was kept below 0.19 ppb/ppb to sustain VOC-limited conditions. For the lowest concentration 1.7 ppb, 73 ppb NO_x was added. For $[\alpha\text{-pinene}]_0$ of 7.4 ppb, 74 and 142 ppb NO_x were tested leading to $[\text{VOC}]_0/[\text{NO}_x]_0$ 0.1 and 0.05 ppb/ppb, respectively. For $[\alpha\text{-pinene}]_0 = 13$ ppb, 135 and 214 ppb NO_x was added, leading to similar $[\text{VOC}]_0/[\text{NO}_x]_0$ ratios. This procedure was performed to control the VOC limitation of $P(O_3)$.

Table 3-3 The initial VOC and NO_x concentrations and P(O₃) of five events of O₃ formation with Holm oak.

Event	VOC ₀ [ppb]	NO _{x,0} [ppb]	VOC ₀ /NO _{x,0} [ppb/ppb]	P(O ₃) [ppb/h]
1	13.6	214	0.06	71.4
2	13.3	134	0.10	80.7
3	7.4	142	0.05	55.0
4	7.4	74	0.10	65.0
5	1.7	73	0.02	47.8

Table 3-3 listed [VOC]₀, [NO_x]₀ and P(O₃) of these five events. Generally, under VOC-limited conditions, higher [VOC]₀ caused higher P(O₃). In cases with two higher [VOC]₀, higher [VOC]₀/[NO_x]₀ ratio caused less O₃ production. Probably the suppression of [OH] in reactions with NO₂ already affected P(O₃).

Therefore, event 2, 4 and 5 were chosen and the O₃ formation rate (P(O₃)) versus the loss rate of BVOC (L(BVOC)) was plotted in Fig. 3-21. A slope of 2.4 shows that on average 2.4 molecules O₃ were produced per molecule consumed VOC. This value was similar as found in the series of α-pinene under VOC-limited conditions.

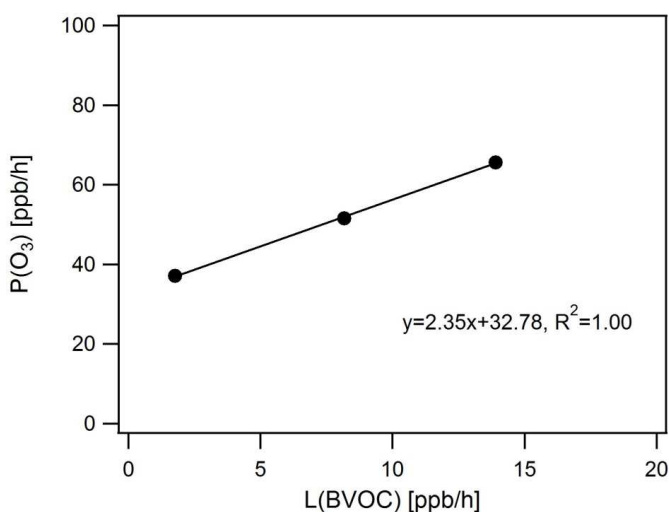


Fig. 3-21 O₃ formation rate (P(O₃)) versus loss rate of VOC mixture (L(BVOC)) from the experiment with Holm oak.

3.4.4 Summary

By testing one vertical cut and one horizontal cut of O₃ isopleth plot, the O₃ formation of single compound α-pinene at our chamber conditions was compared to the model simulation. The results

from these two series show a good qualitative agreement with O₃ isopleth diagrams from Finlayson-Pitts and Pitts Jr (1986). The O₃ formation was controlled by [NO_x]₀, by [α-pinene]₀, and by the ratio of them. When the ratio of [VOC]₀/[NO_x]₀ was high, the system was limited by NO_x. When the ratio of [VOC]₀/[NO_x]₀ was low, it is limited by VOC. A ratio of 0.22 was found under which the chamber system was VOC limited.

Although the problems in the determination of O₃ concentration constrained quantitative analysis of the NO_x dependence of the O₃ forming potential of VOCs, the slope of the plot P(O₃) versus L(BVOC) indicated 2–3 ppb O₃ was formed at the chamber conditions with 1 ppb loss of VOC.

Using plant emitted VOC mixture instead of α-pinene, similar slope of the plot P(O₃) versus L(BVOC) was observed under VOC-limited conditions, indicating similar potential of O₃ formation from BVOC mixture compared to α-pinene. In the VOC-limited range, the O₃ production was increased when the BVOC concentrations were increased either by applying higher light intensity or changing inlet flows.

3.5 The role of plants for tropospheric ozone balance

The role of plants for the O₃ balance is a combined effect of above mentioned processes: O₃ uptake through plant surfaces, gas phase reactions with BVOCs leading to O₃ losses at low NO_x conditions and photochemical O₃ production at high NO_x conditions. Drought and heat stress directly affect the behavior of plants and changed the fluxes of BVOC emissions and O₃ uptake. Dependent on the NO_x concentrations, changes of BVOC emissions alter O₃ balance by either altering O₃ losses by gas phase reactions or altering O₃ formation.

In order to calculate the net effect, these processes were separated into two steps: 1) the fluxes of BVOC emissions and O₃ loss on leaf surfaces were checked in the plant chamber; 2) the potential of BVOC emissions as a sink or a source of O₃ was studied in the reaction chamber.

If the system is at low NO_x conditions (< 300 ppt), the net O₃ flux is equal to the sum of O₃ loss flux on leaf surface and O₃ loss flux by gas phase reactions. In high NO_x system, the O₃ formation superimposes O₃ losses in gas phase reactions. Plants can be a source of O₃ when the net O₃ fluxes are positive as a result of photochemical O₃ formation (equation 2-17).

As a first step of this experiment, the impacts of temperature (Exp. 5.1), PAR (Exp. 5.2) and soil water status (Exp. 5.3) on O₃ uptake and BVOC emission were studied. In a second step, net O₃ fluxes were measured under high NO_x conditions (Exp. 5.4). O₃ uptake and photochemical O₃ formation were checked simultaneously using the two-chamber system. Determinations of net O₃ fluxes were performed at different soil moisture to check the possible impacts of drought for plants on the ozone balance.

3.5.1 Impacts of temperature, PAR and drought stress

Holm oak exhibits mainly *de-novo* MT emissions, which are affected by temperature, PAR and soil water status. Meanwhile, O₃ losses on leaf surfaces are also affected by these factors. Therefore, impacts of temperature, PAR and soil water status on the ratio O₃ uptake/BVOC emission were studied respectively.

3.5.1.1 Impacts of temperature

Table 3-4 shows O₃ uptake fluxes and BVOC emission fluxes from test days with T = 20°C, 25°C and 30°C and with PAR = 600 μmol m⁻² s⁻¹. O₃ added to the plant chamber was constant, ~85 ppb.

Table 3-4 Ozone uptake fluxes, BVOC emission fluxes, and the ratio of them from Holm oak with different leaf temperatures.

Leaf T [°C]	O ₃ uptake rate [nmol m ⁻² s ⁻¹]	VOC flux density [nmol m ⁻² s ⁻¹]	O ₃ uptake/BVOC emission
23.6	2.5 ± 0.1	1.6 ± 0.2	1.6
28.1	2.6 ± 0.0	2.9 ± 0.1	0.9
33.1	2.5 ± 0.1	4.2 ± 0.1	0.6

As expected, higher temperature caused higher BVOC emissions, whereas the O₃ uptake rate remained similar and didn't show any systematical change. The latter was caused by the low impacts of temperature on stomatal conductance. The ratio of O₃ uptake/BVOC emission decreased from 1.6 to 0.6, when temperature was increased by ~10°C.

3.5.1.2 Impacts of PAR

On another two test days, three different PAR were applied to the plant with constant chamber T = 30°C. Table 3-5 shows the results with PAR of 200, 400 and 600 μmol m⁻² s⁻¹. O₃ added to the plant chamber was constant, ~85 ppb. The ratio with 200 μmol m⁻² s⁻¹ was 1.1, which shows the amount of VOC emitted was in the same level as the amount of O₃ taken up by the plant. With increasing PAR, both VOC flux and O₃ uptake fluxes increased. However, the ratios of O₃ uptake/BVOC emission with 400 and 600 μmol m⁻² s⁻¹ were 0.9 and 0.6, which reveals the emissions of this plant were more sensitive to changes of PAR than stomatal opening.

Table 3-5 Ozone uptake fluxes, BVOC emission fluxes and the ratio of them from Holm oak with different PAR.

PAR [μmol m ⁻² s ⁻¹]	O ₃ uptake rate [nmol m ⁻² s ⁻¹]	VOC flux density [nmol m ⁻² s ⁻¹]	O ₃ uptake/BVOC emission
200	1.5 ± 0.0	1.4 ± 0.0	1.1
400	2.1 ± 0.0	2.4 ± 0.1	0.9
600	2.5 ± 0.1	4.1 ± 0.1	0.6

3.5.1.3 Impacts of drought

Drought stress also alters the ozone balance by altering both BVOC emission and O₃ uptake. Exp. 5.3 started with full irrigation and the volumetric water content of the soil ~0.5 m³ m⁻³. This plant went through a severe drought period (~25 days). Fig. 3-22 shows the responses of BVOC emission flux and O₃ uptake flux to drought stress (Exp. 5.3).

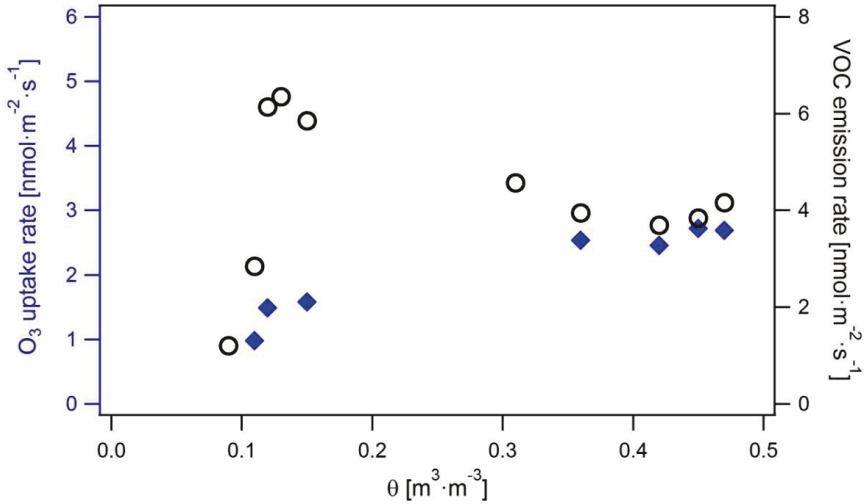


Fig. 3-22 O₃ uptake rate (blue diamonds) and BVOC fluxes (black circles) of Holm oak in dependence of soil water content (θ). Only the data with the same chamber temperature and the same PAR are shown.

Without drought stress ($\theta > 0.3 \text{ m}^3 \text{ m}^{-3}$ in Fig. 3-22), the leaf temperature and transpiration (not shown here) remained constant, O₃ uptake rate and BVOC emission rate also kept constant. When the drought stress started ($\theta \approx 0.15 \text{ m}^3 \text{ m}^{-3}$), transpiration decreased, which caused less cooling effect by evaporation and higher leaf temperature. The O₃ uptake was synchronized with the transpiration, which proved that the O₃ uptake was controlled by stomatal opening. Meanwhile, the emissions, as expected, increased firstly from $\sim 4 \text{ nmol m}^{-2} \text{ s}^{-1}$ to $\sim 6 \text{ nmol m}^{-2} \text{ s}^{-1}$ for the first days of the drought period and then decreased to almost zero afterwards.

It is clear, that the changes of BVOC emissions and O₃ uptake under drought stress were not in parallel. Mild drought increases BVOC emissions but decreases O₃ uptake, thus the ratio of O₃ uptake/BVOC emission decreased a lot. Severe drought diminishes both O₃ uptake and BVOC emission and diminished total impacts of the plant. Drought with different severities impacts the role of plants for the ozone balance differently.

3.5.2 Case study of ozone balance under high NO_x conditions

The role of the Holm oak for the ozone balance was checked with 4 case studies (Exp. 5.4). Either chamber temperature or soil water status was varied in order to simulate the possible impacts of temperature and drought on the behavior of plants and on the ozone balance. All cases were under high NO_x conditions. In table 3-6, both O₃ uptake fluxes and BVOC emission fluxes were listed. The ration of P(O₃)/L(BVOC) was from Fig. 3-23. The net O₃ fluxes, $\Phi(\text{O}_3)_{\text{net}}$, were calculated based on equation (2-17).

Table 3-6 Results from 4 case studies of ozone balance.

Remark	Plant chamber		Reaction chamber	Ozone balance
	O ₃ loss rate [nmol m ⁻² s ⁻¹]	BVOC emission [nmol m ⁻² s ⁻¹]	P(O ₃)/L(BVOC) C [ppb/ppb]	Φ(O ₃) _{net} [nmol m ⁻² s ⁻¹]
Case 1 Standard	2.5 ± 0.1	3.9 ± 0.2	2.8	8.4
Case 2 Low temperature	2.5 ± 0.1	1.6 ± 0.2	2.8	2.0
Case 3 Mild drought	1.4 ± 0.1	6.0 ± 0.3	2.8	15.4
Case 4 Severe drought	0.6 ± 0.1	0.2	2.8	-0.04

In Table 3-6, the ratio of P(O₃)/L(BVOC) was determined using the data from these four cases. The procedure was similar as that in Exp. 4.2 and Exp. 4.3. P(O₃) was plotted as a function of L(BVOC). The value of 2.8 ppb/ppb was obtained from the following figure and used in the calculation of net ozone fluxes.

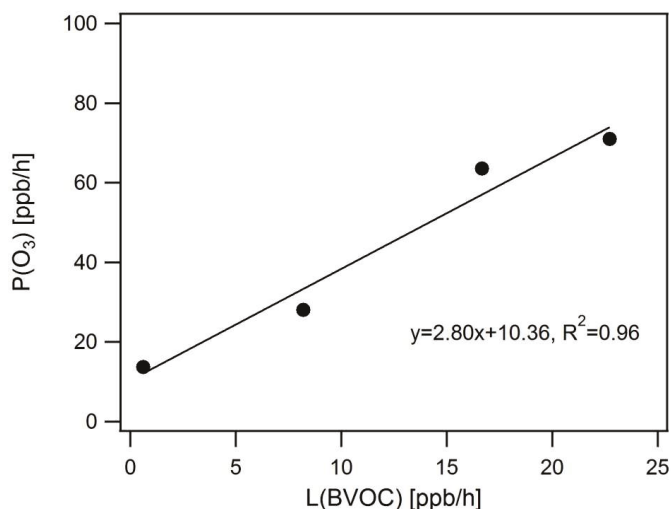


Fig. 3-23 O₃ formation rate (P(O₃)) versus VOC loss rate (L(BVOC)) from the experiment with Holm oak.

Comparing case 1 and 2, temperature, as mentioned in 3.5.1, had almost no effect on the stomatal opening. With the same amount of O₃ in the chamber, O₃ uptake fluxes were similar. However, BVOC emission rates increased by a factor of ~3 and caused a big change of the net O₃ production. With the ratio of P(O₃)/L(BVOC) = 2.8 ppb/ppb, the net O₃ flux increased from 2.0 nmol m⁻² s⁻¹ to 8.4 nmol m⁻² s⁻¹.

Cases 1, 3, and 4 were performed at different soil water statues. Mild drought stress (case 3) caused increase of BVOC emissions and decrease of O₃ uptake. The net gain of O₃ increased from 8.4 nmol m⁻² s⁻¹ to 15.4 nmol m⁻² s⁻¹. However, severe drought stress (case 4) diminished both processes and then diminished the effects of plants on the ozone balance. The net effect of plant on the ozone balance was near to zero.

3.5.3 Summary

The BVOC emission fluxes and O₃ uptake fluxes were affected by a lot of environmental variables: higher temperature caused increased emissions from Holm oak, but didn't substantially alter O₃ uptake rates. Higher PAR enhanced both BVOC emission fluxes and O₃ uptake fluxes. But as O₃ fluxes showed light saturation effects, the ratio of O₃ uptake/BVOC emission decreased. Depending on the severity of drought stress, increase or decrease of BVOC emissions appeared and at the same time O₃ uptake was suppressed. All of these variables impact the ratio of O₃ uptake/BVOC emission and thus influence the ozone balance.

The net effect of plants on O₃ flux depends on NO_x concentration. At low NO_x conditions, VOCs act as a sink of O₃, while at high NO_x conditions, ~2.8 ppb O₃ was produced from 1 ppb VOC mixture from the Holm oak. NO_x switched the role of this plant from a sink to a source of O₃. As long as the air is polluted and with high NO_x concentration, this plant tends to be a net source of O₃.

4 Discussion

4.1 Dry deposition of ozone on plant surfaces

4.1.1 Comparison to literatures

A connection between O_3 uptake and stomatal opening has been observed in previous studies (Laisk et al., 1989; Fares et al., 2008; Neubert et al., 1993). In these studies, the measured total conductivities of O_3 were compared to the calculated stomatal conductivities of O_3 . The intercepts obtained from such plots were negligible in all cases reflecting that O_3 loss caused by cuticular conductivity or reactions of O_3 with compounds at the surface of the cuticle are of minor importance. The slopes of the plots were close to the theoretical value of 1 for sunflower (*Helianthus annuus* L.), tobacco plants (*Nicotiana tabacum* L.) and black poplar (*Populus nigra* L.) indicating that O_3 losses on plant surfaces are limited by diffusion of O_3 through the plants stomata. The plants studied in these experiments emit only a small amount of BVOC suggesting that gas phase losses of O_3 in reactions with the emitted BVOCs are of minor importance. However, for the strong MT-emitter Holm oak, the slope is higher than 1 and the gas phase reaction of O_3 with the MT emissions contribute significantly to non-stomatal O_3 destruction (Fares et al., 2008).

The aim of the present experiments was to investigate whether such relation remains the same when the plant is suffering from drought stress. Since the tested species, Aleppo pine and Holm oak, were strong MT-emitters, the gas phase losses of O_3 with BVOCs were considered and subtracted from the total conductivities of O_3 .

In the experiment with Aleppo pine, mild drought stress was applied. The intercepts of the plots of the measured total conductivity of O_3 versus the calculated stomatal conductivity of O_3 were very low and the slopes with consideration of gas phase reaction were close to 1, even when the plant was under mild drought stress. Low intercepts indicate again that O_3 losses caused by cuticular conductivity or reactions with compounds at the surface of the cuticle are negligible. The slopes show that the stomatal O_3 uptake contributed almost all O_3 losses caused by plant. These results are consistent with the findings described in the studies mentioned above.

In the experiment with Holm oak, intercepts obtained with well-watered plants and under water-stress conditions were both low, but the slope in the latter case was much higher than 1 indicating that transpiration rate and the O_3 uptake rate are not as tightly connected under severe drought stress as they are under well-watered conditions.

4.1.2 Higher slopes under severe drought stress

During the time when the Holm oak was under severe drought stress, the diurnal variation of transpiration was quite small, leading to low values of the calculated stomatal conductivity of O_3 , $1.6 \times 10^{-3} \text{ mol m}^{-2} \text{ s}^{-1}$ during the day and $9 \times 10^{-4} \text{ mol m}^{-2} \text{ s}^{-1}$ during the night. O_3 uptake rates were nearly an order of magnitude higher, $1.2 \times 10^{-2} \text{ mol m}^{-2} \text{ s}^{-1}$ during the day and $4 \times 10^{-3} \text{ mol m}^{-2} \text{ s}^{-1}$ (Fig. 4-1). Nevertheless, the high coefficient of determination ($R^2 = 0.81$) obtained for plots of the total conductivity of O_3 versus the calculated stomatal conductivity of O_3 shows that the O_3 uptake was still related to the stomatal opening. However, the high slope of 9.6 indicates that either the calculation of stomatal conductivity is not correct or the network resistance shown in Fig. 2-2 is not complete.

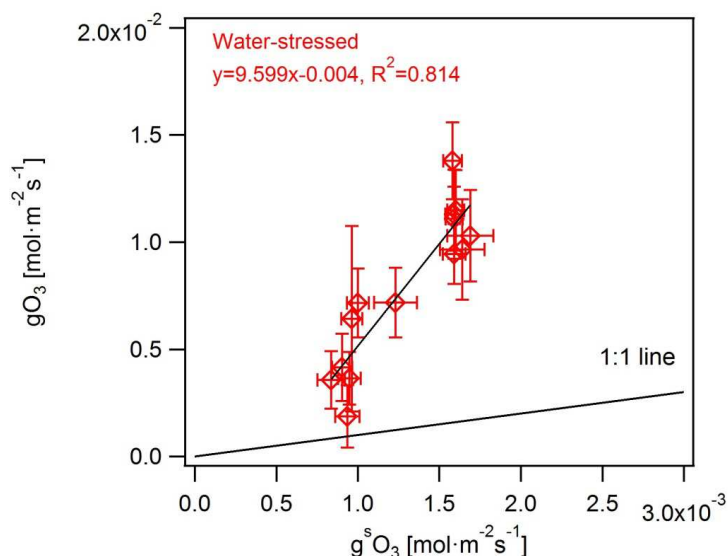


Fig. 4-1 Measured total conductivity of O_3 (g_{O_3}) versus calculated stomatal conductivity of O_3 ($g_{O_3}^s$) of Holm oak under and water-stressed conditions (red open diamonds).

The assumptions for the calculation include: 1) the air in the substomatal cavity is saturated with water vapor at the temperature of the leaf. 2) O_3 concentration in the substomatal cavity is zero. If the latter assumption is wrong, even higher total conductivity of O_3 would be observed. O_3 concentration in the substomatal cavity above 0 is obviously not the reason for the high slope. Other variables, like vapor pressure and O_3 concentration of the air outside the leaf were accurately measured.

The plant in this study grew in potted soil, which was different from previous studies conducted with the plants being situated in nutrient solutions providing the plants with sufficient amounts of water (Neubert et al., 1993). In the case of severe drought stress, the delivery of water vapor from the roots to the substomatal cavity was probably limited. On this occasion, transpiration would be at least partially limited by the internal water transport of the plant, rather than the width of the stomatal opening. Hence the relative humidity in the substomatal cavity could no longer be 100% as

assumed. If so, the stomatal opening was wider than that calculated based on this assumption. Correcting this would lead to slopes lower than that obtained in the plots.

Another reason could be an error in the measurement of BVOCs or unknown compounds that were emitted but not measurable with the existing equipment. Erroneous determination of gas phase losses may also cause too high slopes in the case of emissions of unknown compounds if the emissions are related to stomatal conductivity. Under drought stress, though the transpiration was low, BVOC mixing ratios measured under these conditions were still high, ~8 ppb, which may have caused 0.25 ppb O₃ loss in the chamber. Although gas phase losses may be somewhat higher than estimated, O₃ reactions with the known emissions cannot explain the high value for the slope.

Another possible error may be a wrong measurement of leaf temperature. For instance, reducing leaf temperature by 2°C results in a reduction of the numerical value of the slope from 9.6 to 8.5. In this experiment, the chamber temperature was accurately measured and the leaf temperature was 3-4°C higher than the chamber temperature. Considering that under the conditions in the plant chamber, leaf temperature is typically 2–4°C higher than the chamber temperature and drought stress can only lead to higher leaf temperature. The wrong measurement of leaf temperature as possible explanation is excluded.

Therefore, the most probable reason is a limitation of water supply to the substomatal cavity. This is equivalent to a non-negligible mesophyll resistance for the release of water (Fig. 2-2, R_M). In order to control this hypothesis, another approach is needed to calculate the stomatal O₃ uptake during conditions with shortage of water.

4.2 BVOC emissions under drought and heat stress

All *de-novo* and pool MT emissions from the plants investigated in this study were influenced by soil moisture and temperature, nevertheless, with different responses. Besides different emission mechanisms for MT, different severities of both stresses, drought and heat, caused also quite different impacts on emissions.

4.2.1 *De-novo* emissions under drought stress

Under drought stress, *de-novo* MT emissions showed a clearer relationship with stresses compared to pool emissions: *de-novo* MT emissions increased under mild drought stress and decreased under severe drought stress.

4.2.1.1 Comparison with literatures

The observation of substantial decreases of *de-novo* MT emissions under severe drought stress was similar to previous studies (Bertin and Staudt, 1996; Llusà and Peñuelas, 1998; Šimpraga et al., 2011; Bourtsoukidis et al., 2014; Plaza et al., 2005; Lavoit et al., 2009) as well as increases after re-watering (Peñuelas et al., 2009). Llusà and Peñuelas (1998) found strong suppression of *de-novo* MT emissions from non-storing species such as Holm oak. Lavoit et al. (2009) reported a significant exponential decrease of *de-novo* MT emissions from Holm oak forest when the leaf water potential fell below -2 MPa. Šimpraga et al. (2011) reported strong attenuation of *de-novo* MT emissions from European beech with progressing severe drought stress.

There are also several studies reported an increase of emissions under mild drought (Bertin and Staudt, 1996; Blanch et al., 2007; Ormeño et al., 2007). Blanch et al. (2007) investigated *de-novo* MT emissions from Holm oak. They reported a 33% increase of emissions from the plant with a reduction to one-third of full watering. In the study of Šimpraga et al. (2011), a significant increase of sabinene emission from European Beech was observed before the sharp decay of emissions under severe drought stress. The trend of sabinene emission measured in this study (Fig. 3-5) was nearly identical to such increasing-decreasing trend observed by Šimpraga et al. (2011), which indicates that the same general effect was found.

Though these studies agree with the finding in this study, a quantitative comparison is impossible because different reference quantities are used to characterize the degree of drought stress.

4.2.1.2 Increase of MT under mild drought stress – indirect effect caused by increasing T

Under mild drought stress ($\theta > \theta_1$), increases of emissions were found in almost all experiments. One possible reason is the increase of leaf temperature during drought period. In this study, leaf temperatures were reasonably well measured for the broadleaf species. Although the temperature of chambers was well controlled, the illumination adds extra heat load on leaf surfaces causing

increases of leaf temperature. A portion of this energy is released by evaporative cooling because the evaporation of water requires energy.

In Fig. 4-2, the change of leaf temperature of a Holm oak (Exp. 2.4a) under drought stress was shown, together with transpiration and net assimilation. The plant was irrigated at day 0 ($\theta = 0.4 \text{ m}^3 \text{ m}^{-3}$). Under well-watered conditions, the leaf temperature was $\sim 2^\circ\text{C}$ higher than the chamber temperature (25°C). On day 5, both transpiration and assimilation started to decrease. Meanwhile the leaf temperature showed an opposite trend. The closure of stomata led into the decreases of both transpiration and net assimilation. Thus, the leaf temperature increased because of the less evaporative cooling effect. In this case, the leaf temperature increased from $\sim 27^\circ\text{C}$ to $\sim 30^\circ\text{C}$, about 3°C . Such $2\text{--}3^\circ\text{C}$ increase was also found in the experiments with other species.

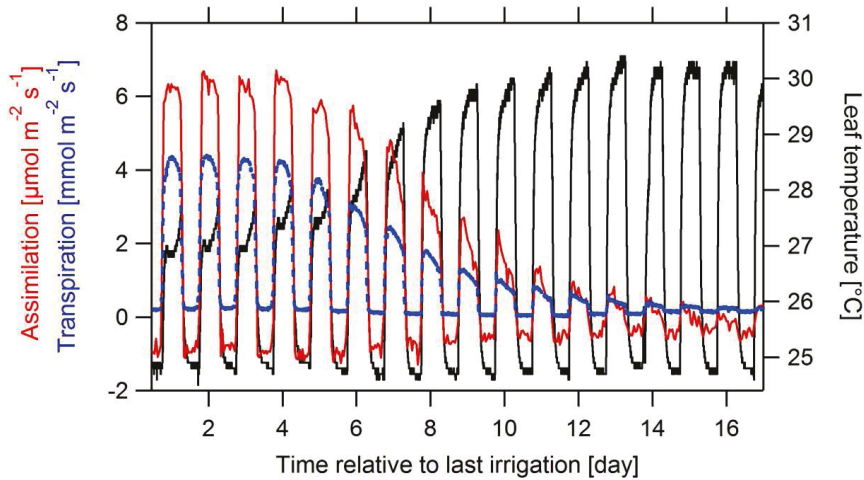


Fig. 4-2 Temporal development of transpiration (blue dashed line, left y scale), assimilation (red line, left y scale) and leaf temperature (black line, right y scale, average of three leaves) at the example of a Holm oak (Exp. 2.4a). Chamber temperature 25°C , PAR = $600 \mu\text{mol m}^{-2} \text{s}^{-1}$.

In the Exp. 2.4c, an average temperature coefficient β of 0.12 K^{-1} was measured for *de-novo* MT emissions from Holm oak. It was used here to calculate the hypothetical increase expected according to the increased leaf temperature. The range of expectable increase of MT emissions was 25–40%, which was similar to the measured increase in the cases of the beech (Exp. 2.3) and three Holm oaks (Exp. 2.4 b, c and d). In all these experiments, increases of MT emissions were found with the value less than 50%.

There was only one case (Exp. 2.4a) where the increase was not explainable by increasing leaf temperature alone. The measured increase of leaf temperature was also $\sim 3^\circ\text{C}$, but the increase of emission was $\sim 150\%$. This could be explained only with a temperature coefficient of $\sim 0.5 \text{ K}^{-1}$, which is atypically high. Therefore, the increase in MT emissions must have been caused by another effect. However, this plant suffered from drought before it was irrigated. The recovery might cause an increase in addition to the increase caused by increased leaf temperature.

4.2.1.3 Use of θ -dependencies of *de-novo* monoterpene emissions in MEGAN

In MEGAN, impacts of drought have been considered so far only for isoprene but not for MT emissions (Guenther et al., 2006;2012). A simple algorithm was used, which relates isoprene emission activity to soil moisture and wilting point (the soil moisture below which plants cannot extract water from soil). Volumetric water content of the soil (θ) was used as reference quantity. Isoprene emissions are not affected when θ is above a threshold θ_1 , but decrease linearly between θ_1 and θ_w , and remain zero as long as θ is below θ_w . The value of θ_w is taken from the study of (Chen and Dudhia, 2001) and $\Delta\theta_1 = 0.06 \text{ m}^3 \cdot \text{m}^{-3}$ is taken from Pegoraro et al. (2004).

One of the aims of this study is to provide a dataset to support modelling of impacts of soil moisture on *de-novo* MT emissions using MEGAN. Since basic parts of isoprene and *de-novo* MT biosynthesis pathways are identical, the possible impacts of drought on the emissions should be also similar (Wu et al., 2015). Therefore, the same reference quantity θ was used and an empirical relationship between *de-novo* MT emissions and θ was established.

As expected, the dependence of *de-novo* MT emission on θ was similar as that of isoprene. An average $\Delta\theta_1 = 0.08 \pm 0.05 \text{ m}^3 \cdot \text{m}^{-3}$ from all tested species was quite similar to than given in MEGAN. The measured lowest volumetric water content of soil, θ_0 , may not directly reflect θ_w . Since a recovery of the transpiration and emission was observed for most of the plants, θ_0 should be slightly above the level at which a plant gets permanently damaged. However, the transpiration rate was unmeasurably low at θ near to θ_0 , thus θ_0 was quite close to θ_w .

Furthermore, the interdependencies of individual factors temperature, light intensity and θ were tested in order to control the justification of a factorial approach, which is often used in modelling BVOC emissions (Guenther et al., 2006;2012).

The temperature dependence and PAR dependence of *de-novo* MT emissions were measured at different soil water status. There were no significant differences of them between under well-watered and under water-stressed conditions. Vice versa, by comparing the zero point and threshold of θ (θ_0 and θ_1) with different temperature or PAR (see Table 3-1), no obvious change of these two values was found. This reflects θ -dependence of emission remained similar although measured at different T or PAR.

Missing interdependencies of temperature, PAR and θ justify describing MT emissions from Holm oak by a factorial approach. Since the basic processes leading to *de-novo* MT emissions are similar for other plant species, it is postulated that the interdependencies of temperature, PAR and θ are also negligible. The datasets provided from this study allow considering the impacts of soil moisture in MEGAN (Guenther et al., 2006;2012) together with impacts of temperature and light intensity.

4.2.2 Comparison of *de-novo* and pool emissions

Compared to the *de-novo* MT emission, no clear relationship was found between θ and pool emissions. Therefore, only temporal changes of emissions under drought stress were shown for the two conifers (Fig. 3-11 and Fig. 3-13). Nevertheless, general trends were found from these two examples: under severe drought stress, the emissions trended to remain constant and showed only

slight decreases. After re-watering, huge peaks of emissions appeared and lasted for a time period of several days.

Different mechanisms of *de-novo* and pool emissions determine the different responses of them under stresses (Grote and Niinemets, 2008). As shown in Fig. 2-3, the size of the storage pool within the leaves determined the relationship between the synthesis and emission rates of isoprenoid. Without storage pool, *de-novo* emissions are directly related to the synthesis, which is controlled by both temperature and light intensity. Under drought, when the stress affects the performance of the plant, reduce of synthesis causes direct reduction of emission. Conifers have large storage pools and the emissions are directly from storage pools. Under drought stress, decreasing transpiration and net assimilation were found for both plants when $\theta < 0.2 \text{ m}^3 \text{ m}^{-3}$, similar as for other species. However, the emissions trended to be constant and were not affected much by even severer drought stress ($\theta < 0.1 \text{ m}^3 \text{ m}^{-3}$) (Fig. 3-11 and Fig. 3-13). This proved again, for storing species, the rate of synthesis and emission are somehow decoupled. The emissions rely on slow vaporization and diffusion from storage pools and follow temperature dependence of compound volatility (Guenther et al., 1993; Grote and Niinemets, 2008). Blanch et al. (2011) reported the relationship between α -pinene emission rates of the storing species Aleppo pine and the mean temperature of previous days. The highest correlation coefficient is found with the mean temperature of the previous 13 days rather than that of the current day.

There are also many studies reporting responses of pool MT emissions to progressive water loss. Ormeño et al. (2007) and Peñuelas and Llusà (1997) reported that pool MT emission of Rosemary (*Rosmarinus officinalis* L) remain stable under water deficit conditions. Blanch et al. (2007) investigated the impacts of drought (reduction to 1/3 of full watering) on Aleppo pine. According to the measurements in this study, drought with 2/3 water loss is not that severe to cause substantial changes of pool emissions. In the study of Blanch et al. (2007), drought causes decreases of pool emissions from Aleppo pine.

As mentioned in the experiments of broadleaf species, the leaf temperature increased 2–3°C during drought period because of the less evaporative cooling effect. Although, for conifers, the leaf temperature were not reliably measureable, it is reasonable to assume that the needle temperature also increased during drought period.

However, the two experiments in this study didn't show substantial increases of pool emissions during early drought periods. Instead, the slight reduction with severe drought maybe related to some limitation of emissions, possibly caused by stomatal closure (Niinemets and Reichstein, 2003; Harley et al., 2014). Moreover, the huge emission peaks appearing after re-watering hint to some accumulation of pool emissions during the drought period. Turtola et al. (2003) investigated changes of MT contents in resin of Scots pine and Norway spruce. They reported 39% and 32% increase of total MT and resin acids in resin caused by severe drought stress, respectively. This study supported a possible relationship between pool emission and accumulated production from certain previous time period.

These findings indicate that the mechanisms of pool MT emissions are so far not that clear. However, although the pool MT emissions are not directly driven by the synthesis, if drought stress causes any reduction of MT synthesis, it will reduce the pool sizes and then the total emissions in the long run.

4.2.3 Impacts of heat stress

In Kleist et al. (2012), the impacts of heat stress on the emissions from plant species with (Scots pine, Norway spruce) and without storage pools (European beech and Palestine oak) were studied. They separated reversible temperature impacts and irreversible effects of heat on BVOC emissions. The latter is defined as thermal stress. In their study, thermal stress causes irreversible decrease of *de-novo* MT emissions from broad leaf species but additional large release of pool MT from conifers.

In the experiment with Norway spruce (Exp. 2.5), the responses of the emissions with different types to heat stress were compared. Before heat application, the emissions of α -pinene (mainly pool emission) and myrcene (mixture of *de-novo* and pool emission) followed temperature dependence nicely. As long as temperature didn't exceed the threshold, increase of T caused higher emissions of both *de-novo* and pool emissions by enhancing either the enzymatic activates of synthesis (for *de-novo* emissions) or by raising the BVOCs vapor pressure and by decreasing the resistance of the diffusion pathway (for pool emissions) (Grote and Niinemets, 2008; Tingey et al., 1991). After the heat stress, large increases of α -pinene, which was a pure pool emission, were observed. According to Kleist et al. (2012), resin ducts are damaged by the thermal stress, which causes an increased release of pool MT during and after the heat application. However, the relative increase of myrcene emission was less than that of α -pinene. Since myrcene emissions were partly *de-novo* emissions, the less pronounced increase could be expected.

It was expected that a 3-h 55°C heat application would cause damage to both resin ducts and MT synthesis. Nevertheless, in this experiment, the pure *de-novo* emission, 1,8-cineole, didn't show an obvious decrease after the heat stress. This hints that the application of 3-h 55°C to this plant might have been not severe enough to suppress the synthesis, though it caused the damage of the resin ducts. The thresholds of temperature above which *de-novo* MT emissions decrease may vary broadly (Kleist et al., 2012).

4.3 Gas phase reaction

Gas phase reactions of O₃ with BVOCs occurred in both the plant chamber and the reaction chamber. In order to determine the dry deposition of O₃ in the plant chamber and formation of O₃ in the reaction chamber, the correct calculation of gas phase reactions is important for separating it from other processes related to O₃.

In order to confirm this, one experiment was carried out in the reaction chamber for the gas phase reaction of O₃ with BVOC mixture. The losses of O₃ and losses of BVOCs were measured and compared to the calculated amount. This result confirmed that the gas phase losses of O₃ in the chamber were mainly due to the reactions with BVOCs.

With respect to the O₃ balance such losses can contribute considerably in the absence of NO_x, similar as for photochemical O₃ formation. Maximum O₃ losses in such gas phase reactions can be expressed as fluxes,

$$\Phi(\text{O}_3)_{\text{gr}} = \sum_i \Phi(\text{VOC}_i) \times d_{\text{VOC}_i} \quad (4-1)$$

where $\Phi(\text{O}_3)_{\text{gr}}$ is the O₃ loss flux by gas phase reactions, $\Phi(\text{VOC}_i)$ is the emission flux of VOC_{*i*} and d_{VOC_i} is the number of double bonds in VOC_{*i*}. At low NO_x conditions, the impacts of vegetation on the net ozone flux could be calculated by equation (4-2)

$$\Phi(\text{O}_3)_{\text{net}} = -\Phi(\text{O}_3)_{\text{uptake}} - \Phi(\text{O}_3)_{\text{gr}} \quad (4-2)$$

In the real environment, the emitted BVOC are oxidized by OH and NO₃ which diminishes the fraction of BVOCs remaining for reactions with O₃. This fraction *f* is given by equation (4-3)

$$f = \frac{k_{\text{O}_3} [\text{O}_3]}{k_{\text{OH}} [\text{OH}] + k_{\text{NO}_3} [\text{NO}_3] + k_{\text{O}_3} [\text{O}_3]} \quad (4-3)$$

As an example, using typical daytime OH concentration of 2×10^6 molecule cm⁻³ and O₃ mixing ratios of 40 ppb, the fraction for α -pinene would be ~0.38, i.e. O₃ losses due to reactions with α -pinene can be expressed as $\Phi(\text{O}_3) = -\Phi(\alpha\text{-pinene}) \times 1 \times 0.38$ ($d = 1$).

The fraction *f* certainly depends on the abundance of oxidants as well as on the respective rate constants. As a lower limit for O₃ destruction by gas phase reactions in the absence of NO_x would certainly be zero in case *f* approaches zero.

In the same experiment, the calculated BVOC losses by the reaction with O₃ contributed ~50 % of total BVOC losses. With [NO_x] < 300 ppt in inlet air, NO₃ concentrations must be also negligible, and the reactions of BVOC with O₃ and OH dominated. The source of OH was the reaction of BVOCs and O₃. Table 4-1 lists the OH radical formation yield of different alkenes calculated by Atkinson et al. (1992). The formation yields of the OH radicals were determined by the experiments conducted in the presence of sufficient cyclohexane to scavenge > 95% if any OH radicals formed.

Table 4-1 Yields of OH radicals formation in reactions of O₃-alkene-cyclohexane-air mixtures at 296 ± 2 K and 740 Torr total pressure (Atkinson et al., 1992).

Alkene	OH radical formation yield
α-pinene	0.85
β-pinene	0.35
Sabinene	0.26
Camphene	≤0.18
Carene	1.06
Limonene	0.86
Myrcene	1.15
Cis- and trans-β-ocimene	0.63

Water vapor concentration, 2.5×10^{16} molecules cm⁻³

The main compounds emitted from this Holm oak were α-pinene and neo-allo-ocimene, which contributed 76% of the total emissions. The reaction of 1 molecule α-pinene and 1 molecule neo-allo-ocimene with O₃ could yield 0.85 and 0.63 (assumed to be the same as for trans-β-ocimene) molecule OH radicals, respectively. Other compounds have different formation yields of OH radicals in the range of 0.1 to 1.2. Following our assumption that ~1 molecule OH radical from 1 molecule ozonolysis of VOCs, ~50% VOC losses caused by the reaction of OH could be well explained.

4.4 Photochemical ozone formation

In the following section, uncertainties in the determination of O_3 formation from BVOCs are analyzed. Two important concepts of photochemical O_3 formation are discussed: NO_x -VOC sensitivity and O_3 forming potential.

4.4.1 Uncertainty of ozone formation rate

The problem with determination of O_3 concentrations constrained quantitative analysis of O_3 formation from BVOCs. This error may have affected the calculation of $J(O^1D)$. $J(O^1D)$ was measured on blank days, when no NO_x was added but VOC(s). VOC(s) were needed because they react with OH and thus avoid substantial reaction of O_3 with OH. Otherwise, the latter reaction would cause more O_3 loss and overestimation of $J(O^1D)$. However, if the added VOC(s) were not enough to scavenge OH, $J(O^1D)$ would have been overestimated. Besides, the reactions of VOC(s) with O_3 could also cause some error. By testing $J(O^1D)$ with high amount of 1,8-cineole, which only reacts with OH but not with O_3 , the impacts of the reaction of VOCs(s) with O_3 or insufficient addition of VOC were excluded. The value was similar as $J(O^1D)$ measured in the Exp. 4.1 to Exp. 4.3.

The problem may also be caused by other compounds which are capable of absorbing light with the same detection wavelength of the O_3 detector. These compounds may generated in the reaction chamber or evaporating from the chamber wall. In this case, by assuming constant production or release rate of the compounds, the certain amount of fake O_3 could be excluded, and the slope of the plot of $P(O_3)$ versus $L(BVOC)$ will not change substantially, i.e., the potential of O_3 formed by BVOC will remain the similar with such correction. Fig. 4-3 concluded the three series of O_3 formation experiments: one with α -pinene (Exp. 4.2) and two with Holm oaks (Exp. 4.3 and Exp. 5.4). Although different chamber conditions and history of use of the chamber caused different intercepts, similar slopes of 2–3 ppb/ppb were found. The slopes were used in this study for further calculation of net O_3 fluxes.

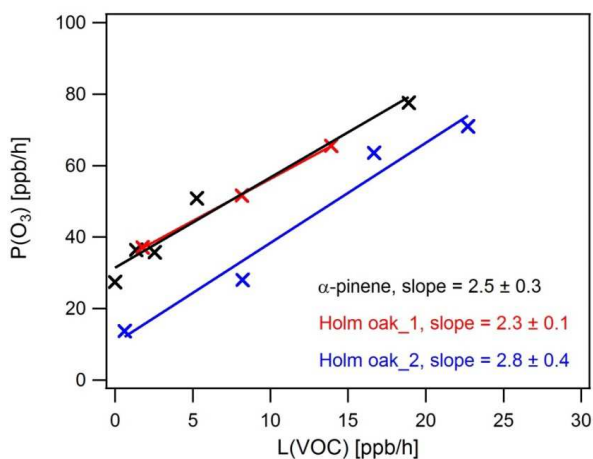


Fig. 4-3 O₃ formation rate (P(O₃)) versus VOC loss rate (L(VOC)) from the experiments of α-pinene (Exp. 4.2) and two Holm oaks (Exp. 4.3 and Exp. 5.4).

4.4.2 NO_x-VOC sensitivity - effective control of tropospheric ozone

Over the past twenty years, researchers have created many photochemical models and conducted a lot of field measurements to get a view of the relation between O₃ and its major precursors: VOCs and NO_x. The O₃-NO_x-VOC chemical system is fundamentally split into NO_x-sensitive (or NO_x-limited) and VOC-sensitive (or VOC-limited) regimes (Finlayson-Pitts and Pitts, 1997; Sillman, 1999). The isopleth plot (Fig. 2-5) illustrates the central feature of the relationship.

In the two series of α-pinene experiments, a horizontal cut and a vertical cut of the isopleth plot were tested. By testing the horizontal cut, a high NO_x condition was simulated, which is typical in urban and polluted rural sites. With high NO_x, the reaction RO₂ + NO represents the dominant reaction pathways for RO₂. In this case, O₃ production rates are controlled by the availability of RO₂, i.e. by the hydrocarbon-OH reaction. O₃ production rates increase with increasing VOC. This system is VOC-limited (Sillman, 1999). As shown in Fig. 3-20, an almost linear relationship was found between O₃ formation rate (P(O₃)) and α-pinene loss rate (L(α-pinene)) when the system was VOC-limited ($[\text{VOC}]_0/[\text{NO}_x]_0 < 0.22$ ppb/ppb). When VOC concentration kept on increasing, the system switched from VOC-limited to NO_x-limited. The rate of reaction RO₂ + NO was limited by [NO] again. One can expect, in the VOC-limited regime, the most effective way to reduce O₃ is reducing the BVOC emissions (Finlayson-Pitts and Pitts, 1997).

By testing the vertical cut, a fixed α-pinene concentration of 19 ppb simulated a high VOC condition, which is typical for example in forest areas (Ammann et al., 2004). When NO_x is low, OH mainly reacts with VOC and produces RO₂. In such case, the formation of O₃ increases with increasing NO_x and is largely unaffected by VOC, the system is NO_x-limited. In such case, reducing NO_x emissions could largely reduce the O₃ concentration.

NO_x-VOC-sensitivity is important for this chemistry system and the sensitivity analysis was used in many studies for efficient control of O₃ (Tie et al., 2013; Wu et al., 2009).

4.4.3 Ozone formation potential

There are a lot of model calculations conducted to quantify the reactivity or O₃ formation potential of VOCs. Photochemical ozone creation potential (POCP) was introduced by Derwent and Jenkin (1991) and used in many models (Derwent et al., 1996; Simpson, 1995). It is a relative value and describes the O₃ forming potential of VOC, *i*, relative to that of ethene

$$\text{POCP}_i = 100 \times \frac{\text{change in (mean or excess) ozone when species } i \text{ reduced}}{\text{change in (mean or excess) ozone when ethene reduced}}. \quad (4-4)$$

One conclusion from this study is that compared to the unreactive hydrocarbons, reactive hydrocarbons are more likely to achieve the theoretical ozone forming potential.

In the study of Carter (1994), Maximum Incremental Reactivity (MIR) of VOCs was calculated using single-cell box models to simulate how O₃ formation in one-day episodes is affected by changes in reactive VOC and NO_x inputs. VOCs have their greatest effect on O₃ under high NO_x conditions. The MIRs for isoprene, α-pinene and β-pinene are listed in Table 4-2. Such numbers match the results in Derwent et al. (1996). MIR has been widely used in many global model simulations (Kroeger et al., 2014; Schifer et al., 2011).

Table 4-2 Maximum incremental reactivity (MIRs) from Carter (1994).

	MIRs [g O ₃ /g VOC]	MIRs [ppb O ₃ /ppb VOC]
isoprene	9.1	12.9
α-pinene	3.3	9.4
β-pinene	4.4	12.5

Wagner et al. (2003) compared O₃ production simulated using Master Chemical Mechanism Version 3 with the experimental data from smog chamber. The compound tested in this study was toluene, which is a VOC with high POCP (Derwent et al., 1996). The results revealed that the model overestimated O₃ concentration by 55%.

For O₃ formation potential of MT, few experimental studies could be found. In my study, the O₃ formation rate (P(O₃)) was compared to the BVOC loss rate (L(BVOC)). The ratio of P(O₃)/L(BVOC) is different from POCP or MIR defined in the above mentioned studies. But in principle, P(O₃)/L(BVOC) reflects the similar potentials of O₃ formation from BVOCs. O₃ formation was measured when the chamber system was not limited by NO_x. That means that the dominant fraction of RO₂ produced by the reaction of OH + VOC could join the reaction RO₂ + NO to produce NO₂. P(O₃)/L(BVOC) was in the range of 2–3 ppb/ppb for α-pinene and also for the mixtures from Holm oak.

Compared to field conditions, similar O₃, NO_x, VOCs, RH conditions were simulated in our chamber. Since the residence time of gases in the chamber is relatively short (40–50 min), an internal UV lamp was equipped, which produced OH at concentrations up to ~10⁷ molecules cm⁻³, around an order of magnitude higher than that in the field. High [OH] allowed the reaction in the chamber to be much faster. However, in many events, there were still VOC left (considered in the calculation of L(BVOC)).

Even for those cases with no VOC left, OH might be not enough for the reactions of secondary products in the limited residence time. The maximal O₃ formation potential might not have been reached under our chamber conditions. But still, the much lower values got in this study indicate the possible overestimation of O₃ forming potential by model simulation.

4.5 The role of vegetation for tropospheric ozone balance

The role of vegetation for tropospheric ozone balance is determined by the amount of O₃ removed by plant and by the amount of O₃ formed from its BVOC emissions. In this study, the impacts of Holm oak on the ozone balance were tested. Both heat and drought stress was applied on the plant causing significant impacts on ozone balance. The results showed how wide the net ozone balance could be varied according to the performance of the plant.

Here the performance of vegetation without stress is discussed and followed by the possible impacts of heat and drought stress on the plants' performance and on the ozone balance.

4.5.1 The ratio of ozone uptake/BVOC emission - the potential to be an ozone source

The ratio of O₃ uptake/BVOC emission links two major processes of the ozone balance, which are related to the plant. In principle, plants are always a sink of O₃ in unpolluted area. Plants take up O₃ and emit BVOCs, which react with O₃. In polluted areas with high NO_x concentrations, destruction by O₃ + BVOCs reactions is replaced by photochemical O₃ formation from the emitted BVOCs. In such case, the ratio of O₃ uptake/BVOC emission reflects the plants' potential to be a source of ozone.

This ratio varies with different environmental variables. BVOC emission flux for certain species is affected by temperature, light intensity, leaf age, etc. (Guenther et al., 2012), while O₃ uptake rate is affected by O₃ concentration and stomatal conductance, which also varies with availability of water, light, temperature, carbon dioxide and other factors (Haworth et al., 2011).

For the first assessment, Holm oak was used as plant species. Holm oak is a strong MT emitter and the individual investigated here emitted $\sim 4.0 \text{ nmol m}^{-2} \text{ s}^{-1} \text{ MT}$ at a chamber temperature of 30°C and a PAR of $600 \mu\text{mol m}^{-2} \text{ s}^{-1}$. Exposing the plant to $\sim 76 \text{ ppb O}_3$ led to the uptake of $\sim 2.5 \text{ nmol m}^{-2} \text{ s}^{-1} \text{ O}_3$. By applying the ratio $P(\text{O}_3)/L(\text{BVOC})$ of 2.8 ppb/ppb, this plant was able to cause a net O₃ flux of $8.4 \text{ nmol m}^{-2} \text{ s}^{-1}$ at VOC limited conditions. The ratio of O₃ uptake flux and BVOC emission flux varied significantly with PAR and temperature. In particular the temperature had a strong effect because MT emissions were strongly relied on temperature but stomatal conductivity was not that much affected by temperature. In general, increasing temperature increased the net ozone emission flux from Holm oak.

It is clear that strong emitters like Holm oak can easily switch from a net O₃ sink to a net O₃ source with increasing NO_x concentration. However, BVOC emissions strongly depend on plant species (Kesselmeier and Staudt, 1999). For species like sunflower, tobacco or barley which emit quite little BVOC, the ratios of O₃ uptake/BVOC emissions are very high. Even the emitted BVOCs act as a source of O₃ with a high ratio of $P(\text{O}_3)/L(\text{BVOC})$, such plants are still a net sink of O₃. There are several studies about the O₃ forming potential of plants. Benjamin and Winer (1998) estimated the O₃ forming potential for tree and shrub species by combining the daily per tree emission rates with published maximum incremental reactivities (MIRs) for isoprene and MT. Strong emitters, like

Norway spruce, Holm oak, and Beech, all belong to the group of trees with high ozone forming potential, which contribute greater than $10\text{g O}_3\text{ d}^{-1}$.

Drewniak et al. (2014) simulated the impacts of a shift in forest composition on O_3 formation at rural and urban sites. Their results of simulation showed that the shift between strong emitter Holm oak to non-emitter maple causes reductions in O_3 concentration of up to 5–6 ppb, which may benefit air quality.

4.5.2 Vegetation under future climate conditions - a sink or a source of ozone?

Plants affect the ozone balance by direct O_3 uptake and by BVOC emissions. Besides temperature and PAR, stresses also affect the performance of plants and their roles for the O_3 balance. The impacts of heat and drought stress on this balance were investigated in this study because the importance of both stresses may increase with future climate change.

4.5.2.1 Heat stress

A lot of studies reported correlations between high O_3 concentration and high temperatures in polluted regions (Lin et al., 2001; Bloomer et al., 2009; Rasmussen et al., 2012).

Moderate heat increases BVOC emissions but does not substantially affect the dry deposition. As shown in table 3-4, an increase of leaf temperature from 23.6°C to 33.1°C didn't cause significant increases or decreases of O_3 uptake rate because stomatal conductance is not sensitive to temperature. Nevertheless, BVOC emissions are quite sensitive. The same increase of temperature caused ~150% increase of emissions. This caused the strong change of the ratio of O_3 uptake/BVOC emission rate. When the BVOC emission rate was combined with $P(\text{O}_3)/L(\text{BVOC})$ (Case. 1 and Case. 2 in table 3-6), the net O_3 flux increased from $2.0\text{ nmol m}^{-2}\text{ s}^{-1}$ to $8.4\text{ nmol m}^{-2}\text{ s}^{-1}$.

However, if the system is at low NO_x conditions, one can expect that, increasing BVOC emissions leads to a higher O_3 destruction. In this case, Holm oak would act as a stronger sink for O_3 with higher temperature.

Such effects are already considered in models. For example, Wu et al. (2008) modeled O_3 formation under consideration of higher temperature in the future climate. The emission of isoprene and other BVOCs (including MT and SQT) in the United States shall increase by 25% and 20%, respectively. Such increase contributes to an increase of O_3 in the northern United States but causes a decrease in the southeast. In the latter region, NO_x emissions are relatively low, which causes little net impacts of climate change on O_3 .

It is worth mentioning that the temperature dependence of emissions has an optimal range (Guenther et al., 2006; Steiner et al., 2010). If temperature is too high and exceeds the threshold, it causes damage of plants which then decreases O_3 uptake as well as BVOC synthesis and emissions (as described in section 3.2.2). In case of heat episodes with temperature increasing such thresholds, the total effect could be opposite.

4.5.2.2 Drought stress

Compared to the impacts of heat stress, fewer studies have been conducted to investigate the impacts of drought on future ozone balance. It is clear that severe drought brings closure of stomata, which subsequently decreases O_3 uptake (Panek and Goldstein, 2001). Meanwhile, BVOC emissions also decrease with severe water deficit (Guenther et al., 2012; Lavoie et al., 2011; Wu et al., 2015). Thus, severe drought stress changes both processes and diminishes the impacts of plants for ozone balance.

However, the impacts of drought on BVOC emissions depend on the severity of the drought. As shown in Fig. 3-22, with progressing drought, transpiration and O_3 uptake decreased before MT emissions were affected by the drought. Moreover, due to the less cooling effect by evaporation, leaf temperature increased as well as MT emissions. Compared to the well-watered conditions, the ratio of O_3 uptake/BVOC emissions was much lower at moderate drought. Such decoupling of BVOC emissions and transpiration with mild drought was observed in all experiments independent of the investigated species. Therefore, in polluted areas, the increasing O_3 formation potential should be a general trend under mild to moderate drought.

As the drought induced decrease of O_3 uptake was caused by lowered stomatal conductivity, it seems evident that drought also causes lowered uptake of NO_2 . Hence, the sink strengths for both O_3 and NO_2 are lowered. In NO_x limited regime, lower uptake of NO_2 caused higher NO_x in the air which might increase the O_3 formation. The uptake of NO_x adds more complexity into the whole ozone balance.

5 Summary and conclusion

In this study, impacts of plant performance on the ozone balance were investigated in the two-chamber system. In the plant chamber, O₃ losses on leaf surfaces and BVOC emissions by plants were measured for different species, which are representative for European climate zones. In the reaction chamber, O₃ losses by the reaction with BVOCs were tested under NO_x-free conditions and photochemical O₃ formation from these BVOCs was tested under high NO_x conditions.

In summary, plants are a sink of tropospheric O₃ in clean air. The dry deposition of O₃ on plant surfaces directly decreases the O₃ concentration. This process is dominated by O₃ uptake through the plant stomata with negligible losses on cuticle and stem. Meanwhile, BVOCs emitted by plants also act as a sink of O₃. O₃ destructions by gas phase reactions were significant in the reaction chamber at NO_x-free conditions. However, at high NO_x conditions, BVOC emissions switched from a sink to a source and O₃ destructions by gas phase reactions were superimposed by photochemical O₃ production. A ratio of O₃ formation rate over BVOC loss rate, in the range of 2–3 ppb/ppb, was observed for both α -pinene and VOC mixture from Holm oak.

Hence, an estimate about the role of plants for O₃ balance was obtained by the ratio of O₃ uptake rate over BVOC emission rate. This ratio reflects the capability of a plant as a potential source of O₃. The lower this ratio, the more likely the plant is to be a source of O₃ at high NO_x conditions. The O₃ uptake/BVOC emission ratio strongly depends on environmental variables such as light intensity, temperature and soil moisture.

Drought causes closure of stomata and fewer uptake of O₃. At the same time, drought affects MT emissions. Mild drought causes increases of *de-novo* MT emissions while severe drought causes decreases of *de-novo* MT emissions. Compared to *de-novo* emissions, pool emissions show a less pronounced response to both mild and severe drought stress. However, independent of the basic mechanism of MT emissions, moderate drought decreases the O₃ uptake/BVOC emission ratio, hence increases the role of a plant as a potential source of O₃. Severe drought stress diminishes the total performance of a plant and diminishes its impacts on the O₃ balance.

As long as high temperatures do not impose thermal stress, stomatal conductivity and O₃ uptake are insensitive to temperature. Due to the distinct temperature dependence of BVOC emissions, the O₃ uptake/BVOC emission ratio decreases. Therefore moderate increase of temperature increases the role of plants as potential O₃ source. However, when temperature exceeds the threshold and causes irreversible damage to plants, for those without storage pools, decreases of BVOC emissions attenuate their role as a potential O₃ source. For plant species with storage pools, increasing emissions enhance their role as O₃ precursors under high NO_x conditions.

Climate change is associated with more frequent and more intense extreme weather events including heat waves and drought (IPCC, 2013; Allen et al., 2010). Estimations of future ozone balance must consider the contribution of vegetation because they impact both sink and source processes of tropospheric ozone. Furthermore, all these processes will be substantially affected by heat and drought stress expected under future climate conditions.

6 Reference

- Allen, C. D., Macalady, A. K., Chenchouni, H., Bachelet, D., McDowell, N., Vennetier, M., Kitzberger, T., Rigling, A., Breshears, D. D., Hogg, E. H., Gonzalez, P., Fensham, R., Zhang, Z., Castro, J., Demidova, N., Lim, J.-H., Allard, G., Running, S. W., Semerci, A., and Cobb, N.: A global overview of drought and heat-induced tree mortality reveals emerging climate change risks for forests, *Forest Ecology and Management*, 259, 660-684, <http://dx.doi.org/10.1016/j.foreco.2009.09.001>, 2010.
- Ammann, C., Spirig, C., Neftel, A., Steinbacher, M., Komenda, M., and Schaub, A.: Application of PTR-MS for measurements of biogenic VOC in a deciduous forest, *International Journal of Mass Spectrometry*, 239, 87-101, <http://dx.doi.org/10.1016/j.ijms.2004.08.012>, 2004.
- Ashmore, M.: Assessing the future global impacts of ozone on vegetation, *Plant, Cell & Environment*, 28, 949-964, 2005.
- Atkinson, R., Aschmann, S. M., Arey, J., and Shorees, B.: Formation of OH radicals in the gas phase reactions of O₃ with a series of terpenes, *Journal of Geophysical Research: Atmospheres*, 97, 6065-6073, 10.1029/92JD00062, 1992.
- Atkinson, R., Baulch, D. L., Cox, R. A., Hampson, R. F., Kerr, J. A., Rossi, M. J., and Troe, J.: Evaluated Kinetic, Photochemical and Heterogeneous Data for Atmospheric Chemistry: Supplement V. IUPAC Subcommittee on Gas Kinetic Data Evaluation for Atmospheric Chemistry, *Journal of Physical and Chemical Reference Data*, 26, 521-1011, doi:<http://dx.doi.org/10.1063/1.556011>, 1997.
- Atkinson, R.: Atmospheric chemistry of VOCs and NO_x, *Atmospheric Environment*, 34, 2063-2101, [http://dx.doi.org/10.1016/S1352-2310\(99\)00460-4](http://dx.doi.org/10.1016/S1352-2310(99)00460-4), 2000.
- Benjamin, M. T., and Winer, A. M.: Estimating the ozone-forming potential of urban trees and shrubs, *Atmospheric Environment*, 32, 53-68, 1998.
- Bertin, N., and Staudt, M.: Effect of water stress on monoterpene emissions from young potted holm oak (*Quercus ilex* L.) trees, *Oecologia*, 107, 456-462, 1996.
- Blanch, J. S., Penuelas, J., and Llusia, J.: Sensitivity of terpene emissions to drought and fertilization in terpene-storing *Pinus halepensis* and non-storing *Quercus ilex*, *Physiologia Plantarum*, 131, 211-225, 10.1111/j.1399-3054.2007.00944.x, 2007.
- Blanch, J. S., Llusia, J., Niinemets, U., Noe, S. M., and Penuelas, J.: Instantaneous and historical temperature effects on alpha-pinene emissions in *Pinus halepensis* and *Quercus ilex*, *Journal of Environmental Biology*, 32, 1-6, 2011.
- Bloomer, B. J., Stehr, J. W., Piety, C. A., Salawitch, R. J., and Dickerson, R. R.: Observed relationships of ozone air pollution with temperature and emissions, *Geophysical Research Letters*, 36, L09803, 10.1029/2009GL037308, 2009.
- Bourtsoukidis, E., Kawaletz, H., Radacki, D., Schütz, S., Hakola, H., Hellén, H., Noe, S., Mölder, I., Ammer, C., and Bonn, B.: Impact of flooding and drought conditions on the emission of volatile organic compounds of *Quercus robur* and *Prunus serotina*, *Trees*, 28, 193-204, 10.1007/s00468-013-0942-5, 2014.
- Bowman, F. M., and Seinfeld, J. H.: Fundamental basis of incremental reactivities of organics in ozone formation in VOC/NO_x mixtures, *Atmospheric Environment*, 28, 3359-3368, [http://dx.doi.org/10.1016/1352-2310\(94\)00165-H](http://dx.doi.org/10.1016/1352-2310(94)00165-H), 1994.
- Calfapietra, C., Fares, S., Manes, F., Morani, A., Sgrigna, G., and Loreto, F.: Role of Biogenic Volatile Organic Compounds (BVOC) emitted by urban trees on ozone concentration in cities: A review, *Environmental Pollution*, 183, 71-80, 2013.

- Carter, W. P.: Development of ozone reactivity scales for volatile organic compounds, *Air & waste*, 44, 881-899, 1994.
- Chameides, W., Lindsay, R., Richardson, J., and Kiang, C.: The role of biogenic hydrocarbons in urban photochemical smog: Atlanta as a case study, *Science*, 241, 1473-1475, 1988.
- Chen, F., and Dudhia, J.: Coupling an advanced land surface-hydrology model with the Penn State-NCAR MM5 modeling system. Part I: Model implementation and sensitivity, *Monthly Weather Review*, 129, 569-585, 2001.
- Dai, A.: Increasing drought under global warming in observations and models, *Nature Climate Change*, 3, 52-58, 2013.
- Derwent, R., and Jenkin, M.: Hydrocarbons and the long-range transport of ozone and PAN across Europe, *Atmospheric Environment. Part A. General Topics*, 25, 1661-1678, 1991.
- Derwent, R., Jenkin, M., and Saunders, S.: Photochemical ozone creation potentials for a large number of reactive hydrocarbons under European conditions, *Atmospheric Environment*, 30, 181-199, 1996.
- Dodge, M.: Combined use of modeling techniques and smog chamber data to derive ozone-precursor relationships, International conference on photochemical oxidant pollution and its control: Proceedings, 1977a, 881-889.
- Dodge, M. C.: Effect of selected parameters on predictions of a photochemical model, Environmental Protection Agency, Research Triangle Park, NC (USA). Environmental Sciences Research Lab., 1977b.
- Drewniak, B. A., Snyder, P. K., Steiner, A. L., Twine, T. E., and Wuebbles, D. J.: Simulated changes in biogenic VOC emissions and ozone formation from habitat expansion of *Acer Rubrum* (red maple), *Environmental Research Letters*, 9, 014006, 2014.
- Fares, S., Loreto, F., Kleist, E., and Wildt, J.: Stomatal uptake and stomatal deposition of ozone in isoprene and monoterpene emitting plants, *Plant Biology*, 10, 44-54, 2008.
- Felzer, B., Reilly, J., Melillo, J., Kicklighter, D., Sarofim, M., Wang, C., Prinn, R., and Zhuang, Q.: Future effects of ozone on carbon sequestration and climate change policy using a global biogeochemical model, *Climatic Change*, 73, 345-373, 2005.
- Finlayson-Pitts, B. J., and Pitts Jr, J. N.: Atmospheric chemistry. Fundamentals and experimental techniques, 1986.
- Finlayson-Pitts, B. J., and Pitts, J. N.: Tropospheric air pollution: ozone, airborne toxics, polycyclic aromatic hydrocarbons, and particles, *Science*, 276, 1045-1051, 1997.
- Fiscus, E. L., Booker, F. L., and Burkey, K. O.: Crop responses to ozone: uptake, modes of action, carbon assimilation and partitioning, *Plant, Cell & Environment*, 28, 997-1011, 2005.
- Grote, R., and Ninemets, Ü.: Modeling volatile isoprenoid emissions—a story with split ends, *Plant Biology*, 10, 8-28, 2008.
- Guenther, A., Hewitt, C. N., Erickson, D., Fall, R., Geron, C., Graedel, T., Harley, P., Klinger, L., Lerdau, M., and McKay, W.: A global model of natural volatile organic compound emissions, *Journal of Geophysical Research: Atmospheres* (1984–2012), 100, 8873-8892, 1995.
- Guenther, A., Karl, T., Harley, P., Wiedinmyer, C., Palmer, P., and Geron, C.: Estimates of global terrestrial isoprene emissions using MEGAN (Model of Emissions of Gases and Aerosols from Nature), *Atmospheric Chemistry and Physics*, 6, 3181-3210, 2006.
- Guenther, A., Jiang, X., Heald, C., Sakulyanontvittaya, T., Duhl, T., Emmons, L., and Wang, X.: The Model of Emissions of Gases and Aerosols from Nature version 2.1 (MEGAN2. 1): an extended and updated framework for modeling biogenic emissions, 2012.
- Guenther, A. B., Zimmerman, P. R., Harley, P. C., Monson, R. K., and Fall, R.: Isoprene and monoterpene emission rate variability: model evaluations and sensitivity analyses, *Journal of Geophysical Research: Atmospheres* (1984–2012), 98, 12609-12617, 1993.
- Harley, P., Eller, A., Guenther, A., and Monson, R.: Observations and models of emissions of volatile terpenoid compounds from needles of ponderosa pine trees growing in situ: control by light, temperature and stomatal conductance, *Oecologia*, 176, 35-55, 10.1007/s00442-014-3008-5, 2014.
- Haworth, M., Elliott-Kingston, C., and McElwain, J. C.: Stomatal control as a driver of plant evolution, *Journal of Experimental Botany*, 62, 2419-2423, 10.1093/jxb/err086, 2011.

- Heiden, A., Kobel, K., Langebartels, C., Schuh-Thomas, G., and Wildt, J.: Emissions of oxygenated volatile organic compounds from plants Part I: Emissions from lipoxygenase activity, *Journal of Atmospheric Chemistry*, 45, 143-172, 2003.
- Horowitz, L. W., Walters, S., Mauzerall, D. L., Emmons, L. K., Rasch, P. J., Granier, C., Tie, X., Lamarque, J. F., Schultz, M. G., and Tyndall, G. S.: A global simulation of tropospheric ozone and related tracers: Description and evaluation of MOZART, version 2, *Journal of Geophysical Research: Atmospheres* (1984–2012), 108, 2003.
- IPCC: Climate Change 2013: The Physical Science Basis. Contribution of Working Group I to the Fifth Assessment Report of the Intergovernmental Panel on Climate Change, Cambridge University Press, Cambridge, United Kingdom and New York, NY, USA, 1535 pp., 2013.
- IUPAC: Subcommittee for Gas Kinetic Data Evaluation, <http://www.iupac-kinetic.ch.cam.ac.uk/>, 2009.
- Jacob, D. J., and Wofsy, S. C.: Photochemistry of biogenic emissions over the Amazon forest, *Journal of Geophysical Research: Atmospheres* (1984–2012), 93, 1477-1486, 1988.
- Karnosky, D., Pregitzer, K. S., Zak, D. R., Kubiske, M. E., Hendrey, G., Weinstein, D., Nosal, M., and Percy, K.: Scaling ozone responses of forest trees to the ecosystem level in a changing climate, *Plant, Cell & Environment*, 28, 965-981, 2005.
- Kesselmeier, J., and Staudt, M.: Biogenic Volatile Organic Compounds (VOC): An Overview on Emission, Physiology and Ecology, *Journal of Atmospheric Chemistry*, 33, 23-88, 10.1023/A:1006127516791, 1999.
- Kleist, E., Mentel, T., Andres, S., Bohne, A., Folkers, A., Kiendler-Scharr, A., Rudich, Y., Springer, M., Tillmann, R., and Wildt, J.: Irreversible impacts of heat on the emissions of monoterpenes, sesquiterpenes, phenolic BVOC and green leaf volatiles from several tree species, *Biogeosciences*, 9, 5111-5123, 2012.
- Kroeger, T., Escobedo, F. J., Hernandez, J. L., Varela, S., Delphin, S., Fisher, J. R., and Waldron, J.: Reforestation as a novel abatement and compliance measure for ground-level ozone, *Proceedings of the National Academy of Sciences*, 111, E4204-E4213, 2014.
- Kulmala, M., Vehkamäki, H., Petäjä, T., Dal Maso, M., Lauri, A., Kerminen, V.-M., Birmili, W., and McMurry, P. H.: Formation and growth rates of ultrafine atmospheric particles: a review of observations, *Journal of Aerosol Science*, 35, 143-176, 2004.
- Laisk, A., Kull, O., and Moldau, H.: Ozone concentration in leaf intercellular air spaces is close to zero, *Plant Physiology*, 90, 1163-1167, 1989.
- Lavoir, A., Staudt, M., Schnitzler, J., Landais, D., Massol, F., Rocheteau, A., Rodriguez, R., Zimmer, I., and Rambal, S.: Drought reduced monoterpene emissions from the evergreen Mediterranean oak *Quercus ilex*: results from a throughfall displacement experiment, *Biogeosciences*, 6, 2009.
- Lavoir, A. V., Duffet, C., Mouillot, F., Rambal, S., Ratte, J. P., Schnitzler, J. P., and Staudt, M.: Scaling-up leaf monoterpene emissions from a water limited *Quercus ilex* woodland, *Atmospheric Environment*, 45, 2888-2897, 10.1016/j.atmosenv.2011.02.005, 2011.
- Lefohn, A.: Surface level ozone exposures and their effects on vegetation, 1992.
- Leighton, P. A.: Photochemistry of air pollution, Academic Press, 93-94, 1961.
- Lin, C. Y. C., Jacob, D. J., and Fiore, A. M.: Trends in exceedances of the ozone air quality standard in the continental United States, 1980–1998, *Atmospheric Environment*, 35, 3217-3228, [http://dx.doi.org/10.1016/S1352-2310\(01\)00152-2](http://dx.doi.org/10.1016/S1352-2310(01)00152-2), 2001.
- Llusà, J., and Peñuelas, J.: Changes in terpene content and emission in potted Mediterranean woody plants under severe drought, *Canadian Journal of Botany*, 76, 1366-1373, 10.1139/b98-141, 1998.
- Marrero, T., and Mason, E. A.: Gaseous diffusion coefficients, *Journal of Physical and Chemical Reference Data*, 1, 3-118, 1972.
- Meehl, G. A., and Tebaldi, C.: More intense, more frequent, and longer lasting heat waves in the 21st century, *Science*, 305, 994-997, 2004.
- Mentel, T. F., Wildt, J., Kiendler-Scharr, A., Kleist, E., Tillmann, R., Maso, M. D., Fisseha, R., Hohaus, T., Spahn, H., and Uerlings, R.: Photochemical production of aerosols from real plant emissions, *Atmospheric Chemistry and Physics*, 9, 4387-4406, 2009.

- Mentel, T. F., Kleist, E., Andres, S., Dal Maso, M., Hohaus, T., Kiendler-Scharr, A., Rudich, Y., Springer, M., Tillmann, R., Uerlings, R., Wahner, A., and Wildt, J.: Secondary aerosol formation from stress-induced biogenic emissions and possible climate feedbacks, *Atmos. Chem. Phys.*, 13, 8755-8770, 10.5194/acp-13-8755-2013, 2013.
- Monks, P., Granier, C., Fuzzi, S., Stohl, A., Williams, M., Akimoto, H., Amann, M., Baklanov, A., Baltensperger, U., and Bey, I.: Atmospheric composition change—global and regional air quality, *Atmospheric Environment*, 43, 5268-5350, 2009.
- Müller, J. F.: Geographical distribution and seasonal variation of surface emissions and deposition velocities of atmospheric trace gases, *Journal of Geophysical Research: Atmospheres* (1984–2012), 97, 3787-3804, 1992.
- Neubert, A., Kley, D., Wildt, J., Segschneider, H. J., and Förstel, H.: Uptake of NO, NO₂ and O₃ by sunflower (*Helianthus annuus* L.) and tobacco plants (*Nicotiana tabacum* L.): dependence on stomatal conductivity, *Atmospheric Environment. Part A. General Topics*, 27, 2137-2145, [http://dx.doi.org/10.1016/0960-1686\(93\)90043-X](http://dx.doi.org/10.1016/0960-1686(93)90043-X), 1993.
- Niinemets, Ü., and Reichstein, M.: Controls on the emission of plant volatiles through stomata: A sensitivity analysis, *Journal of Geophysical Research: Atmospheres*, 108, 4211, 10.1029/2002JD002626, 2003.
- Ormeño, E., Mévy, J. P., Vila, B., Bousquet-Mélou, A., Greff, S., Bonin, G., and Fernandez, C.: Water deficit stress induces different monoterpene and sesquiterpene emission changes in Mediterranean species. Relationship between terpene emissions and plant water potential, *Chemosphere*, 67, 276-284, <http://dx.doi.org/10.1016/j.chemosphere.2006.10.029>, 2007.
- Panek, J. A., and Goldstein, A. H.: Response of stomatal conductance to drought in ponderosa pine: implications for carbon and ozone uptake, *Tree Physiology*, 21, 337-344, 10.1093/treephys/21.5.337, 2001.
- Pegoraro, E., Rey, A., Bobich, E. G., Barron-Gafford, G., Grieve, K. A., Malhi, Y., and Murthy, R.: Effect of elevated CO₂ concentration and vapour pressure deficit on isoprene emission from leaves of *Populus deltoides* during drought, *Functional Plant Biology*, 31, 1137-1147, 2004.
- Peñuelas, J., and Llusà, J.: Effects of Carbon Dioxide, Water Supply, and Seasonality on Terpene Content and Emission by *Rosmarinus officinalis*, *J Chem Ecol*, 23, 979-993, 10.1023/B:JOEC.0000006383.29650.d7, 1997.
- Peñuelas, J., Filella, I., Seco, R., and Llusà, J.: Increase in isoprene and monoterpene emissions after re-watering of droughted *Quercus ilex* seedlings, *Biol Plant*, 53, 351-354, 10.1007/s10535-009-0065-4, 2009.
- Plaza, J., Núñez, L., Pujadas, M., Pérez-Pastor, R., Bermejo, V., García-Alonso, S., and Elvira, S.: Field monoterpene emission of Mediterranean oak (*Quercus ilex*) in the central Iberian Peninsula measured by enclosure and micrometeorological techniques: Observation of drought stress effect, *Journal of Geophysical Research: Atmospheres*, 110, D03303, 10.1029/2004JD005168, 2005.
- Rasmussen, D. J., Fiore, A. M., Naik, V., Horowitz, L. W., McGinnis, S. J., and Schultz, M. G.: Surface ozone-temperature relationships in the eastern US: A monthly climatology for evaluating chemistry-climate models, *Atmospheric Environment*, 47, 142-153, <http://dx.doi.org/10.1016/j.atmosenv.2011.11.021>, 2012.
- Schifter, I., Díaz, L., Rodríguez, R., and Salazar, L.: Oxygenated transportation fuels. Evaluation of properties and emission performance in light-duty vehicles in Mexico, *Fuel*, 90, 779-788, <http://dx.doi.org/10.1016/j.fuel.2010.09.034>, 2011.
- Schimang, R., Folkers, A., Kleffmann, J., Kleist, E., Miebach, M., and Wildt, J.: Uptake of gaseous nitrous acid (HONO) by several plant species, *Atmospheric Environment*, 40, 1324-1335, 2006.
- Schuh, G., Heiden, A., Hoffmann, T., Kahl, J., Rockel, P., Rudolph, J., and Wildt, J.: Emissions of volatile organic compounds from sunflower and beech: dependence on temperature and light intensity, *Journal of Atmospheric Chemistry*, 27, 291-318, 1997.
- Seinfeld, J. H., and Pandis, S. N.: Atmospheric chemistry and physics: from air pollution to climate change, 2006.

- Sillman, S.: A numerical solution for the equations of tropospheric chemistry based on an analysis of sources and sinks of odd hydrogen, *Journal of Geophysical Research: Atmospheres*, 96, 20735-20744, 10.1029/91JD01967, 1991.
- Sillman, S.: The relation between ozone, NO_x and hydrocarbons in urban and polluted rural environments, *Atmospheric Environment*, 33, 1821-1845, [http://dx.doi.org/10.1016/S1352-2310\(98\)00345-8](http://dx.doi.org/10.1016/S1352-2310(98)00345-8), 1999.
- Šimpraga, M., Verbeeck, H., Demarcke, M., Joó, É., Pokorska, O., Amelynck, C., Schoon, N., Dewulf, J., Van Langenhove, H., Heinesch, B., Aubinet, M., Laffineur, Q., Müller, J. F., and Steppe, K.: Clear link between drought stress, photosynthesis and biogenic volatile organic compounds in *Fagus sylvatica* L, *Atmospheric Environment*, 45, 5254-5259, <http://dx.doi.org/10.1016/j.atmosenv.2011.06.075>, 2011.
- Simpson, D.: Hydrocarbon reactivity and ozone formation in Europe, *Journal of Atmospheric Chemistry*, 20, 163-177, 1995.
- Steiner, A. L., Davis, A. J., Sillman, S., Owen, R. C., Michalak, A. M., and Fiore, A. M.: Observed suppression of ozone formation at extremely high temperatures due to chemical and biophysical feedbacks, *Proceedings of the National Academy of Sciences*, 107, 19685-19690, 2010.
- Stevenson, D., Dentener, F., Schultz, M., Ellingsen, K., Van Noije, T., Wild, O., Zeng, G., Amann, M., Atherton, C., and Bell, N.: Multimodel ensemble simulations of present - day and near - future tropospheric ozone, *Journal of Geophysical Research: Atmospheres* (1984–2012), 111, 2006.
- Strong, J., Whyatt, J. D., Metcalfe, S. E., Derwent, R. G., and Hewitt, C. N.: Investigating the impacts of anthropogenic and biogenic VOC emissions and elevated temperatures during the 2003 ozone episode in the UK, *Atmospheric Environment*, 74, 393-401, 2013.
- Tarvainen, V., Hakola, H., Hellén, H., Bäck, J., Hari, P., and Kulmala, M.: Temperature and light dependence of the VOC emissions of Scots pine, *Atmospheric Chemistry and Physics*, 5, 989-998, 2005.
- Tie, X., Geng, F., Guenther, A., Cao, J., Greenberg, J., Zhang, R., Apel, E., Li, G., Weinheimer, A., Chen, J., and Cai, C.: Megacity impacts on regional ozone formation: observations and WRF-Chem modeling for the MIRAGE-Shanghai field campaign, *Atmos. Chem. Phys.*, 13, 5655-5669, 10.5194/acp-13-5655-2013, 2013.
- Tingey, D. T., Manning, M., Grothaus, L. C., and Burns, W. F.: INFLUENCE OF LIGHT AND TEMPERATURE ON MONOTERPENE EMISSION RATES FROM SLASH PINE, *Plant Physiology*, 65, 797-801, 10.1104/pp.65.5.797, 1980.
- Tingey, D. T., Turner, D. P., and Weber, J. A.: Factors controlling the emissions of monoterpenes and other volatile organic compounds, *Trace gas emissions by plants*, 65, 797-801, 1991.
- Turtola, S., Manninen, A.-M., Rikala, R., and Kainulainen, P.: Drought Stress Alters the Concentration of Wood Terpenoids in Scots Pine and Norway Spruce Seedlings, *J Chem Ecol*, 29, 1981-1995, 10.1023/A:1025674116183, 2003.
- Wagner, V., Jenkin, M. E., Saunders, S. M., Stanton, J., Wirtz, K., and Pilling, M. J.: Modelling of the photooxidation of toluene: conceptual ideas for validating detailed mechanisms, *Atmos. Chem. Phys.*, 3, 89-106, 10.5194/acp-3-89-2003, 2003.
- Wang, Y., Logan, J. A., and Jacob, D. J.: Global simulation of tropospheric O₃ - NO_x - hydrocarbon chemistry: 2. Model evaluation and global ozone budget, *Journal of Geophysical Research: Atmospheres* (1984 - 2012), 103, 10727-10755, 1998.
- WHO: Air quality guidelines: global update 2005: particulate matter, ozone, nitrogen dioxide, and sulfur dioxide, World Health Organization, 2006.
- Wildt, J., Kley, D., Rockel, A., Rockel, P., and Segschneider, H.: Emission of NO from several higher plant species, *Journal of Geophysical Research: Atmospheres* (1984–2012), 102, 5919-5927, 1997.
- Wildt, J., Mentel, T. F., Kiendler-Scharr, A., Hoffmann, T., Andres, S., Ehn, M., Kleist, E., Müssgen, P., Rohrer, F., Rudich, Y., Springer, M., Tillmann, R., and Wahner, A.: Suppression of new particle formation from monoterpene oxidation by NO_x, *Atmos. Chem. Phys.*, 14, 2789-2804, 10.5194/acp-14-2789-2014, 2014.

- Wu, C., Pullinen, I., Andres, S., Carriero, G., Fares, S., Goldbach, H., Hacker, L., Kasal, T., Kiendler-Scharr, A., Kleist, E., Paoletti, E., Wahner, A., Wildt, J., and Mentel, T. F.: Impacts of soil moisture on de novo monoterpene emissions from European beech, Holm oak, Scots pine, and Norway spruce, *Biogeosciences*, 12, 177-191, 10.5194/bg-12-177-2015, 2015.
- Wu, S., Mickley, L. J., Jacob, D. J., Rind, D., and Streets, D. G.: Effects of 2000–2050 changes in climate and emissions on global tropospheric ozone and the policy-relevant background surface ozone in the United States, *Journal of Geophysical Research: Atmospheres* (1984–2012), 113, 2008.
- Wu, S., Duncan, B. N., Jacob, D. J., Fiore, A. M., and Wild, O.: Chemical nonlinearities in relating intercontinental ozone pollution to anthropogenic emissions, *Geophysical Research Letters*, 36, 2009.

7 Appendix

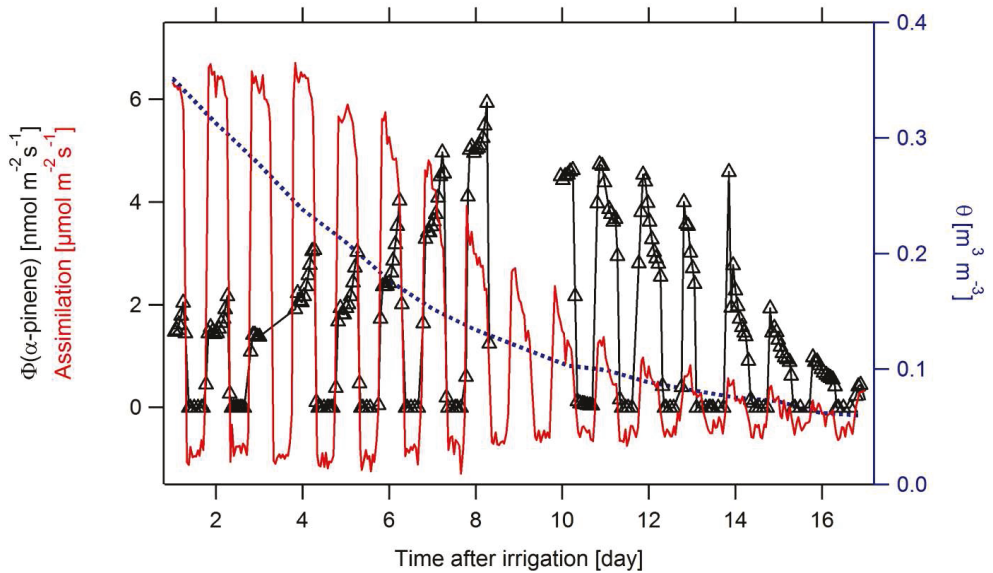


Fig. A1: Temporal shape of α -pinene emissions from a Holm oak, Exp. 2.4a (black triangles, left y scale), net assimilation (red line, left y scale, multiplied by -1) and volumetric water content of the soil (blue dashed line, right y scale). Plant was irrigated at day 0. Gaps in α -pinene emissions are due to time periods when the GC MS device was switched to calibration.

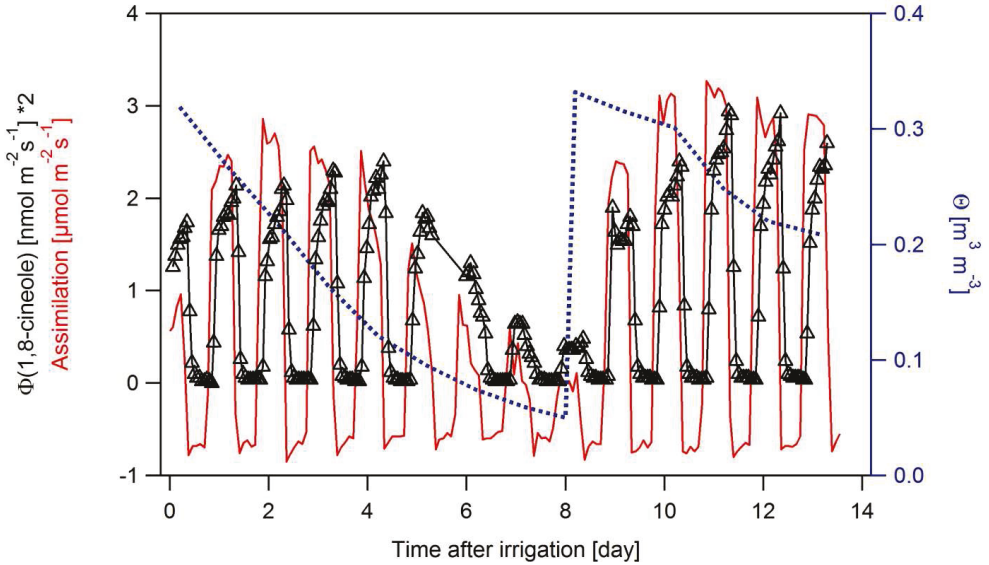


Fig. A2: Temporal shape of 1,8-cineole emissions from a Scots pine, Exp. 2.2 (black triangles, left y scale, data are multiplied by 2) and net assimilation (red line, left y scale, multiplied by -1) and volumetric water content of the soil (blue dashed line, right y scale). Plant was irrigated at day 0 and re-watered at day 8. Gap in the trace showing α -pinene emissions is due to a calibration.

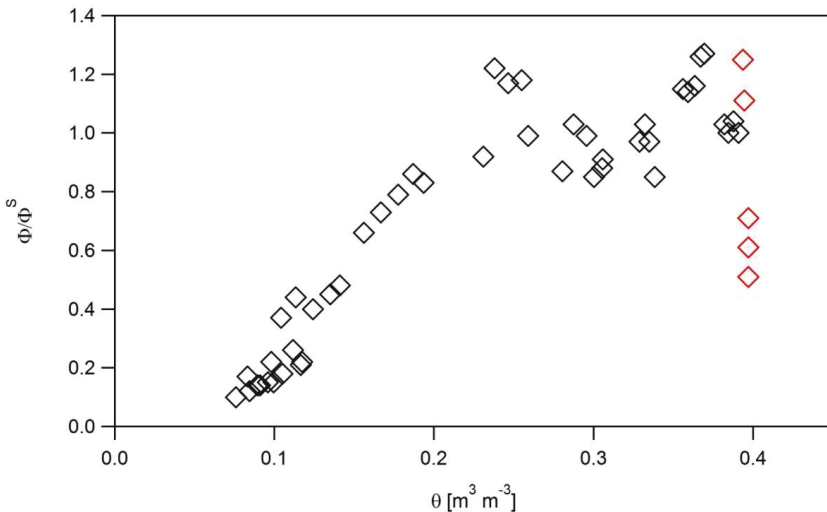


Fig. A3: Normalized 1,8-cineole emissions from a Norway spruce (Exp. 2.1) during a progressing drought period (black diamonds) and recovery (red diamonds) in dependence of the volumetric water content of the soil.

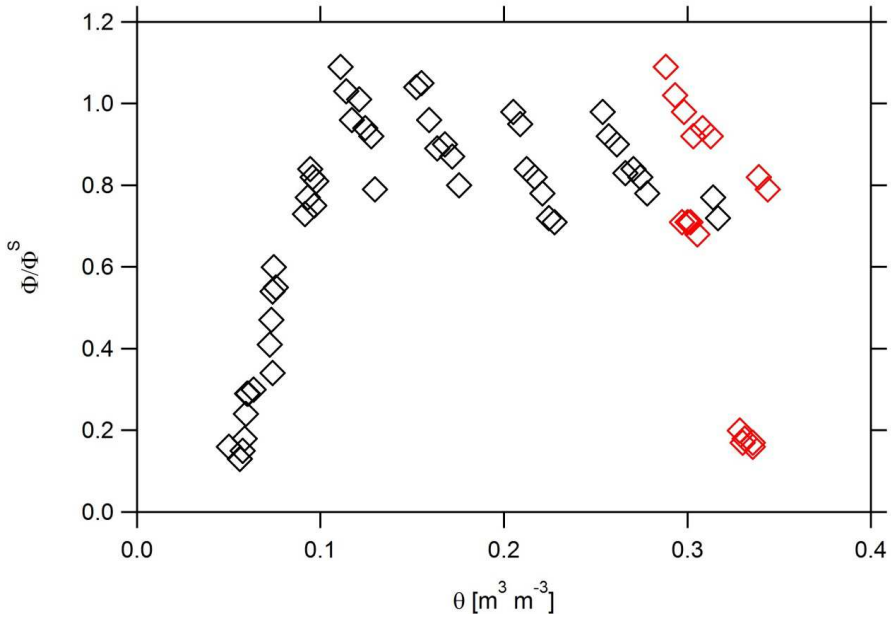


Fig. A4: Normalized 1,8-cineole emissions from a Scots pine (Exp. 2.2) during a progressing drought period (black diamonds) and recovery (red diamonds) in dependence of the volumetric water content of the soil.

8 Abbreviations

BVOCs	Biogenic volatile organic compounds
CH ₄	Methane
CO	Carbon monoxide
CSTRs	Continuously stirred tank reactors
GC-MS	Gas chromatography-mass spectrometry
IR	Infrared
θ	Volumetric water content of the soil
J(O ¹ D)	O ₃ photolysis frequencies
JPAC	Jülich plant atmosphere chamber
MT	Monoterpene
NMHC	Non-methane hydrocarbon
NO _x	Nitrogen oxides
O ¹ D	Excited oxygen
O ³ P	Ground state oxygen
O ₃	Ozone
OH	Hydroxyl radicals
PAR	Photosynthetic active radiation
ppb	Parts per billion
ppm	Parts per million
ppt	Parts per trillion
PSS	Photostationary steady state

PTR-MS	Proton-transfer-reaction mass spectrometry
RH	Relative humidity
SQT	Sesquiterpenes
T	Temperature
VOCs	Volatile organic compounds

9 Acknowledgement

First and foremost I want to thank Prof. Dr. Andreas Schäffer not only for accepting the supervision of this thesis, but also for his valuable guidance and consistent encouragement. Your advices on both research as well as my career have been invaluable.

I would also like to express my sincere gratitude to Prof. Dr. Andreas Wahner and Prof. Dr. Astrid Kiendler-Scharr for providing the opportunity to work at Forschungszentrum Jülich and especially to Prof. Dr. Andreas Wahner for accepting the scientific supervision as second examiner.

I would like to express the deepest appreciation to my supervisor, PD. Dr. Thomas F. Mentel. I appreciate all his contributions of time, ideas, and funding to make my Ph.D. experience productive and stimulating.

I am extremely grateful to my supervisor PD. Dr. Jürgen Wildt. Without his patient guidance, scholarly inputs, persistent help and encouragement, this dissertation would not have been possible.

I want to thank the JPAC team for supporting me and sharing a lot of sweets and happiness: Dr. Einhard Kleist for operating the chamber and for the helpful suggestions and discussions; Iida Pullinen for her great contribution to the experiments of O₃ uptake and BVOC emissions; and Stefanie Andres, Lina Hacker, Tina Kasal, Monika Springer for their support and help.

I would like to thank all members of staff at IEK-8 who helped me in the past three years. In particular, I would like to thank Dr. Ralf Tillmann for the help of PTR-MS and Dr. Franz Rohrer and Borchardt Joachim for the support of NO_x measurement, and Dr. Defeng Zhao for the inspiring discussion.

In addition, a thank you to Prof. Dr. Hans Toni Ratte and Dr. Monika Ratte who encouraged me to start my Ph.D. at Forschungszentrum Jülich.

I gratefully acknowledge financial support by the integrated EU project ECLAIRE (Contract No. 282910).

Lastly, I would like to thank my family and friends for all their love and backing.

Band / Volume 295

Hydration and dehydration at the tropical tropopause

C. Schiller (2015), 72 pp

ISBN: 978-3-95806-101-9

Band / Volume 296

Influence of Impurities on the Fuel Retention in Fusion Reactors

M. Reinhart (2015), 140 pp

ISBN: 978-3-95806-105-7

Band / Volume 297

The role of abiotic processes in the formation and degradation of gaseous nitrogen compounds in the soil

J. Heil (2015), XIV, 106 pp

ISBN: 978-3-95806-106-4

Band / Volume 298

12th Carolus Magnus Summer School on Plasma and Fusion Energy Physics

edited by Kristel Crombé (2015), 468 pp

ISBN: 978-3-95806-107-1

Band / Volume 299

Optical near-field investigations of photonic structures for application in silicon-based thin-film solar cells

A. M. Ermes (2015), vi, 157 pp

ISBN: 978-3-95806-108-8

Band / Volume 300

Strom- und Gasmärktedesign zur Versorgung des deutschen Straßenverkehrs mit Wasserstoff

M. Robinius (2015), VI, 255 pp

ISBN: 978-3-95806-110-1

Band / Volume 301

Alterung von Vakuum-plasmagespritzten MCrAlY-Schutzschichten und ihre Wechselwirkung mit Nickel- und Cobalt-basierten γ/γ' -Superlegierungen

P. J. Terberger (2015), IX, 149 pp

ISBN: 978-3-95806-113-2

Band / Volume 302

Verbundvorhaben ELFA Effiziente Luftfahrzeuge

Brennstoffzellensysteme zur Energieerzeugung BREZEN –
Teilprojekt: Kerosinaufbereitung

R. Peters, J. Meißner, J. Pasel, R. C. Samsun, D. Stolten
(2016), viii, 84 pp

ISBN: 978-3-95806-114-9

Band / Volume 303

Cavity-Ringdown-Spektroskopie zur Untersuchung der Rolle höherer Stickoxide für den nächtlichen Schadstoffabbau in der unteren Atmosphäre

S. Schrade (2016), II, 118 pp
ISBN: 978-3-95806-116-3

Band / Volume 304

Thermo-mechanical Properties of Mixed Ionic-Electronic Conducting Membranes for Gas Separation

V. K. Stournari (2016), 167 pp
ISBN: 978-3-95806-117-0

Band / Volume 305

Untersuchungen zu suspensionsplasmagespritzten Wärmedämmschichtsystemen

N. Schlegel (2016), X, 136 pp
ISBN: 978-3-95806-118-7

Band / Volume 306

Laser processing for the integrated series connection of thin-film silicon solar cells

B. Turan (2016), XII, 190 pp
ISBN: 978-3-95806-119-4

Band / Volume 307

Development and Application of a Multiscale Model for the magnetic Fusion Edge Plasma Region

F. Hasenbeck (2016), 190 pp
ISBN: 978-3-95806-120-0

Band / Volume 308

Emissions of Biogenic Volatile Organic Compounds and Ozone Balance under Future Climate Conditions

C. Wu (2016), VI, 93 pp
ISBN: 978-3-95806-121-7

Weitere **Schriften des Verlags im Forschungszentrum Jülich** unter
<http://www.zwb1.fz-juelich.de/verlagextern1/index.asp>

éclairé

Effects of climate change on air pollution impacts
and response strategies for European ecosystems



**Energie & Umwelt /
Energy & Environment
Band / Volume 308
ISBN 978-3-95806-121-7**

